DISORDERED SYSTEMS: ELECTRONIC PROPERTIES

By

VASUNDHRA CHOUDHRY

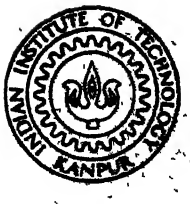

DEPARTMENT OF PHYSICS

INDIAN INSTITUTE OF TECHNOLOGY KANPUR

AUGUST, 1981

DISORDERED SYSTEMS: ELECTRONIC PROPERTIES

A Thesis Submitted
in Partial Fulfilment of the Requirements
for the Degree of

DOCTOR OF PHILOSOPHY

By

VASUNDHRA CHOUDHRY

to the

DEPARTMENT OF PHYSICS

INDIAN INSTITUTE OF TECHNOLOGY KANPUR

AUGUST, 1981

many an afflatus, inflatus and brutus
say many-a-time to a many-of-us
half done is done
since nothing-is-ever-completus

—anon.

Ph. D. 1984

PHY-1981-D-CHO-DIS

ACKNOWLEDGEMENTS

Dr. Abhijit Mookerjee has provided me with expert guidance and wise counsel throughout my Ph.D. program. I personally feel that while his supervision is professional, it is at the same time, amicable. Working with him has been a rich experience.

I am thankful to Dr. Kalyan Banerjee for his enthusiastic supervision of the work done on anharmonic oscillators.

I must thank my colleagues, Mr. Pankaj Joshi, Mr. V.K. Srivastava and Mr. R.P. Singh for endless discussions.

I am, also, pleased with all friends who thanked me profusely at completion.

My thanks to Mr. J.K. Misra for the patience and unflagging enthusiasm which he showed during the preparation of the manuscript.

Lastly, I wish to thank Mr. H.K. Panda and Mr. L.S. Rathore for satisfactory duplication work.

Vasundhra Choudhry

CONTENTS

A Copy of 'On the Size of the Localisation', Mookerjee, A. and Choudhry, V., (1976), Phys. Lett. 59A, 136-8

A Copy of 'Localisation of Electrons in Disordered System,' by A. Mookerjee and V. Choudhry (1977), 80C 411-413. Proc. NP&SSP Symp.

In case of configurations of a cluster that are mixed, the question of interactions between two different kinds of bonds arises. For example in case of the $Ga_xIn_{1-x}As$ alloys, a configuration of the kind 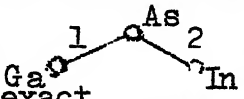

may be a part of a cluster. The interaction H_{12}^{exact} between these bonds 1 and 2 is of a H_1^A kind but between a Ga-As and an In-As bond. It is demonstrated in the following that this interaction is the average of H_1^A's corresponding to pure Ga-As and pure In-As crystals, as a reasonable approximation.

Let bonds 1 and 2 be described by quantum states $|b_1\rangle$ and $|b_2\rangle$ respectively. Then,

$$|b_1\rangle = (|As_1\rangle + |Ga_1\rangle)\frac{1}{N}$$

and $$|b_2\rangle = (|As_2\rangle + |In_2\rangle)\frac{1}{N}$$

in terms of the sp^3 hybridised orbitals at the various sites directed along the respective bonds and N is the normalisation constant ~ 2, assumed to be the same for the Ga-As and In-As bonds. We are concerned with H_{12}^{exact}, i.e.

$$\langle b_1|\underline{H}^{exact}|b_2\rangle = \frac{1}{N^2}[\{\langle As_1| + \langle Ga_1|\}\ \underline{H}\ \{|As_2\rangle + |In_2\rangle\}]$$

$$= \frac{1}{N^2}[\langle As_1|\underline{H}|As_2\rangle + \langle Ga_1|\underline{H}|As_2\rangle$$

$$+ \langle As_1|\underline{H}|In_2\rangle + \langle Ga_1|\underline{H}|In_2\rangle]$$

LIST OF FIGURES

probabilities are indicated in Fig. 3.7(c). Configurations $C_4^{(v)}$ and $C_4^{(vi)}$ are identical but are listed separately to retain symmetry under exchange of the alloyed ions Ga and In. Now,

$$\underline{G}^{(4)} = \begin{bmatrix} G_0 & G_1^A & G_1^A & G_1^A \\ G_1^A & G_0 & G_1^A & G_1^A \\ G_1^A & G_1^A & G_0 & G_1^A \\ G_1^A & G_1^A & G_1^A & G_0 \end{bmatrix}$$

where G_o and G_1^A are the matrix elements of the CPA Green's operator. H_{ij}^{exact} are similarly determined and the n x n matrix $\underline{H}^{exact}$ written for each configuration by substituting in the correc parameters depending on whether the bonds i and j are the Ga-As or the In-As type. An average over the trace of the averaged Green's operator matrix is taken to yield the averaged diagonal Green's operator sought, since the four bonds are not symmetrical in all the configurations.

(d) Next, the seven bond cluster consisting of a bond and its six nearest neighbours is considered. The matrices involved are therefore 7 x 7. Eight configurations and their respective statistical probabilities of occurrence are shown in Fig.3.7(d). Matrix elements of the CPA Green's operator between common cation and common anion adjacent bonds, second nearest neighbouring parallel and non-parallel bonds, and the diagonal elements all

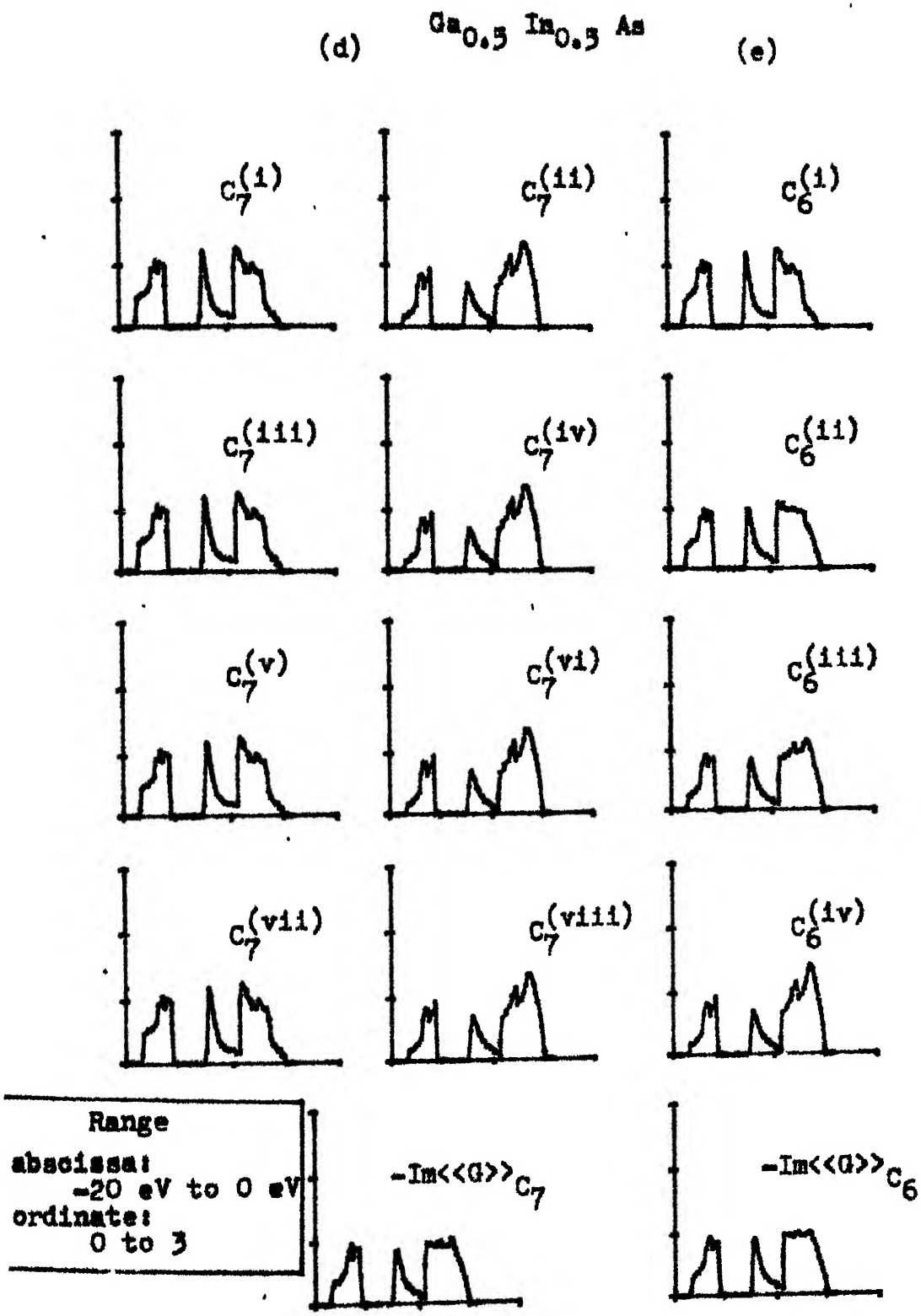

ig. 3.11: Density of electron states per bond in units of π^{-1} (-Im G) for the alloy $Ga_{0.5}$ $In_{0.5}$As corresponding to each configuration (Fig. 3.7(a) to (e)) of the clusters (a) C_1 (b) C_4 (c) $C_{4'}$ (d) C_7 and (e) C_6 and those averaged over configurations of each cluster, using the fitted parameters.

CHAPTER IV

THE CHEMICAL PSEUDOPOTENTIAL THEORY, APPLICATION AND COMPARISONS

4.1 Introduction:

The parameters used to describe the III-V semiconductors in Chapter III have been obtained by fitting with experimental observations of the photoelectric thresholds and x-ray photomission spectra. The procedure is unsatisfactory due to two main reasons. Firstly, experimental results obtained by different workers differ. So much so that differences in parameters for the same alloy obtained from different sources vary more than parameters corresponding to different alloys (See Table 3.2). Chen and Sher (1978) in fact, first determine parameters corresponding to the six III-V semiconducting materials considered, separately from two or three different sources of experimental observations differing sometimes widely. Finally, the best fitted values are determined by a hit-and-trial method, such that after an energy dependent broadening is imposed, the density of states function obtained best resembles the experimental x-ray photoemission spectra curves. This involves much arbitrariness. Secondly, the bond basis set is non-orthogonal, with considerable overlap between bonds on different pairs of atoms.

where T is the kinetic energy operator and V_{ac} is the effective bond potential. A functional form for the V_{ac} may be obtained in terms of the atomic potentials V_a and V_c at the sites labelled by a and c, and the corresponding orbital functions ϕ_a and ϕ_c respectively which constitute the bond under consideration, by writing Eq. (4.14) as

$$(T + V_{ac}) [|a\rangle + |c\rangle] = \varepsilon_b [|a\rangle + |c\rangle]$$

the normalisation constant being irrelevent here. This can be simplified to

$$T_a|a\rangle + T_c|c\rangle + V_{ac}[|a\rangle + |c\rangle] = \varepsilon_b[|a\rangle + |c\rangle]$$

i.e. $$(\varepsilon_a - V_a)|a\rangle + (\varepsilon_c - V_c)|c\rangle + V_{ac}[|a\rangle + |c\rangle] = \varepsilon_b[|a\rangle + |c\rangle]$$

i.e. $$V_{ac} = \varepsilon_b + \frac{(V_a - \varepsilon_a)\,\phi_a + (V_c - \varepsilon_c)\,\phi_c}{\phi_a + \phi_c} \qquad (4.15)$$

where T_a and T_c are the kinetic energy operators corresponding to the electrons bound to the atoms at sites a and c respectively. In case of carbon and silicon in a diamond lattice this potential along the bond is symmetric (Bullett 1975) while in case of III-V semiconductors forming a zinc-blende structure, the potential is asymmetric.

The pseudopotential off diagonal matrix elements are therefore like $\langle a'c'|V^{(ac)}_{a'c'}|ac\rangle$, where $|a'c'\rangle$ is a bond orbital neighbouring to $|ac\rangle$. To evaluate these, one could use the 'Wigner trick' similar to the one used by Anderson for his

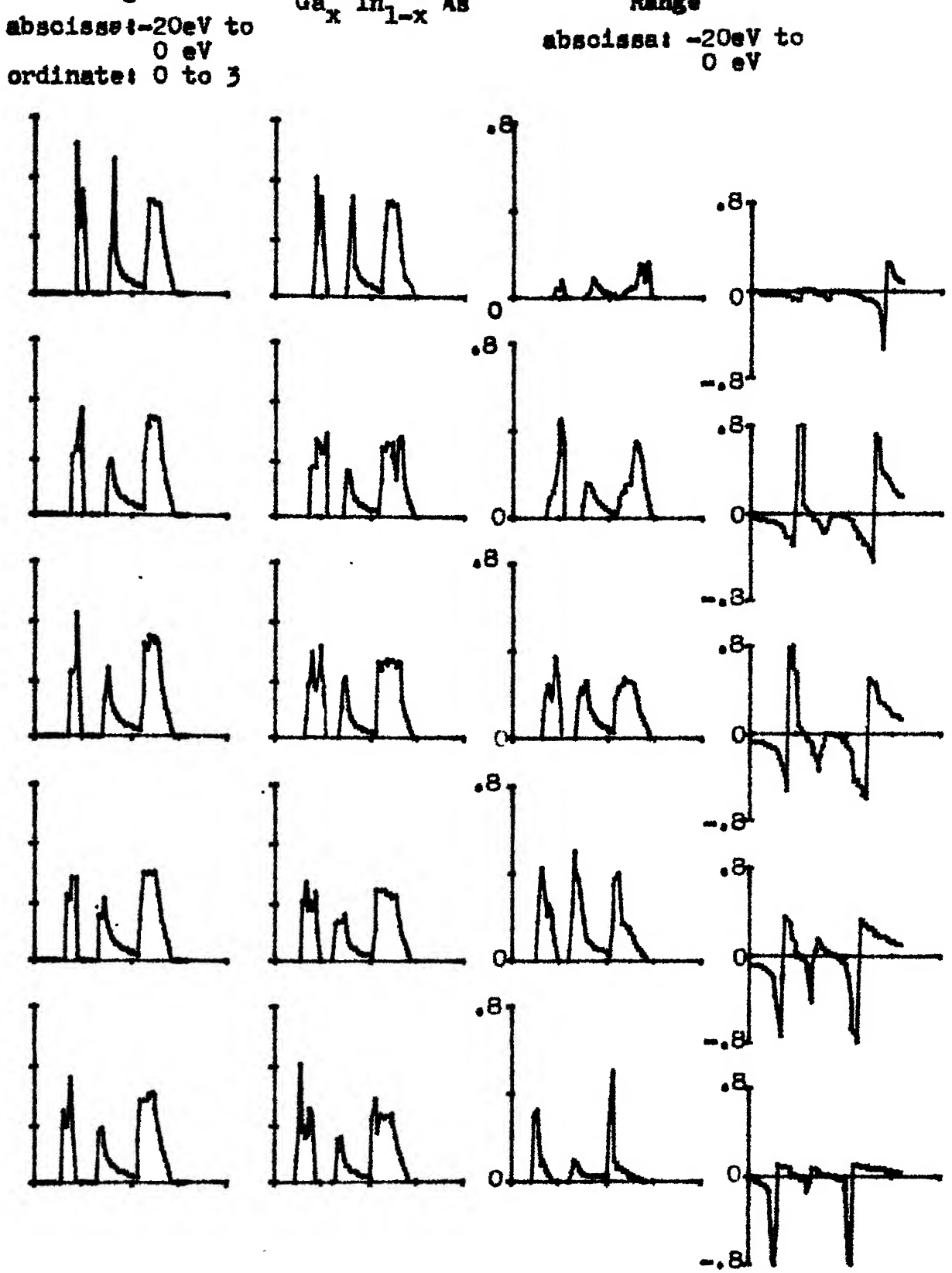

Fig. 4.4: (i) $-\mathrm{Im}\, G^{VCA}$ (ii) $-\mathrm{Im}\, G^{CPA}$ (iii) $-\mathrm{Im}\, \Sigma$ and (iv) $\mathrm{Re}\, \Sigma$ for the specific alloys $Ga_x In_{1-x} As$ with $x = 0.1, 0.3, 0.5, 0.7$ and 0.9 obtained

LIST OF TABLES

SYNOPSIS

The study of metallic alloys like brass, steels and white metal has had a long history. Semi conductors and their alloys like Si, Ge, GaAs, InAs and $GaAs_x P_{1-x}$ have attracted attention with the advent of photovoltaic cells, as have amorphous semi-conductors like hydrogenated a-Si films as proposed cheap, but efficient solar cells. For a long time the study has been empirical, essentially a metallurgical approach. Till recently there has been a lack of underlying unity of theory, and consequently controversy over seemingly contradictory experimental data.

Often, the properties of the alloys and the constituents or that of the crystalline and the amorphous materials differ drastically. In order to understand why these systems exhibit these properties and to be able to predict specific properties, not only must one understand how these arise in the pure or ordered systems but also how they change on introducing disorder. Clearly, this requires a microscopic theoretical study that is systematic. The thesis is an attempt in this direction. Our attention is confined to the electronic properties of disordered systems.

A self consistent cluster CPA formalism to obtain a configurationally averaged Green's function for electronic

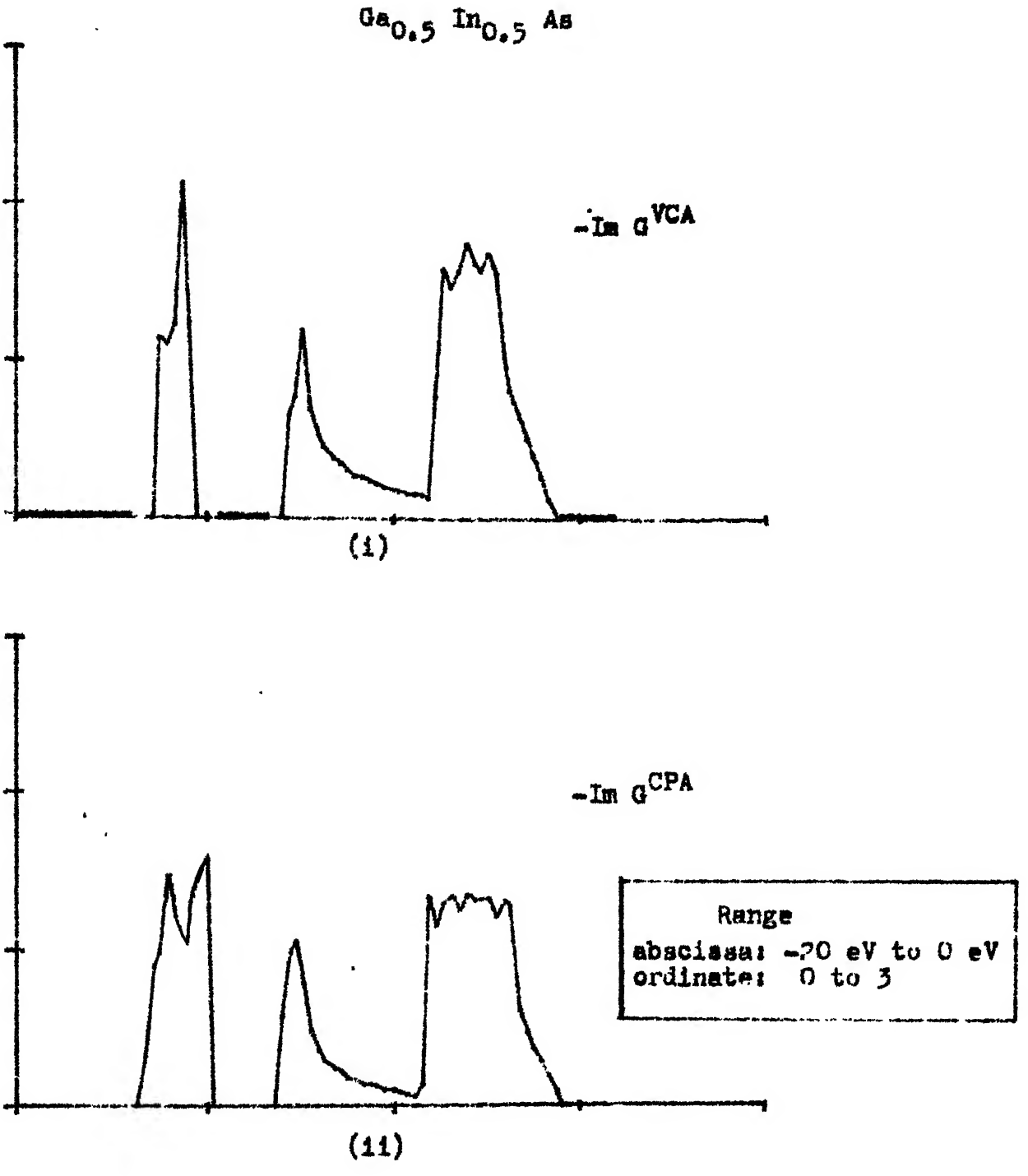

Fig. 4.9: (i) $-Im\ G^{VCA}$ and (ii) $-Im\ G^{CPA}$ for $Ga_{0.5}$ $In_{0.5}$ As using chemical bond pseudopotential parameters.

tree is always more diffusive than the same on the real lattice from which the tree was formed by 'delinking'. Estimates of the localisation length in the CTA are thus always over-estimates, as are the estimates of the mobility edges.

We can rewrite Eqn. (5.1) somewhat. Following Economou and Cohen (1972),

if $G_{00}(Z) = [Z-\varepsilon_0-\sigma_0(Z)]^{-1}$, $\sigma_0(Z)$ being the self energy, then,

$$P_0(E) = \int_{-\infty}^{+\infty} dE \lim_{\eta \to 0^+} \{n_0(E)/[1 + \frac{\mathrm{Im}\sigma_0(E + i\eta)}{\eta}]\}$$

We have used the herglotz property of the Green's function and the self energy,

$$\text{i.e. } \mathrm{sgn}\,[\mathrm{Im}\, G_{00}(Z)] = -\,\mathrm{sgn}\,[\mathrm{Im}\, Z];$$

$$\lim_{\eta \to 0^+} \frac{1}{\pi} \mathrm{Im}\, G_{00}(E - i\eta) = n_0(E)$$

the local density of states; and since $\sigma_0(Z)$ is analytic in the entire upper half plane Im $Z > 0$,

$$\lim_{\eta \to 0^+} \frac{\mathrm{Im}\,\sigma_0(E-i\eta)}{\eta} = -\frac{d\sigma_0(E)}{dE}$$

Now, within the band, $n_0(E) \neq 0$. If the state is extended, $d\sigma_0/dE$ diverges and $P_0(E) = 0$. On the other hand, in the localised domain, $d\sigma_0/dE$ is finite and $\to 0$ when the degree

spectra is developed in Chapter III. This is based on the Augmented Space method of Mookerjee. The method is superior to the CPA (reviewed in Chapter II) in that statistical clustering effects and off-diagonal disorder over finite clusters are successfully taken into account without destroying the herglotz property of the Green's function. This is essential for physical relevance.

The theory is applied to the valence bands of substitutional alloys, in particular to those consisting of pairs of GaAs, InAs, GaSb, InSb, GaP, InP with a common cation or anion mixed in various properties e.g. $Ga_xIn_{1-x}As$, $\forall\ 0 \leq x \leq 1$. These materials form tetrahedrally coordinated, strong covalently bonded solids in a zinc-blende lattice structure. In the alloys the fcc sublattice of the common ion is 'regular', while that of the other ion is randomly occupied by the constituent atoms.

These are studied in the Bond Orbital Model (BOM) which has the advantage over the Site Orbital Model of having rapidly falling off-diagonal terms. In doing this we are neglecting the bonding-antibonding overlaps. Also the antibonding orbital bases have been found to be inappropriate for the study of the conduction band, and we do not get any estimates of the band gaps. A parameterised hamiltonian fitted to experimental data is used to obtain the Green's

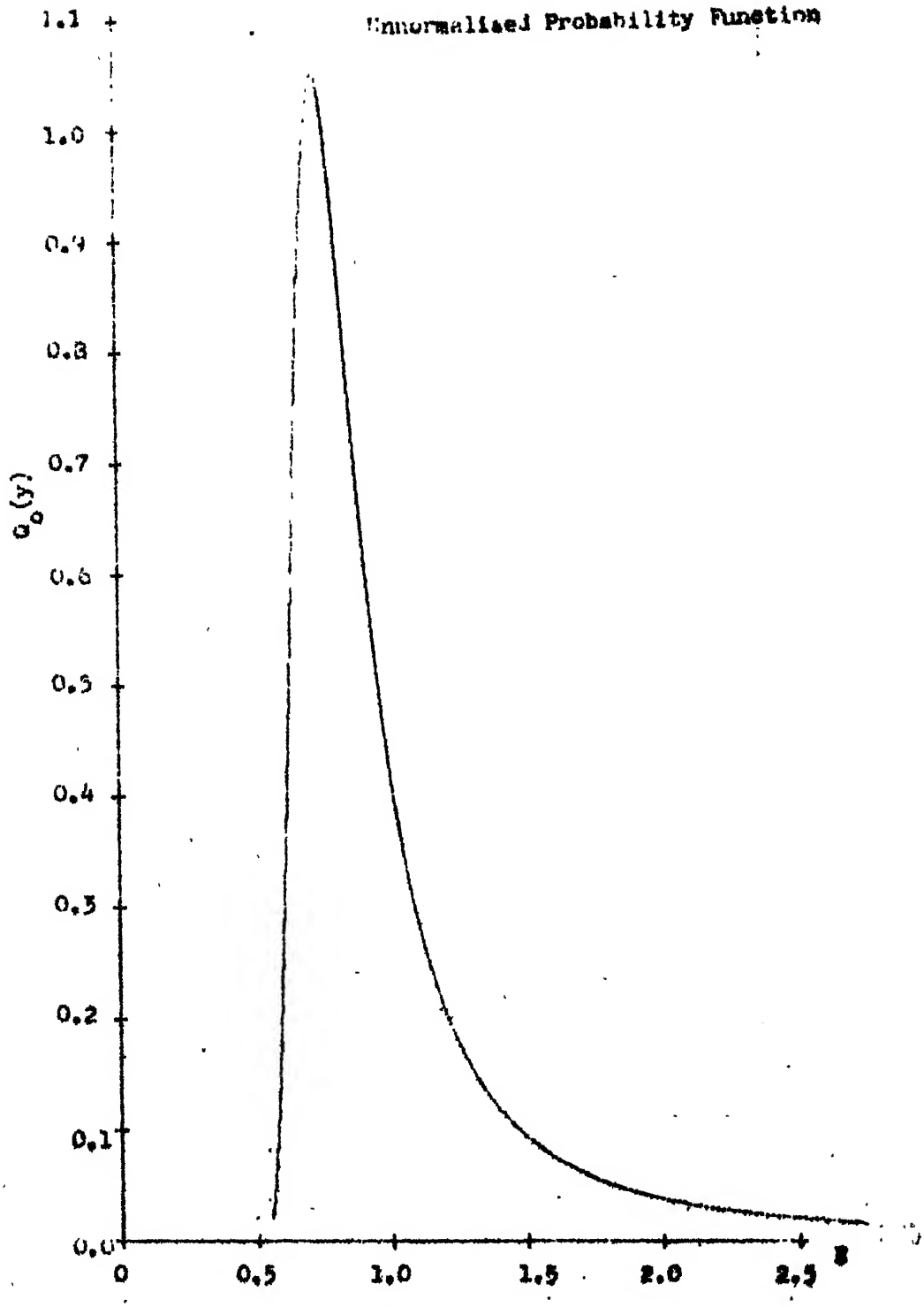

Fig. 5.2: A typical $Q_o(y)$ for E near E_s.

functions for the ternary alloys in the Virtual Crystal Approximation (VCA). A Ray Diagram technique, described in Appendix A, is employed to evaluate density of states and consequently the complete Green's functions by the use of Kramers-Kronig relations. A similar technique is used to obtain the off-diagonal elements of the Green's operator, required for the cluster embedding in the effective medium. The VCA result is used as a starting point for the subsequent CPA calculation. Cluster CPA Green's functions corresponding to exact clusters of various kinds embedded in the CP-medium are then obtained. A weighted average of these gives the required configurationally averaged Green's functio Results are obtained for one-bond, four-bond, seven-bond and six-bond-ring clusters. The CP-medium is not made self-consi tent with respect to the clusters larger than one-bond. Consequently, there is no improvement of the band edges or th structure near them. But the cluster characteristics near th band centres are reproduced. In addition, hypothetical alloy with widely differing potentials are studied, revealing the 'impurity bands'. These show considerable sensitivity to clustering and off-diagonal disorder.

The parameter fitting procedure to fix the hamiltonian carried out using the photoelectric thresholds and x-ray photoemission spectra involves a degree of arbitrariness depending on different experimental data, often differing

shown to effectively transform the Hill determinant such that, for every eigen energy, most of the contribution is lumped in one term on the diagonal. Opening the Hill determinant about this term gives exceedingly fast converging perturbation expansion for the eigenvalues and eigenfunctions The boundary layer in the (k,λ) plane which has been believed to be unsurpassable by all other methods available before, is crossed with ease, for all anharmonicities. Furthermore the convergence is so fast and the accuracy limited only by the machine precision, that the solutions can be called 'exact' in a numerical sense.

Other problems that can be attempted are a) the double-hump potentials eg. in the ammonia molecule, b) perturbations as by electric fields i.e. Stack effect, c) anharmonicities other than the polynomial ones, etc. The approach is very promising and will probably prove very useful in the study of other non-linear problems.

with each other considerably. The non-orthogonality of the bond bases is claimed to be absorbed in the parameters. This is an approximation of unclear validity. In Chapter IV, we have developed a chemical pseudopotential scheme to determine the parameters, starting from Herman-Skillman tables of self-consistent Hartree-Fock one-electron potentials and orbitals. The chemical pseudopotential method not only takes the non-orthogonality of the bases into account but is illustrative of the chemistry of the bonding in a more transparent fashion. Furthermore, the ab initio procedure is independent of parameter fitting to experiments. The VCA, CPA and the cluster-CPA calculations are likewise made on the same systems and comparisons made.

In both cases, the cluster CPA alters essentially the top of the valence band. This is to be expected because the inner states must see less of the details of the neighbourhood.

In Chapter V, the question of the nature of electronic states in disordered systems is tackled. A criterion for localisation involving the convergence or divergence of the averaged localisation length is introduced. An estimate of localisation lengths of electron states in weakly disordered Cayley trees is made. Results are exact near the mobility edge, producing the linear dependence on energy expected in effective medium theories. In general, nonlinear integral

Eqn. (A.1) for each TT in each tetrahedron of the IBZ and accumulate the sum, (vii) Use Kramers-Krönig relations to evalu the complete function F(E).

When $f(\vec{k})$ in the integrand does not reflect the symmetries of the BZ, contributions in each of the other parts of BZ similar to the IBZ, obtainable by the application of a symme transformation of the complete BZ, may be obtained by inserting the value of $f(\vec{k})$ at points corresponding to the $\vec{k}_r$ in the IBZ scanned. Since the Hamiltonian is necessarily symmetric under these very transformations, all other factors remain the same.

A.3 Generalisation and Application to Off-Diagonal Green's Functions:

The BZ of an fcc lattice is shown in Fig.A.3in which some symmetry points and directions are also indicated. Labels in the band structures for GaAs and InAs on Fig.(3.5) correspond to those shown here. The IBZ is shown in Fig.A.4 which can conveniently be divided into three tetrahedra 1,2 and 3, all apexed at Γ, the centre of the BZ (Fig. A.5). The coordinates shown are in the units of $\pi/16a$, where a is the edge of the direct fcc lattice cubic unit cell. Γ corresponds to $\vec{k} = 0$ and is,therefore,taken to be the origin of the coordinate system, and the coordinate axes x,y,z pass through the centres of the square faces of the BZ (Fig. A.4). Point A and the symmetry points Γ, L, U, X, K are the vertices of the IBZ. LUAK is a sixth of the hexagonal face, while UXA is an eighth

equations are obtained. Close to the band edge, solutions necessitated numerical computation. This has been carried out and the results presented.

As a case of divergent but asymptotic perturbation, the problem of the anharmonic oscillator is also considered. An elegant non-perturbative method using the difference equation, to evaluate eigenvalues and eigenfunctions is presented. The work, done in collaboration with Dr. K. Banerjee, S.S.Kanwal and S.P. Bhatnagar [Proc. Roy. Soc., London, A 360, 575-586 (1978)] does not get worse with higher quantum numbers for, say, the quartic anharmonicity, i.e., $V = kx^2 + \lambda x^4$, or with the anharmonicity parameter λ. The hitherto unsurpassable 'boundary layer' in the (k, λ) plane is crossed with ease. The calculation takes considerably less time than the best methods otherwise available only for some regimes of (k, λ) and few quantum numbers. Fast quadratic convergence and accuracy limited only by the 'PRECISION' of the computer calculation are other highlights of the formalism. Some eigenvalues accurate to 15 significant figures are tabulated, calculated in the Double Precision mode on IBM 7044 and DEC 10.

CHAPTER I

INTRODUCTION

1.1 Disordered Systems:

Until recently, most of the attention of physicists has been occupied by regular or ordered systems. Yet there is no dearth of those essentially disordered. Examples abound. Besides the geophysical and astrophysical systems, liquids, amorphous solids, glasses, random alloys, polymers are some of them.

The original metallurgical approach for discovering useful metal alloys, for example, was to 'mix and see' if a useful, reproducible property is obtained. In this way steels, the discovery of which revolutionised industry, were obtained by alloying iron with small amounts of carbon, chromium, etc. Varied proportions of the same constituents gave steels exhibiting various degrees of hardness, and other associated properties like ductility and tenacity. Similarly, brasses, alloys of copper and zinc, have been in use. White metals too are very useful as antifriction coatings for bearings. Of these, the Babbit metals are composed of mainly tin alloyed with smaller amounts of antimony and copper, while the Brittania metals also contain zinc, lead and bismuth. The latter are also used for making table ware.

APPENDIX C

THE ANHARMONIC OSCILLATOR

eigenfunction just begins to increase in magnitude. The contribution to the moments from the rest of the configuration space is estimated to be less than $O(10^{-16})$ for all the moments of the table 3; (iii) the moments may now be expressed as sums of integrals of the type $\int_0^1 x^{2k} e^{-\alpha x^2} dx$, ($k$ = integer), which are obtained recursively starting from the incomplete Gaussian integral $\int_0^1 e^{-\alpha x^2} dx$. The computation of moments therefore requires no integration; (iv) each moment in table 3 has been checked by varying α in the range (7).

The matrix elements of the operators x and x^2 in the lowest ten states of the quartic oscillator ($H = p^2 + x^4$) are given in table 3. The best known estimates (Chan & Stelman 1963; Reid 1970) of the transition moments of the quartic oscillator were obtained by using variational eigenfunctions. The variational eigenfunctions are known to be much less accurate than the corresponding eigenvalues and are unsuitable for the computation of moments. Thus only the first few (two or three) non-zero moments for the transitions were obtained in these works to some reliability (6 figures). We emphasize that all moments except the lowest one for any transition may be obtained from (12), without integration.

5. Discussion

(i) The confidence in the accuracy of the computed eigenvalues is derived from the following checks: (*a*) The computed eigenvalues are stable with respect to changes in the scaling α (see (7)) and for different initial estimates for the energies; (*b*) Three separate computations with an increasing, a decreasing, and a nearly flat, sequence of determinants (see the discussion after (11)) yielded eigenvalues differing by at most two units in the 16th significant figure; (*c*) The upper and lower bounds for the eigenvalues differing in the 16th figure by at most two units were obtained by the 'sign check' described in § 2.

(ii) It may be emphasized that no integration or diagonalization is necessary in this method which makes it attractive for the eigenvalue problems of the linear operators.

(iii) In perturbation theory with λ as the small parameter, this problem belongs to the singular perturbation class. The uniform applicability of this method for all λ underlines its non-perturbative character. For this reason the method is expected to apply to problems involving large perturbations.

(iv) The need for introducing a scaled basis was realized by Reid (1970) who used the linear variation method with harmonic oscillator basis for the quartic oscillator eigenvalue problem. However, in a variational framework the use of a scaled basis becomes intractably laborious for the following reason. In a variational computation the first n (say) eigenvalues are obtained together. Since the appropriate scaling is different for different n and λ a single scaling is not suitable for the computation of all n eigenvalues. A compromise scaling must therefore be used.

Semiconducting alloys e.g. $Ga_xIn_{1-x}As$, GaAs-GaAlAs have recently become important because of their use in solar cells in search of an alternative energy source. Also GaAsP cells are used as light emitters and HgCdTe as IF-detectors.

The special properties of each of the alloys mentioned above often differ drastically from those of the constituents. In order to really understand why the alloys exhibit these properties and to be able to predict specific properties, not only must one know how these properties arise in the pure constituents, but also how these change on alloying. For example, in case of solar cell materials, how the band gap changes on alloying is an important factor. Of course, in general, the shapes of the bands together with the band gap, determine the optical and optico-electrical properties. The knowledge of how these change on alloying would make it possible to determine the optimum proportions of constituents in an alloy, that would exhibit the desired properties and behaviour, in a theoretically systematic manner, instead of the 'hit and trial' experimental method. Clearly, this requires a study at the microscopic level. This is the view point of the theoretical physicists.

Interest in amorphous states of pure and mixed intrinsic semi-conductors eg a-Si and $Te_{48}As_{30}Si_{12}Ge_{10}$ was sparked off by Ovshinsky's (1968) reported discovery of its switching

property. A-Si now shows tremendous promise in construction of cheap and efficient solar cells. Although solar cells using crystalline Si have been designed fairly successfully in the laboratory, these are not commercially viable, as tedious methods of preparation of large enough crystalline cells are prohibitively expensive. Solar cells using a-Si, on the other hand, are comparatively non-expensive both because of simpler methods of preparation and because thin films require very little material. Thus large areas coated with these films may be easily obtained. Such cells with a working efficiency of 4% are now available commercially. Those working at about 8% efficiency have also been reported but have short lives. Besides, these are not easily reproduced, To understand these features, again a microscopic analysis is indicated.

Glasses, too, are disordered materials in the amorphous state. Other systems like amorphous Sulphur, Selenium, Tellurium,etc. have also been extensively experimented with, though a microscopic understanding of the behaviour of these is yet incomplete.

Experiments to detect presence of voids and dangling bonds, sensitivity to annealing, judged by measuring changes in the ESR response, conductivity, voids, stresses, diamagnetism, etc. as the annealing rates are varied, seem to indicate inherent differences between some materials. Some

materials defy preparation by the method of quenching the liquid state, always ending up in polycrystalline states this way, while some others should better be called 'super cooled liquids' because no latent heat around the apparent change of state is involved. Further, some materials do, while others do not even show a 'glass transition'. Sometimes the essential difference between some materials occurs because some materials can be made in bulk, while some are obtained only as films. The behaviour of the former is governed by bulk properties, while that of latter must essentially be due to surface properties. In fact, studies on silicon-dioxide films have revealed that some properties of silicon samples are truly due to the silicon-dioxide layer that gets very easily formed on the surface due to oxidisation. Surface properties are, likewise important for transition metal alloys in their use as catalysts for chemical reactions. Spin glasses,met-glasses, garnets and other random magnetic systems are some of the other systems of concern.

Such varied behaviour makes a universal theory for all disordered systems virtually impossible. Those mentioned above, and others studied experimentally with a view to reach a better understanding at large, therefore, need to be classified.

1.2 Classification:

1) Compositionally Disordered systems, i.e. those in which the locations of sites form a lattice, occupied randomly by atoms of the constituents. These include (a) defects and impurities in otherwise periodic systems, e.g. colour centres in ionic alloys, (b) metal alloys i.e. the brasses, steels, white metals, and (c) the semi-conducting alloys, e.g. $Ga_xIn_{1-x}As$, Ga_xSe_{1-x}, $GaAs_xP_{1-x}$.

2) Structurally disordered systems include the amorphous materials. These are:

a) Dielectric films like SiO_2 or ionic insulators like V_2O_5.

b) The amorphous semiconductors, which are further subdivided into two classes - (i) the tetrahedrally bonded (TB) type e.g. a-Si, a-Ge, a-GaAs, and (ii) the lone pair (LP) type, e.g. a-Se, a-As_2S_2. These are distinguished because of general differences shown experimentally. For example, the former are generally found only as thin films containing voids and dangling bonds, while the latter, formed in bulk, do not have enough density of these to be detected by the porosity and ESR experiments respectively. Again, the TB a-semiconductors are very sensitive to annealing indicated by the disappearance of the ESR response, increase in resistivity, decrease in the number of voids

and relaxation of internal stress. These also show considerable diamagnetic enhancement in the amorphous state. The LP type of a-semiconductors, on the other hand, are much less sensitive to annealing, show no stress thereafter, and the diamagnetic enhancement is not much. Finally, these exhibit a glass transition, while the TB type can be obtained only as films and show no glass transition, passing into the crystalline state instead.

c) Quasi one-dimensional systems like TTN-TCNQ have been designed and dealt with, essentially to gain understanding, since theoretically the problem is relatively simple.

3) Polymers are a subclass of structural disorder because of their structural peculiarities. These consist of long linear molecules which fill space. Interactions between various parts of a chain as well as other chains exist. These often exhibit a gelling phenomena related to the localisation in disordered systems, which must be understood. Interest in polymers arises from analogous systems like plastics in material science and gels, polymer solutions, DNA, the genetic material etc. in life sciences.

4) Magnetic disorder occurs when the spin orientation is random forming random para- and ferro-magnets. Five systems,

viz. Cu-Mn, Au-Fe, Au-Cr, Ag-Cr and Ag-Mn are crystalline random alloys consisting of moderate concentrations of the magnetic constituent and show a new magnetic phase called the spin glass . Kondo effect, i.e. disappearance of magnetisation below a certain temperature, of very dilute magnetic impurities in a non-magnetic host, is an unusual property exhibited by this class. Finally, met-glasses, garnets etc. consist of a structurally disordered matrix of transition metal atoms embedded in a glass-forming matrix, e.g. Fe_xB_{1-x}.

1.3 Non-Reproducibility of Experimental Results:

Observations made on the same system by different experimentalists sometimes do not tally. Of course, a particular sample can accidentally develop a specific anomaly during its preparation or while observations are made on it, therefore, an experimentalist takes the pre-caution of repeating observations on a sample, as well as various samples prepared under the same conditions before quoting the results.

Some parameters that affect the properties of the sample obtained are (1) method of preparation, (2) the environment, (3) the source of raw material and (4) the consequent analysis of data.

For example, while lone pair amorphous semiconductors can be prepared in bulk by quenching the liquid state,

tetrahedrally bonded amorphous semiconductors form poly-crystalline samples in this process, exhibiting very different properties. Again, thin film of a-Si obtained from rf-sputtering in an inert gas environment is now distinguished from that obtained by glow discharge through silane (SiH_4) gas. The former contains microvoids, with dangling bonds in them, whereas the latter, referred to as hydrogenated a-Si, is different essentially because the available H-atoms enter the sample and satisfy the dangling bonds. Presence of impurities in dilute amounts also can alter properties of a sample, hence the source of raw material used and the environment of preparation must be taken into account while trying to understand the mechanism of behaviour. Finally, the analysis employed to interpret the observations can introduce controversies. For example, band gaps as determined from electrical and optical properties need not give similar results.

There is, therefore, an urgent need to correctly interpret experimental results and clearly understand the various parameters which affect their outcome, in a systematically developed theoretical approach.

1.4 Theoretical View:

The solution of the many body problem of structures and properties of crystalline materials is facilitated to a great extent by the Bloch's theorem. Lattice periodicity,

or translational invariance of the potential is central to the theorem. As a consequence, in the momentum space, the degrees of freedom reduce to a few, and the problem becomes tractable.

The idea of bands and band gaps came out of this. Much of solid state phenomena of crystals is understood in terms of these. For example, the position of the Fermi level E_f within the bands or gaps determines the conductive nature of the material. For the E_f lying within the band gap ΔE, if $\Delta E \sim kT$, the material is semiconducting. For $\Delta E << kT$ or overlapping bands, metallic behaviour is produced. For $\Delta E >> kT$, we have insulators, which are transparent if ΔE is greater than the energy of visible photons. But glass, an amorphous material lacking lattice symmetry, must have a large band gap, because of its transparency to light. Thus, the general belief that Bloch's theorem or lattice symmetry is necessary for the existence of band gaps, is untrue.

Actually, the long range order that Bloch's theorem assumes, is not essential for the existence of bands and gaps between them. That well defined bonding and antibonding energy levels in isolated molecules spread into bands in the solid state has been the view of chemists. In fact, all band structure calculations of the density of states take account only of interactions between near neighbours. To sum up, long range order is not necessary, while the local

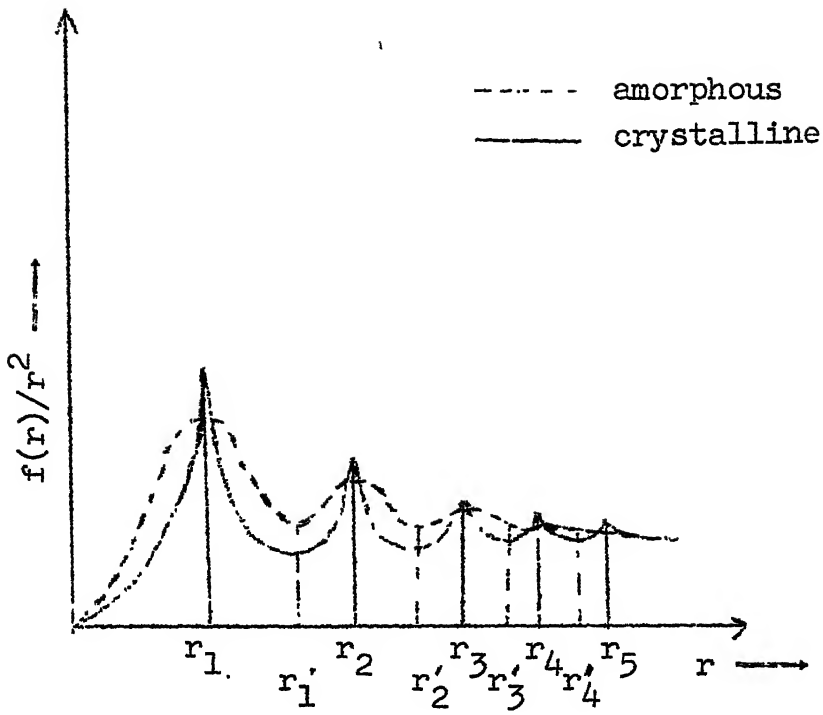

Fig. 1.1: A typical radial distribution function f(r) scaled by r^2 for crystalline (full lines) and amorphous materials (broken lines), where f(r): the number of atoms around distance r per unit volume.

r_n : the n-th near neighbour distance in crystals, and

r'_n : the distance within which all n-th near neighbour are situated in both cases.

bonding behaviour is sufficient to determine the bands and properties arising from these.

Experiments on amorphous materials reveal that the coordination number is retained. Typical radial distribution functions f(r), the number of atoms round the distance r per unit volume, scaled by r^2 to remove the inevitable steady rise in f(r), for crystalline and amorphous states of materials like Ge, Si are shown in Fig. 1.1. In the amorphous states, the peak at r_1' , where r_n' are the n-th near-neighbour distances, though gets broadened, does not shift. That the curve gets smooth earlier than for crystals, is indicative of the absence of long range order in amorphous materials. This observation supports the above view and suggests a local theory based on bonding that must be attempted.

In general, one would like to look into the nature of various excitations, e.g. electrons, phonons, magnons, etc. As Elliott et.al. (1974) have shown, within the Green's operator formalism, studies of each of these can be cast on very similar frameworks. Methods developed for one are, thereafter, easily extended for other excitations. In the following work we concentrate on the electronic properties, in particular,

the density of states. In Chapter II, we review earlier attempts at developing the theory of electronic structure of random alloys. The idea is to examine in detail the drawbacks of these approaches so as to form a basis for our generalisation. The Coherent Potential Approximation (CPA), which has been the most successful development so far, has been examined with a view of determining the best avenue open for generalisation. Unsuccessful or partially successful attempts at generalisation have also been discussed. Finally, an analytically sound cluster CP - generalisation has been developed, which at the same time is tractable for reasonably realistic calculations on real alloys. This generalisation is based on the augmented space approach introduced by Mookerjee (1973) and later developed by various authors (Kaplan, Gray 1976, 1977, Kaplan, Leath,Gray, Diehl 1960). This is presented in Chapter III and applied to III-V semiconducting ternary alloys obtained from pairs of GaAs, InAs, GaSb, InSb, GaP and InP, with a common cation or an anion in various ratios. These are covalently bonded with a four-fold coordination, and fall in the category of compositionally disordered systems, i.e. have a randomly occupied lattice. The approach is basically a tight-binding formalism suitable for our theory. Bond orbitals built out of symmetric combinations of sp^3-hybridised orbitals at each atom site are used as the

bases. Matrix elements of the Hamiltonian are used as parameters. These are determined from fitting to specific experimental results.

In Chapter IV, a chemical pseudopotential method for an ab initio derivation of the crystal Hamiltonian is developed. This is a generalisation of Bullett's (1975) application of the pseudopotential theory to bond orbitals of systems like crystalline carbon and silicon. The method generates the spectrum from atomic potentials, takes into account the non-orthogonality of the basis and leaves us free to predict experimental results, rather than fit to them. The spectra corresponding to the pure constituents are then used as input in the cluster-CPA calculation for the alloy spectra.

The question of the nature of the electron states in disordered systems, diffusive or localised, pioneered by Anderson (1958) has been tackled in Chapter V. Anderson suggested that localised or non-diffusive electron states may exist in disordered systems. Much confusion prevailed regarding the existence of such states. However, presently, there is general acceptance of the existence of localised states and a bulk of experimental data may be explained on the basis of this assumption. Borland (1964) and Ishii (1973) showed that in one-dimension, all states become localised for any

finite disorder. Mott (1967,68) introduced the idea of sharp mobility edges separating extended and localised states in three dimensions and used this concept to explain the electrical properties of amorphous semiconductors. As the degree of disorder increases, the mobility edges move into the band. At a critical disorder all states become localised. This is the Anderson transition.

We develop a criterion for the calculation of the averaged localisation length of electron states and estimate these in weakly disordered systems in the Cayley Tree Approximation. The problem is exactly solvable near the mobility edge giving the linear dependence of the averaged localisation length on the energy as expected in effective medium theories. Away from the mobility edges, the localisation length has been determined numerically.

As a case of divergent but asymptotic perturbation, the problem of the anharmonic oscillator is also considered. An elegant non-perturbative method using the difference equation, to evaluate eigenvalues and eigenfunctions is presented. The work, done in collaboration with Dr. K. Banerjee, S.S.Kanwal and S.P. Bhatnagar, does not get worse with higher quantum numbers for, say, the quartic anharmonicity, i.e., $V = kx^2 + \lambda x^4$, or with the anharmonicity parameter λ. The hitherto unsurpassable boundary layer in the (k, λ) plane is crossed with ease.

The calculation takes considerably less time than the best methods otherwise available only for some regimes of (k, λ) and few quantum numbers. Fast quadratic convergence and accuracy limited only by the 'PRECISION' of the computer calculation are other highlights of the formalism. Some eigenvalues accurate to 15 significant figures are tabulated, calculated in the Double Precision mode on IBM 7044 and DEC 10.

CHAPTER II

CRITICAL REVIEW OF EARLIER THEORIES OF ALLOYS

2.1 Introduction:

In this chapter we shall review critically earlier attempts to calculate density of electronic states in disordered systems. Though attractive at first, some approaches become intractable for a realistic calculation, while others involving simplifying assumptions either become far removed from reality or lose features essential for physical relevence. The objective, therefore, is to highlight shortcomings of these attempts, while at the same time discuss the basic ideas behind the different approaches, so as to expose avenues of generalisation, which not only conform to physical reality but are tractable for actual application.

2.1.1 Rigid Band Model (RBM):

In this model, the density of states function is assumed to be uniform in the alloy. The electronic concentration in the conduction band is altered and set by equalising the Fermi energy at each atomic site. Charge transfer therefore, must occur, although experiments on Cu-Ni alloys seem to indicate

its absence (Wenger et al 1971, Love et al 1971, Bennett et al 1974). The model predicts disappearance of ferromagnetism as concentration of Ni is increased (Kirkpatrick et al 1969), since the partially filled d-bands in pure Ni responsible for ferromagnetism would have to be filled when alloyed with Cu having one more electron and hence a higher Fermi level. Qualitative agreement with experiments is found, though not quantitatively (Mott and Jones 1979). The RBM predicts this disappearance to occur at Cu concentration of 10% while it actually occurs at 60%. The model, however, agrees well even quantitatively with observed optical gaps and many features of the Slater Pauling curves of saturation magnetisation vs. electron concentration for some of the alloys of transition metal series (Hill and Matthias 1968).

Needless to say, the RBM is too crude for cases when distinct bands corresponding to each of the constituents of the alloy are present, as when many properties of the alloy sensitive to the constituents are of concern.

2.1.2 Virtual Crystal Approximation (VCA):

In this model, the actual random alloy potential is replaced by an average,

$$\bar{V} = c\, V_A + (1 - c)\, V_B$$

if V_A and V_B are the potentials of the constituents A and B

present in atomic concentrations c and (1-c) respectively. The model Hamiltonian,

$$H = \sum_i \bar{\varepsilon}_i + \sum_{ij} \bar{V}_{ij}$$

is then translationally invariant and possesses the crystal symmetries. Band structure and other properties within this model can then be evaluated using standard techniques for crystals.

The VCA cannot be expected to reveal any features characteristic of disorder other than the crude averages. However, it does serve well as a zeroeth approximation for more refined theories. In case the potentials of the constituents are very similar, it is not a bad approximation e.g. Ge-Si alloys, but in cases like Cu-Zn and Li-Mg alloys, or when we are dealing with impurity bands, tally with experimental observations is not even satisfactory. The model can be said to be valid when the mean free path is large. Valence bands of III - V semiconducting alloys studies in this work have been dealt within this model in the past. Some features like Van Hove singularities persist, which are not expected in the real alloys (Fig. 3.9).

Also in general, alloys exhibit bowing of the band gap on alloying (Fig. 2.1). Neither the RBM nor the VCA show this bowing behaviour.

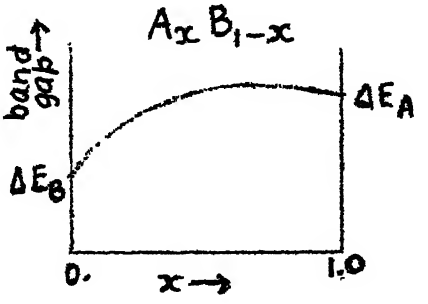

Fig. 2.1: 'Bowing' behaviour of the band gap alloying.

2.1.3 Minimum Polarity Model (MPM):

Van Vleck (1953) imposed electrical neutrality at each atomic site as an ansatz for understanding ferromagnetism in Ni. Negligible charge transfer observed for Ni-Cu alloys indicates applicability of the model. But clearly, the model has limited scope while agreement with experimental observations is crude.

2.1.4 Virtual Bound State Model (VBSM):

Also called the Friedel-Anderson model, this really is between the extremes of the RBM and the MPM and is applicable for transition metal impurities in noble and simple metals. The sharp d-bands of the transition metal impurities overlap in energy with the host conduction band and get broadened, forming virtual bound states. These become strong scattering centres. This idea explains fairly well the optical experiments on noble-metal-rich alloys like AgPd, CuPd, CuAg, CuMn, AgMn and AlMn, AlCu alloys. Again, the model merely has a rough tally with observations while it applies only to the systems listed.

2.2 Effective Medium Theories: The CPA

The effective medium theories, the t-matrix formulation, the Diagrammatic approaches, the Augmented Space method, the Recursion Method, the Method of Moments and the Cumulant Expansion method are attempts at refinements of the theory in

different directions. However, in a single site self consistent approximation, all these yield identical results - the Coherent Potential Approximation (CPA). The Average t-matrix Approximation (ATA) used by some authors is simpler than the CPA but has the disadvantage of being non-self-consistent. These various approaches and their limitations are described in the following after taking a fresh view of the general problem and the use of Green's operator or the resolvent.

2.2.1 The Model:

The study of properties of solids is an example of a many body system. Firstly the Born-Oppenheimer Approximation helps separate the nuclear and the electronic parts of the wave function describing the many particle system consisting of nuclear and electrons in the alloy. The Schrödinger equation is still a many-electron wave equation describing the motion of electrons for a field system of nuclei. The Hartree-Fock scheme then yields a one-electron equation of motion for stationary states in the presence of the nuclei and an average potential due to all other electrons, say,

$$H\psi(\vec{r}) = E\psi(\vec{r})$$

where,

$$H = -\frac{\hbar^2}{2m}\nabla^2 + V(\vec{r})$$

$V(\vec{r})$ being the total single particle potential. In case of crystals, $V(\vec{r})$ is cell periodic and the use of Bloch's theorem gives wave functions of the form,

$$\psi_{\vec{k}}(\vec{r}) = e^{i\vec{k}.\vec{r}} u_{\vec{k}}(\vec{r})$$

where $u_{\vec{k}}(\vec{r})$ is periodic in the real space and the eigen-states of the Hamiltonian are eigen states of the momentum operator also. In case of substitutional binary alloys of the type $A_x B_{1-x}$

$$V(\vec{r}) = \sum_i v_i (\vec{r} - \vec{R}_r)$$

where $\vec{R}_i$ are position vectors corresponding to lattice sites and v_i is V_A or V_B depending on whether the i-th site is occupied by the A type or the B-type constituent. The dependence of $v_i(\vec{r})$ on the configuration around the i-th site is to be ignored. Rather, the occupancies of each site are assumed to be statistically independent. Affinity or short range order is, in other words, not taken into account. The probabilities of finding on A-type or B-type constituent at any site are then directly proportional to their concentrations.

The potential V, and thus also the Hamiltonian, is not periodically symmetric, because the potential in each cell is not identical and depends upon the occupying constituent. The periodic Bloch type electronic states will thus

get scattered from sites and acquire finite life times and the crystal momentum $\vec{k}$ is no longer a good quantum number. Evidently, the eigenstates of momentum are not stationary since these are no longer simultaneous eigenstates of the Hamiltonian; in which case, it does not really make sense to consider the k-dependence of energy, that is, the band structure. Bansil et al (1975) have shown that it is possible to characterise an alloy spectrum in terms of complex energy bands, the real and imaginary parts of which correspond to the energies and life times respectively of the electron waves specified by the momentum $\vec{k}$. However, except in the case of mild disorder, e.g. dilute alloys of very similar constituents, this particular approach, invoking as it does, integration over a complex $\vec{k}$-space, is not very profitable or practicable. The method has been used for surface properties, but not very extensively in the case of disordered alloys.

2.2.2 Role of Configuration Averaging:

Consistently obtained reproducible properties of disordered systems in general are a surprise, considering the fact that each sample is only one of the many configurations possible. In particular, a realistic sample of a random alloy corresponds to a configuration of a very large system. One would like to consider all possible microscopic configurations consistent with known macroscopic

parameters e.g. the concentrations of the constituents and take an average over these, weighted by the probabilities of their occurence. For a binary alloy, the number of configurations is 2^N where N is the number of alloy-sites in the sample. The number consistent with the values of the concentrations of mixing is a fraction of this but is still too large because $N \sim 10^{20}$ even for a tiny sample. One could try to theoretically derive properties of the most probable configuration and propose that these properties are highly likely. But again, the number of different configurations as probable as the most likely, and those of comparable likelihoods of occurrence are intractably numerous.

Since the aim is to be able to theoretically understand and predict properties of a system, one must look at how these properties are obtained. These are necessarily results of experiments, carried out usually using a specific probe, e.g. photons, electrons, which interact with the system, and are subsequently examined to deduce information about the system. In the process, the probe encounters atoms in local environments, statistically numerous as well as varied. This is responsible for reproducible observations just as statistical systems in dynamical equilibrium can be unambiguously labelled by temperature, pressure, etc. despite local fluctuations. The response of an alloy system,

for example, is thus that due to a congregation of these locally varied environments, the net result being an averaged response, not the response of an averaged environment. This warning, that only experimentally observable physical quantities related to the response of the system to a probe must be averaged, has been given by Anderson (1972), to explain source of controversies that arose over non-physical results obtained because non-physical quantities like self energy, the un-Bloch-like wave functions etc, were averaged. The Green's function corresponding to any spectrum like that of the electrons, phonons, etc. can be configurationally averaged since its imaginary part is directly proportional to the density of states, a measurable quantity. Other physical quantities may be derived from it and comparisons with experimental results made.

The above is an additional pointer to a valid local theory, besides the fact that long range order is absent while short range order is retained in the disordered state. The evidence of the latter is in the experimentally obtained field distribution function (Fig. 1.1) indicating that the coordination number and bond lengths remain very nearly the same (Sec. 1.4).

Local orbitals viz. the atomic site orbitals, or the bond orbitals in case of covalently bonded atoms and their interactions between near neighbours only have been used as a

basis by chemists for small as well as very large molecular systems to explain the observed phenomena. In alloy systems too, affinities are known to affect essentially the near neighbour configurations.

The case for a local theory is strong and is welcome because of its implication that considering configurations of local environments, i.e. small clusters may be sufficient.

2.2.3 Resolvent or the Green's Operator:

By definition, the resolvent or the Green's operator G corresponding to a Hamiltonian H is given by,

$$\underline{G}(z) = (z\,\underline{I} - \underline{H})^{-1} \qquad (2.1)$$

where $\underline{I}$ is the identity operator. It is defined for all values of z, the generalised complex energy variable, except on a domain viz. the spectrum of the Hamiltonian $\underline{H}$. Realistic Hamiltonians are self adjoint and hence have only real eigenvalues. The spectrum should thus be entirely on the real axis in the complex z-plane. The Green's operator has poles at each spectral point, i.e. eigenvalue. Projection on to the corresponding eigenstate is the residue at that point. The diagonal members $G_{ss}(z)$ of any representation of $\underline{G}(z)$ with respect to any linearly independent basis $\{|s\rangle\}$ is analytic everywhere in Im $z \neq 0$. Also, Im $G_{ss}(z) < 0$ if Im $z > 0$ and Im $G_{ss}(z) > 0$ if Im $z < 0$. If the spectrum of $\underline{H}$ is bound from above, clearly $G_{ss}(z) \sim 1/z$ as $z \to \infty$ along the real axis. In case H is not bounded from above, we have to further assume

this asymptotic behaviours of $G_{ss}(z)$. Finally $\underline{G}(z) = \underline{G}^{+}(z)$. All these properties define a Herglotz function. $G_{ss}(z)$ is thus herglotz.

From the definition [Eq. (2.1)] of the Green's operator, its diagonal matrix element in some representation $\{|s\rangle\}$ the Green's function is given by,

$$G_{ss}(z) = \langle s | (z \underline{I} - \underline{H})^{-1} | s \rangle$$

$$= \sum_{n} \frac{\langle s|n\rangle \langle n|s\rangle}{z - E_n}$$

where $\{|n\rangle\}$ is the complete set of eigenstates of H, corresponding to the eigenvalues $\{E_n\}$, normalised to unity. Then the trace of the Green's function matrix in this representation,

$$\text{Tr } G_{ss}(z) = \sum_{s} \sum_{i} \frac{\langle s|n\rangle \langle n|s\rangle}{z - E_n}$$

$$= \sum_{n} \frac{1}{z - E_n}$$

where the completeness of the bases set $\{|s\rangle\}$ is used. In case the Green's function is required in the tight binding basis in a crystal, all diagonal elements of this matrix are identical and,

$$g(z) = \frac{1}{N} \text{Tr } G_{ss}(z) = \frac{1}{N} \sum_{n} \frac{1}{z - E_n}$$

It is clear now why $g(z)$ is not defined at the eigenvalues

of the Hamiltonian H, mentioned earlier. Since the eigenvalues are all real, the $g(z)$ is defined along the real axis in the limit that the imaginary part of z becomes infinitesimally small, i.e.,

$$\lim_{\delta \to 0^+} g(E + i\delta) = \lim_{\delta \to 0^+} \frac{1}{N} \sum_n \frac{1}{E + i\delta - E_n}$$

$$= \frac{1}{N} \sum_n \left[\mathcal{P} \frac{1}{E-E_n} - i\pi \delta (E-E_n) \right]$$

E being real, and $\mathcal{P}$ represents the principal part so that

$$-\frac{1}{\pi} \mathrm{Im} \; g(E + i0^+) = \frac{1}{N} \sum_n \delta (E - E_n)$$

$$= n(E)$$

the density of states per site. This relation is very useful because knowing n(E), the complete Green's function at any value z can be obtained from Kramers-Kronig relation,

$$g(z) = -\frac{1}{\pi} \int_{-\infty}^{\infty} \frac{\mathrm{Im} \; g(E+i0^+)}{z - E} \, dE$$

$$= \int_{-\infty}^{\infty} \frac{n(E)}{z-E} \, dE$$

This relation is a consequence of the analyticity of $g(z)$ and its asymptotic behaviour.

2.2.4 Mean Field Approach:

Here, an effective Hamiltonian is defined such that the Green's function corresponding to it is functionally equal

to the configurationally averaged Green's function of the model Hamiltonian under consideration. That is, in a tight binding basis, corresponding to the exact Hamiltonian,

$$\underline{H} = \sum_i \varepsilon_i \underline{P}_i + \sum_{i,j} V_{ij} \underline{T}_{ij}$$

define,

$$\underline{H}' = \underline{H}_o + \sum_{i,j} S_{ij}(E) \underline{T}_{ij}$$

where $\underline{H}_o$ is some crystal Hamiltonian.

$$\underline{H}_o = \sum_i \bar{\varepsilon}_i \underline{P}_i + \sum_{i,j} \bar{V}_{ij} \underline{T}_{ij}$$

say, that corresponding to the pure host or the VCA, such that,

$$\underline{H} = \underline{H}_o + \sum_i \omega_i \underline{P}_i + \sum_{i,j} v_{ij} \underline{T}_{ij}$$

where,

$$\omega_i = \varepsilon_i - \bar{\varepsilon} \quad \text{and} \quad v_{ij} = V_{ij} - \bar{V}_{ij}$$

and the self energy,

$$S_{ij}(E) = \sigma(E)\,\delta_{ij} + \sigma_{ij}(|\vec{r}_i - \vec{r}_j|; E)\,(1 - \delta_{ij})$$

having translational symmetry as in an ordered system. The corresponding Green's operator then is

$$G'(z) = (z\,I - H')^{-1}$$

The idea is to seek those $\sigma(E)$ and σ_{ij} which yield,

$$G' = \langle\langle G^{ex} \rangle\rangle \qquad (2.2)$$

where G^{ex} represents the Green's operator corresponding to the exact Hamiltonian and the double parentheses indicate configuration averaging.

In a single site approximation, the self energy is taken to be diagonal and identical for all sites. The exact Hamiltonian is then different from the effective Hamiltonian only in the diagonal part,

$$\underline{H} = \underline{H}' + \sum_i (\omega_i - \sigma(E)) \underline{P}_i$$

$$= \underline{H}' + \underline{h}$$

h being the difference and is random since ω_i is $(\varepsilon_A - \bar{\varepsilon})$ or $(\varepsilon_B - \bar{\varepsilon})$ with probabilities C and (1 - C) respectively for a $A_C B_{1-C}$ type random binary alloy. Defining now an operator T such that,

$$G = G' + G'T G' \tag{2.3}$$

Then,

$$T = (I - hG')^{-1} h$$

$$= \sum_i \frac{d_i}{1-d_i G} \underline{P}_i$$

$$= \sum_i \underline{t}^{(i)} \text{ say}$$

where $d_i = \omega_i - \sigma(E)$. Then (2.3) implies,

$$\langle\langle G \rangle\rangle = G' + G' \langle\langle T \rangle\rangle G'$$

For (2.2) to hold,

$$\langle\langle t^{(i)} \rangle\rangle = 0$$

This is the CPA equation. Explicitly written, this is

$$\frac{\varepsilon_A - \bar{\varepsilon} - \sigma}{1-(\varepsilon_A - \bar{\varepsilon} - \sigma)g(z-\bar{\varepsilon}-\bar{\sigma})} C + \frac{\varepsilon_B - \bar{\varepsilon} - \sigma}{1-(\varepsilon_B - \bar{\varepsilon} - \sigma)g(z-\bar{\varepsilon}-\sigma)} (1-C) = 0$$

The above is a single site approximation taking into account only single site configurations. Even though the effective Hamiltonian is still non-random, it is an improvement over the VCA since some information about disorder has gone into it. The self energy $\sigma(E)$ is obtained by solving the above equation self consistently at every energy. Physically what is sought is a characteristic crystal at every energy, which has the same Green's function as that obtained after averaging over exact single site configurations. No account can be taken of off diagonal disorder and clusters. We shall make use of this basic picture of clusters (in this case only one site) immersed in a medium which is self-consistently determined by the fact that no extra scattering occurs on immersion (equivalence shown in the next section), when we generalise to our cluster - CPA. As such this idea is of central importance.

2.2.5 The Multiple Scattering Theory and Diagrammatic Techniques

Just as in the case of the Mean Field Approach, use is made of some periodic reference Hamiltonian $\underline{H}_o$, an effective energy dependent Hamiltonian $\underline{H}$ (E) and the exact Hamiltonian $\underline{H}$, different from $\underline{H}$ by $\underline{h}$. This difference h is the perturbation

causing scattering. It is the random part of the exact Hamiltonian and satisfies the requirement of the Multiple Scattering theory in that it can be decomposed as a sum of contributions from each site, i.e.,

$$\underline{h} = \sum_i h_i , \quad h_i = \varepsilon_i - \sigma(E)$$

Also, as defined before,

$$\underline{T} = \underline{h} + \underline{h}\,\underline{G}'\underline{T}$$

$$= \sum_i h_i (I + G'T) = \sum_i \underline{T}_i \text{ say} \qquad (2.5)$$

which, by iteration, gives,

$$T = \sum_i \underline{h}_i + \sum_i \underline{h}_i \underline{G}' \sum_j \underline{h}_j + \sum_i \underline{h}_i \underline{G}' \sum_j \underline{h}_j \underline{G}' \sum_k \underline{h}_k + \ldots \qquad (2.6)$$

which gives with (2.5)

$$T_i = t_i (1 + G' \sum_{j \neq i} T_j)$$

where $t_i = (1 - h_i G') h_i$

$$= h_i + h_i G' h_i + h_i G' h_i G' h_i + \ldots \qquad (2.7)$$

the atomic t-matrix representing complete scattering from the i-th site. Substituting this into (2.6) gives,

$$T = \sum_i t_i + \sum_i t_i G' \sum_{j \neq i} t_j + \sum_i t_i G' \sum_{j \neq i} t_i G' \sum_{k \neq j} t_k + \ldots$$

Each term in this expression for the total T-matrix represents

successive scattering processes that an electron may undergo. Multiple scatterings at a particular site are included in the t_i as seen in eqn. (2.7). But the electron can get scattered again at a site, after atleast one intermediate scattering process, since in the third term k can be equal to i.

As before,

$$<< G^{ex} >> \;=\; G' + G' << T >> G'$$

Now, writing,

$$\underline{H}' \;=\; \underline{H}_o + \sum_i (\sigma(E) - \varepsilon_o)\, \underline{P}_i \;=\; \underline{H}_o + \underline{h}_o$$

and imposing the physical requirement that the scattering matrix for the perturbation h_o is the same as the configuration averaged one for the random perturbation h, we obtain,

$$H' \;=\; H_o + << T >> (I + G' << T >>)^{-1} \qquad (2.8)$$

In the Averaged T-Matrix Approximation (ATA), the $<< T >>$ is substituted into this to obtain the effective Hamiltonian, while setting,

$$<< T >> \;=\; 0$$

gives the CPA equation. This is a self consistent approach while the ATA is not.

Since the set of equations essentially solved (self consistently, of course) for the CPA are,

$$<< T_i >> \;=\; << t_i >> \;(1 + G' \sum_{j \neq i} << T_j >>) \qquad (2.9)$$

the approximation involved is the dropping of the fluctuation term,

$$\langle\langle t_i G' \sum_{j \neq i} (T_j - \langle\langle T_j \rangle\rangle) \rangle\rangle$$

on the right hand side. The CPA equation

$$\langle\langle t_i \rangle\rangle = 0 \quad \forall \; i$$

is solved for any one site because of the periodicity of the averaged quantities.

While the ATA and the CPA yield correct results for various limiting cases, e.g. the low concentration, weak scattering and the atomic limits, only the CPA is reasonable in the strong scattering regime. The CPA has been shown to yield (Schwartz and Siggia, 1972) the first eight moments of the density of states function exactly and the higher moments also fairly accurately. As against this the ATA produces only the first four moments exactly, the RBM the first two and the VCA, the first three. In the split band limit ($|\epsilon_A - \epsilon_B| \gg 0$), the subbands appear in the CPA and the ATA, but the shape of the curve given by the CPA is better because it yields more correct moments. Also both ATA and CPA are invariant with respect to the interchange of the constituents. But the most important advantage of the CPA over the ATA, however, is reflected in the herglotz Green's function (Mookerjee 1979) that it yields and the localisation theorem that it obeys (Kirkpatrick et al, 1970). According to this theorem

there can be no states in the energy region simultaneously forbidden by both the pure crystals of type A and type B constituents (Kumar, Joshi 1978).

2.2.6 Other Approaches:

Besides the (i) Mean field approach and that of (ii) Multiple Scattering of Bloch states of perfect crystals by imperfections described above, there have been other independent attempts yielding the CPA results. These are (iii) Similar to the multiple scattering approach described above, which is a perturbative method using a propagator expansion, a locator formalism based on localised states as the bases set also gives the CPA results in a single site approximation. [Matsubara, Tayozawa 1961, Matsubara, Kaneyoshi 1966, Ziman 1969], (iv) Diagrammatic approaches make use of the perturbation expansion to draw associated diagrams, symbolising product terms of the perturbation terms and the unperturbed propagator, and in this way making systematic partial sums, e.g. those corresponding to all kinds of repeated scattering from a single site, which precisely yield the CPA. This approach was introduced by Yonezawa and Matsubara (1966), Yonezawa (1968) and Leath (1968,1970) using the propagator formalism. Leath (1970) also obtained the identical result using the locator expansion.

A formal equivalence of these and the multiple scattering approaches has been shown by Ziman (1969) and Ducastelle (1971).

Attempts at generalisations of the CPA in the mean field multiple scattering and the equivalent diagrammatic approaches have been frustrated because of the enormous number of terms or diagrams required to be summed. Calculation of the self energy S_{ij} over only near neighbours itself becomes numerically intractable. Electron self energy in a pair approximation using a functional derivative technique due to Kadanoff and Baym (1962)has been calculated by Schwartz and Siggia (1972). Identical results from the multiple scattering technique have been obtained by Cyrot-Lackman and Ducastelle(1971). Outside the nearest neighbour off diagonal self energy in any further cluster generalisation, it becomes virtually impossible to keep track of the terms.

(v) A cumulant expansion method developed by Yonezawa and Matsubara (1966 a,b, 1967) to calculate the configurationally averaged Green's function, also gives the CPA result in the single site approximation after the correction pointed out later by Yonezawa (1968 a,b) is incorporated. Equivalence to retaining terms corresponding to repeated scattering from a single site has been shown. The formalism does admit generalisation to pairs, triplets, etc. but any realistic calculation becomes intractable and any further approximations lead to

violation of herglotz property in various unpredictable energy regions.

(vi) A method of moments developed by Cyrot and co-workers (1970 - 1974) is another approach besides the cumulants expansion method mentioned above, not depending on band structures on Bloch's theorem of any approximate Hamiltonian. It is based on the fact that the p-th moment of the density of states,

$$= \int dE\ E^p\ n(E)$$

can be obtained for a tight binding model by counting the number of paths of length p which start and return to the same lattice point. The density of states can then be obtained from its moments. In principle all moments are required but, Ducastelle and Cyrot-Lackman (1971) show how to get approximate p(E) knowing a finite number of moments, and also how to determine band edges and shapes near singularities which this approximation smoothens. This method yields results closely resembling the CPA results but does not suggest systematic generalisations.

(vii) Introduced by Haydock et al (1972a, 1975), the Recursion Method involves the generation of a new orthonormal bases out of the localised orbitals and their interactions. Within this basis, the Hamiltonian is tridiagonal. The Green's function can then be expressed as an infinite

continued fraction. The method is a purely real space method. It makes no appeal to the Bloch theorem or reciprocal space, and as such is ideally suited to cases where periodicity is absent as in disordered solids, surfaces, solids with defects etc. Cases with more than one active band have also been studied by this method. Basically the method systematically samples the local environment of sites to yield an equivalent semi-infinite linear chain.

The method is ideally suited for realistic calculations with the help of present generation computors. Although in this work the 'Ray' Integration technique has been employed, the Augmented space formalism introduced by Mookerjee (1973) to be described subsequently allow a direct use of the Recursion method in generating configuration averages Green's functions also. The fortunate coupling of these two techniques provides us with the generalisation we have been seeking.

2.3 The Augmented Space Method:

Introduced by Mookerjee (1973a,b) it is an entirely different way of viewing the problem, but yields the single site CPA very naturally. This approach is powerful in that it can systematically be generalised to larger cluster approximations. Essentially the Hilbert Space describing the true configuration dependent Hamiltonian is augmented by another Hilbert space describing the disorder. Methods

applicable to ordered lattices are then used to obtain physical quantities. The self energy concept is not explicitly present in this formalism but later Mookerjee(1975b) furnished the equivalence by considering an electron interacting with a fermion field and derived an expression for self energy identical with the CPA result.

Since the method is rigorous and tractable even when configurations over finite clusters are considered, this seems to be one of the most powerful avenues open for generalisations. Also because of the fact that in this formalism one always obtains Green's functions that are herglotz it is not only attractive because of its elegance but is clearly superior to all other methods examined above. The method and its explicit form in the Cluster-CPA (CCPA) for binary alloys is described in Chapter III. Limitations of the CPA described in the following section, over come in the self-consistent CCPA are also discussed thereafter.

2.4 Limitations of the CPA:

As a single site approximation, the CPA is the best possibility and has been extensively used for almost all disordered systems of concern. It is an approximation all the same and yields, for example, incorrect band widths. Of course, no off-diagonal disorder involving two or more sites can be consistently taken into account in any one site

approximation. In binary alloys, while the centre of gravity of the bands is determined by the orbital energy (diagonal element in tight binding bases - the site orbitals) and the spread by interactions between neighbours, the actual shape of the density of states function is determined by relative values of the various interactions between near, not only the nearest, neighbours. These numbers can be quite different for different substances, even though their atomic potential functions are similar.

Again as mentioned earlier, short range order is important in cases of binary alloys where affinities between the atoms of the constituents cause particular kinds of clusters to occur preferentially. Even in the absence of this effect of chemical clustering that is not reflected in the CPA, the effect of statistical clustering is also absent. This is believed to be important in the impurity bands i.e. when concentration of one component is low and δ, the difference in orbital energies of the two components, is large. In fact, although impurity bands are produced, most of the structure expected in these is lost in the CPA. Machine calculations, however, do reproduce this structure (Payton and Visscher 1967, Dean 1972, Alben et al 1975). The shape of the impurity band, greatly affects quantities like conductivity of such impurity bands, the electronic specific heat, the paramagnetic open susceptibility, the cohesive energy (Van der Rest et al 1975a) etc.

Band tails as given by the CPA fall of much faster than are expected by experiments. These are understood (Lifshitz 1964) to be due to very large sized clusters of atoms. Band edges are particularly important for electronic properties of amorphous semiconductors.

The CPA density of states thus, in general, consists of rounded peaks and fast falling smooth tents. Further, no information regarding the extended or localised nature of the electronic states, and therefore also the mobility edge can be obtained. This information is needed for correctly interpreting data obtained of the electronic spectra from electrical and optical experiments.

Actually, a large number of experiments on concentrated alloys have pointed towards the importance of the local environment on the magnetic as well as electronic properties of these alloys.

The cluster CPA formalism developed in Chapter III accounts for statistical clusters along with off-diagonal disorder over the clusters. The chemical bonding view taken in the application to the III-V ternary semiconducting alloys emphasises the importance of a local environment.

CHAPTER III

THE CLUSTER COHERENT POTENTIAL APPROXIMATION : FORMALISM AND APPLICATION TO III-V TERNARY ALLOYS

3.1 The Augmented Space Method:

The augmented space method and the use of graphical methods to determine Green's function to various approximations is described in this section.

3.1.1 General Theory:

Let $\{e_i\}$ be the set of random numbers describing a configuration and let $P(\{e_i\})$ describe the probability density associated with the configurations. Assuming that the various e_i are statistically independent,

$$P(\{e_i\}) = \pi_i \, p_i(e_i) \tag{3.1}$$

where $p_i(e_i)$ is the probability density of the individual variables. Correlated distributions can also be considered. Short ranged order problem has been considered by Kaplan and Gray (1976, 1977).

The formalism hinges on the observation that the probability density has all the properties of a density of states

corresponding to a Green's function of a hermitian operator,

$$p_i(e_i) \geq 0 \quad \text{and} \quad \int_{-\infty}^{\infty} p_i(e_i)\, de_i = 1$$

so that it is possible to express this as the imaginary part of a Herglotz function which could in turn be the resolvent corresponding to some self-adjoint operator $\underline{M}_i$ in some Hilbert space ϕ_i, i.e.,

$$p_i(e_i) = -\frac{1}{\pi} \operatorname*{Lim}_{e \to e_i + i0^+} \langle f_o^i | (e\underline{I} - \underline{M}_i)^{-1} | f_o^i \rangle \qquad (3.2)$$

where $|f_o^i\rangle$ is a member of the basis set $\{|f_o^j\rangle\}$ spanning ϕ_i.

Given a p(e), if one could find a convergent continued fraction of the kind,

$$\cfrac{1}{e-a_1 - \cfrac{b_1^2}{e-a_2 - \cfrac{b_2^2}{e-a_3 - \cfrac{b_3^2}{\cdots}}}}$$

then a representation of the operator $\underline{M}$ is a tridiagonal matrix with a_1, a_2, ..., etc. along its diagonal and b_1, b_2, ... etc. along the off-diagonal i.e.,

$$\begin{bmatrix} a_1 & b_1 & 0 & 0 & 0 & . & . & . \\ b_1 & a_2 & b_2 & 0 & 0 & . & . & . \\ 0 & b_2 & a_3 & b_3 & 0 & . & . & . \\ . & . & . & . & . & . & . & . \\ . & . & . & & & & & \end{bmatrix}.$$

in some bases $\{|f_n\rangle\}$. Of course, we have to restrict ourselves to probability distributions all of whose moments are finite. However, almost all physical problems conform to this. The notable exception is the Lorenzian. The procedure involved in Haydock's (1972) method of Recursion for determining matrix elements of Green's operator is the inverse of this.

The question of the uniqueness of $\underline{M}$ is irrelevant for our purpose. Any operator $\underline{M}$ that yields the correct p(e) suffices.

For the binary alloy case with diagonal disorder only, e.g., A_cB_{1-c}, e represents the diagonal element of the Hamiltonian in a tight binding (or atomic orbital) bases, and the p(e) is a two-peaked delta function at e_A and e_B of strengths c and (1-c) respectively. Setting the zero of energy at e_A and letting $e_0 = e_B - e_A$,

$$p(e) = c\delta(e) + (1-c)\,\delta(e-e_o)$$

And since,

$$p(e) = -\frac{1}{\pi} \lim_{z \to e+i0^+} g(z),$$

therefore,

$$g(z) = \frac{c}{z} + \frac{(1-c)}{z-e_o} \qquad (3.3)$$

$$= \cfrac{1}{z-a_1 - \cfrac{b_1^2}{z-a_2}}$$

were $a_1 = (1-c)\ e_o$, $a_2 = ce_o$, $b_1^2 = c(1-c)\ e_o^2$. A representation of the matrix $\underline{M}$ is thus the 2 x 2 matrix,

$$\begin{bmatrix} (1-c)\ e_o & \sqrt{c(1-c)}\ e_o \\ \sqrt{c(1-c)}\ e_o & ce_o \end{bmatrix} \qquad (3.4)$$

eigenvalues of which are 0 and e_o. Its eigenstates $|f_1\rangle$ and $|f_2\rangle$ describe occupancies corresponding to these eigenvalues. The g(z) corresponds to $\langle f_o|(z\underline{I}-\underline{M})^{-1}|f_o\rangle$, where $|f_o\rangle = c^{1/2}|f_1\rangle + (1-c)^{1/2}\ |f_2\rangle$ (See Eq. (3.3)).

The 'Disorder Field' is now introduced. To each variable e_i we have associated a 2-dimensional vector space ϕ_i and a representation of a self-adjoint operator $\underline{M}_i$ corresponding to the probability density of that variable in some bases $\{|f_n^i\rangle\}$. If the set of eigenvectors say $\{h_n^i\rangle\}$ of $\underline{M}_i$ were taken as the bases, then each $|h_n^i\rangle$ in ϕ_i would correspond to one particular value taken by the variable e_i. In general, any element in ϕ_i is a linear combination of the $\{|h_n^i\rangle\}$. ϕ_i thus describes all possible states or configurations of the variable e_i.

The product space $\Phi = \pi_i \otimes \phi_i$ can now be constructed which contains in its description, all possible states of the set $\{e_i\}$ i.e., all configurations of the disordered system. The bases in the product space are,

$$|f\rangle = \{|f_i^1\rangle\} \otimes \{|f_i^2\rangle\} \otimes \ldots \qquad (3.5)$$

and if $g_i(z) = (z\underline{I} - \underline{M}_i)^{-1}$

then,

$$P(\{e_i\}) = -\frac{1}{\pi} \mathrm{Im} \langle f_o | \underline{G} | f_o \rangle$$

where,

$$|f_o\rangle = |f_o^{\,1}\rangle \otimes |f_o^{\,2}\rangle \otimes |f_o^{\,3}\rangle \otimes \ldots \qquad (3.6)$$

and,

$$G(z) = g_1(z) \otimes g_2(z) \otimes g_3(z) \otimes \ldots$$

Φ can now be appropriately called the disorder field. All information about various statistical configurations is contained in this, while that of probability of these is described by the operator $\underline{M}_i$ defined on this field.

Configuration averaging procedure can now be described. Consider first, a function f(e) of one variable only. Its average is,

$$\bar{f} = \int_{-\infty}^{\infty} f(e)\, p(e)\, de$$

$$= \int_{-\infty}^{\infty} f(e) \left\{ -\frac{1}{\pi} \mathrm{Im} \lim_{z \to e+i0^+} g^{(\underline{M})}(z) \right\} de$$

where,

$$g^{(\underline{M})}(z) = \langle f_o | (z\underline{I} - \underline{M})^{-1} | f_o \rangle$$

$$= \langle f_o | \underline{G}^{(\underline{M})}(z) | f_o \rangle, \text{ say}$$

so that,

$$p(e) = -\frac{1}{\pi} \mathrm{Im}\, g^{(\underline{M})}(e+i0^+) = -\frac{1}{\pi} \mathrm{Im} \langle f_o | \underline{G}^{(\underline{M})}(e+i0^+) | f_o \rangle$$

Assuming now that f(z) as a function of a complex variable z has no singularities on that part of the real axis which forms a branch cut of the function $g^{(\underline{M})}(z)$, or in its neighbourhood,

$$\bar{f} = -\frac{1}{2\pi i} \oint f(z)\, g^{(\underline{M})}(z)\, dz$$

The contour, over which the integration is carried out, is taken around the branch cut of g(z) along the real axis, not including any singularities of f(z). Since $\underline{M}$ is a hermitian operator on ϕ, we can write,

$$g^{(\underline{M})}(z) = \int_{-\infty}^{\infty} (z-h)^{-1}\, p(h)\, dh$$

Hence,

$$\bar{f} = -\frac{1}{2\pi i} \oint f(z)\, dz \int_{-\infty}^{\infty} (z-h)^{-1}\, p(h)\, dh$$

$$= -\frac{1}{2\pi i} \int_{-\infty}^{\infty} p(h)\, dh \oint f(z)\, (z-h)^{-1}\, dz$$

$$= -\frac{1}{2\pi i} \int_{-\infty}^{\infty} \mathrm{Im} \langle f_o | G^{(\underline{M})}(h+i0^+) | f_o \rangle\, dh \oint f(z)\, (z-h)^{-1} dz$$

$$= \langle f_o | [\int_{-\infty}^{\infty} \{ \mathrm{Im}\, G^{(\underline{M})}(h+i0^+) \}\, dh\, f(h)] | f_o \rangle \qquad (3.7)$$

$$= \langle f_o | \underline{f}(\underline{M}) | f_o \rangle$$

where $\underline{f}(\underline{M})$ is the same functional of $\underline{M}$ as f is of h, $\underline{f}(\underline{M}) = \int f(h)\, d\underline{P}(h)$ where $\underline{P}(h)$ is the spectral projection operator of $\underline{M}$. The average has thus been expressed as a representation of a suitably constructed operator. The generalisation to a function of several variables is straightforward with one $\underline{M}^{(i)}$ for each variable e_i. In case f(e) is itself a matrix element of the kind, say, $\langle r_i | \underline{F}(e) | r_j \rangle$, state vectors

$$\tilde{\underline{H}} = \sum_i \underline{P}_i \otimes \underline{Q}_i + V \sum_{i,j} \underline{T}_{ij} \otimes \underline{I} \qquad (3.11)$$

where,

$$\underline{Q}_i = \underline{I} \otimes \underline{I} \otimes \ldots \otimes \underline{M}_i \otimes \underline{I} \otimes \ldots \qquad (3.12)$$

The expanded Hamiltonian $\tilde{\underline{H}}$ contains complete information about the system and is defined on the expanded Hilbert space $\Psi = \mathcal{H} \otimes \Phi$. Description of the dynamical behaviour is in the subspace $\mathcal{H}$, while that of the statistical behaviour is in Φ, the disorder space. The configuration averaged Green's function is a particular representation in this expanded space Ψ. The problem has thus been reduced to the determinationof the resolvent of the Hamiltonian $\tilde{\underline{H}}$ in the expanded space Ψ, ensuring, in the process, the necessary herglotzicity of the resolventso obtained. Notice that upto the final stage of configuration averaging no approximations are involved. After averaging it is much simpler to introduce physically valid approximations.

3.1.2 Graphical Methods:

The graphical method (Haydock 1972) for determining various functionals of the Hamiltonian by renormalisation is summarised below. Its use in the application of the cluster CPA formalism for a general alloy system is made later in Secs. 3.1.3 and 3.1.4.

Let $\{|i\rangle\}$ be any complete linearly independent bases in which the Hamiltonian is described. This may be the tight

binding bases, the bond orbitals, the Wannier functions, the Bloch functions etc. The overlap matrix,

$$S_{ij} = \langle i|j\rangle$$

is a unit matrix in case the bases is orthonormal. Matrix elements of an operator $\underline{A}$ are given by, say,

$$A_{ij} = \langle i|\underline{A}|j\rangle$$

A graph is associated with every bases $\{|i\rangle\}$. To every element $|i\rangle$ of the bases set $\{|i\rangle\}$ is associated a vertex v_i, and to each distinct pair of elements $(|i\rangle, |j\rangle)$ a link or bond l_{ij} which may be directional (i.e. l_{ij} may be distinct from l_{ji}) or otherwise. To any operator $\underline{A}$ there corresponds a graph consisting of vertices and those links for which $A_{ij} \neq 0$. In general, the graph does not look like the lattice. It does so in case the chosen bases is a tight binding one, e.g. the Wannier functions and an operator whose off-diagonal matrix elements in this bases are finite only for near neighbours.

Suppose we want to invert an operator $\underline{A}$. Then the contribution of each vertex v_i is defined as $k(v_i) = 1/A_{ii}$ and that of a link l_{ij} as $k(l_{ij}) = A_{ij}$.

A path of length N is defined as a series of ordered vertices and links $P_N = \{v_{i_o}\, l_{i_o i_1}\, v_{i_1}\, l_{i_1 i_2}\, v_{i_2} \cdots v_{i_N}\}$. Contribution of a path is defined as $k(P_N) = \pi_n k(v_{i_n}) \pi_{np} k(l_{i_n i_p})$ A self avoiding path of length N, $Q_N = \{v_{i_o}, l_{i_o i_1}, v_{i_1} \cdots v_{i_N}\}$

is a path such that $v_{i_n} \neq v_{i_m}$ $\forall$ $n \neq m$, with the only exception that v_{i_o} may be the same as v_{i_N} in which case it is a self-avoiding polygonal path.

The renormalised contribution of a vertex v_{i_N} in a path Q_N is defined as,

$$K(v_{i_n}) = \sum_{N=0}^{\infty} \sum_{Q'_N} K(Q'_N) \qquad (3.13)$$

where Q'_N are all polygonal self-avoiding paths from v_{i_n} and back, on the graph from which the vertices $v_{i_0} \ldots v_{i_{n-1}}$ have been removed.

The following theorem then follows (Haydock 1972, Mookerjee 1978).

Theorem:

$(\underline{A}^{-1})_{ij} = \sum_{N=0}^{\infty} \sum_{Q_N} K(Q_N)$ where Q_N are all self-avoiding paths from v_i to v_j.

The proof is lengthy and a thorough discussion exists in the above two references. However, if $\underline{A}^{-1}$ is the resolvent $\underline{G} = (z\underline{I} - \underline{H})^{-1}$, then the theorem simply reduces to the Watson-Greenwood renormalised perturbation expansion for the Green's functions G_{ij}.

The main purpose of the graphical representation is to simply visualise the extremely cumbersome algebraic expressions

involved in the renormalised perturbation expressions, particularly when we shall be involved in generating approximations like the cluster coherent potential approximation.

3.1.3 1-CPA by the Graphical Method in the Augmented Space:

Once the Hamiltonian $\tilde{\underline{H}}$ is defined on the extended space $\Psi = \mathcal{H} \otimes \Phi$ it can be written in a site-field representation $|nf\rangle$ as,

$$\tilde{\underline{H}}_{nf,mf'} = \underline{M}^{n}_{ff'}\delta_{nm} + \underline{V}_{nm}\,\delta_{ff'} \qquad (3.15)$$

where $\underline{M}^{n}_{ff'}$ is the operator in Φ associated with the probability distribution and V_{nm}, that on $\mathcal{H}$. The disorder field states are specified by the set of states $\{|f^{n}_{i}\rangle\}$ occupied in all individual fields ϕ_n, the exact form depending on the probability distribution p(e). In general, one chooses the bases in ϕ_n such that the representation of $\underline{M}_n$ is tridiagonal so that p(e) is given by a continued fraction. For a bimodal density (Eq. 3.3) the $\underline{M}^{n}_{ff'}$ for each n is given by Eq. (3.4) and its graph is a single-link chain like

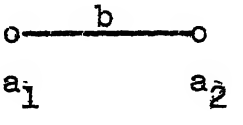

where $a_1 = (1-c)\,e_o$, $a_2 = e_o c$, $b = \sqrt{c(1-c)}\,e_o$. Finally the configuration averaged Green's function is the resolvent corresponding to the Hamiltonian $\tilde{\underline{H}}$ (Eq. (3.14).

Until now the expressions are exact. Approximations are made while employing the graphical technique; the exact graph, on which the calculation from Eq. (3.13) is formidable, is replaced by a simpler graph on which the path counting is simpler and tractable.

Choosing for $\underline{A}$ in Eq. (3.13) as $(z\underline{I} - \underline{\tilde{H}})$, the configuration averaged Green's functions $\bar{G}_{nm}(z)$ can be determined by considering self avoiding non intersecting paths in the complete augmented space $\Psi = \otimes \Phi$. Walks in the augmented space imply the following. An electron at a site labelled by n and the field state $|f\rangle = |f_i^1\rangle \otimes |f_j^2\rangle \otimes \ldots |f_k^n\rangle \ldots$ can be induced by $\underline{\tilde{H}}$ either to make spatial hops to one of the near neighbours of n with the matrix element V, keeping the field state the same, or it can remain on the same spatial site, while the field at the site n changes according to $\underline{M}^n$, the fields at all other spatial sites remaining unchanged. For $|f\rangle = |f_o^1\rangle \otimes |f_o^2\rangle \otimes \ldots$,

$$\bar{G}_{nm}(z) = \langle nf|(z\underline{I} - \underline{\tilde{H}})^{-1}|mf\rangle \qquad (3.16)$$

The problem is reduced, therefore, to one similar to that in the ordered system at the expense of a largerspace in which the matrix element is to be evaluated. The superiority of this method over all other approaches attempted earlier is in the fact that approximations retaining herglotzicity of the configuration averaged Green's functions are easily made. This has been virtually impossible beyond the 1-CPA in all other approaches attempted so far.

Starting from a vertex labelled (o f), the first steps possible (Fig. 3.1) are to the near neighbours l_i in the direct space (shown by single lines) or to a different configuration state of the site o labelled by (o f_o) by a disorder field hop (shown by double lines)

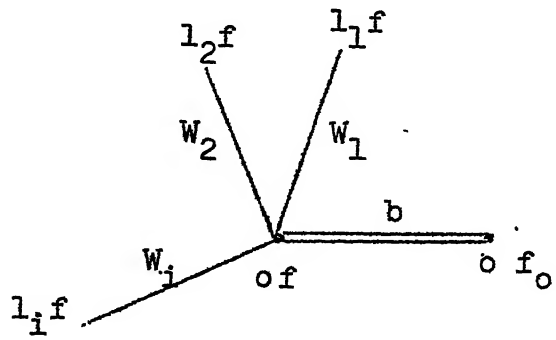

Fig. 3.1: First steps of 'walks' corresponding to $\underline{H}$ in the augmented space.

If $R_o(z)$ is the contribution of all self-avoiding non-intersecting paths from the vertex 'o' and back in the space $\mathcal{H}$, then, the resolvent in an ordered system would be,

$$P_{oo}(z) = \frac{1}{z - R_o(z)} \qquad (3.17)$$

It includes contributions $\sum_i V_i^2 P_{ii}^{(o)}$ where i are various neighbours of 'o' and $P_{ii}^{(o)}$ corresponds to the resolvent calculated from a subgraph in which the vertex 'o' has been removed, besides contributions of closed self-avoiding loops in $\mathcal{H}$. In the extended space, the configuration averaged Green's function $\bar{G}(z)$ can be similarly written as,

$$\bar{G}(z) = 1/[z - R(z) - T(z)] \qquad (3.18)$$

where R(z) includes contributions entirely in the spatial part $\mathcal{H}$ of the complete augmented Hilbert space $\mathcal{V}$, as well as those from non-intersecting paths which include field hops but not as parts of closed loops. The latter are contained in T(z).

The simplifying approximation is now made: Closed paths involving both the spatial and field hops are delinked. As a result T(z) = 0. Hence the graph consists of essentially that in the ordered system together with an extra field hop with the off-diagonal element of $\underline{M}^n$ in the tridiagonal representation ($b = \sqrt{c(1-c)}\, e_o$ in case of binary alloys) as the link function. It may be noticed that then, starting from a vertex 'nf' and hopping to a vertex 'nf_n' one faces a subgraph with the vertex 'nf' missing, which is exactly similar to the original one. That is,

$$G^{(of)}_{of_o, of_o} = G_{of, of} = \bar{G}_{oo} = G(z) \qquad (3.19)$$

Delinking of closed paths involving mixed hops is essential for this to hold.

The above delinking procedure amounts of the 1-CPA (Bishop & Mookerjee, 1974). This is shown below.

Let $G^{DL}(z)$ be the resolvent corresponding to the graph in the augmented space after delinking in the manner described above, and let,

$$M_{ij} = W_i \, \delta_{j,i+1}$$

be the tridiagonal representation of the operator $\underline{M}^n$ in each subspace ϕ_n of Φ. Then,

$$G^{DL}(z) = 1/[z-R_o(z - W_1^2 G_1(z)) - W_1^2 G_1(z)]$$

$$= P_{oo}\,[z - W_1^2\, G_1(z)] \qquad (3.20)$$

where,

$$G_i(z) = 1/[z-R_o(z-W_1^2 G_1) - W_{i+1}^2\, G_{i+1}\,(z)] \qquad (3.21)$$

In the conventional 1-CPA formalism a self energy $\Sigma(z)$ is defined by,

$$G^{CP}(z) = 1/[z - \Sigma(z) - R_o\,(z - \Sigma)]$$

$$= P_{oo}\,[z - \Sigma(z)] \qquad (3.22)$$

where $G^{CP}(z)$ is the 1-CPA Green's function. The self energy $\Sigma(z)$ is determined self consistently from the 1-CPA equation,

$$\int_{-\infty}^{\infty} \frac{x - \Sigma(z)}{1-G(z)(x-\Sigma(z))}\, p(x)\, dx = 0 \qquad (3.23)$$

so that,

$$G^{CP}(z) = \int_{-\infty}^{\infty} \frac{p(x)\, dx}{A(z) - x} \qquad (3.24)$$

where,

$$A(z) = \frac{1 + G^{CP}\,\Sigma}{G^{CP}} \qquad (3.25)$$

Now, just as in Eq. (3.7), $G^{CP}(z)$ from Eq. (3.24) can be written as,

$$G^{CP}(z) = \langle f_o|[A(z)\,\underline{I} - \underline{M}]^{-1}|f_o\rangle.$$

Graphically, therefore,

$$G^{CP}(z) = 1/[A(z) - W_1^2 G_1^{CP}(z)]$$

where,

$$G_i^{CP}(z) = 1/[A(z) - W_{i-1}^2 G_{i+1}^{CP}(z)]$$

But A(z) from Eqs. (3.22) and (3.25) above is,

$$A(z) = z - R_o [z - \Sigma(z)]$$

Hence $G^{CP}(z)$ from Eqs. (3.26) and (3.27) is the same as $G^{DL}(z)$ from Eqs. (3.20) and (3.21). The formal equivalence of the two-approximations has also been shown by Mookerjee (1974) using multiple scattering diagrams.

3.1.4 n-CPA in the Augmented Space Method:

The essential approximation involved in the 1-CPA described in the last section is to ignore closed non-intersecting paths involving both spatial and the disorder field hops in the augmented space. Generalisation to an n-cluster CPA involves including only those closed non-intersecting paths which involve disorder field hops over the n sites of the cluster. A self energy renormalising the interaction between each pair of sites in this cluster can then be defined. The corresponding n x n matrix $\underline{\Sigma}$ will have less than n^2 independent components. These can be determined self consistently by an iterative procedure starting with a diagonal form corresponding to the 1-CPA.

Of course, the method will be useful only if this procedure converges. Mookerjee et.al. (1980) have shown that for the diamc lattice with off diagonal disorder, rapid convergence is obtained, the band width increases and cluster features in the minority regions appear.

The shortest closed path involves spatial and disorder field hops over two sites and consists of eight vertices as shown in Fig. (3.2).

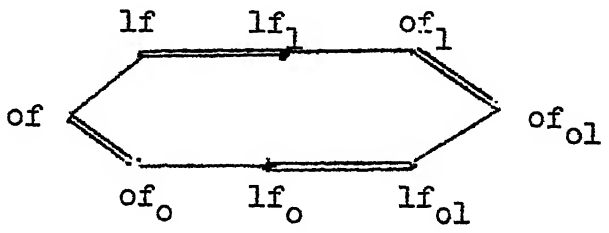

Fig. 3.2: Shortest self avoiding closed path in the full augmented space involving both spatial and disorder field hops.

3.1.5 Cluster Embedding:

Once the self consistent medium with respect to a cluster of n sites C_n is determined, i.e. for $i,j \in C_n$,

$$G_{ij}^{(n)}(z) = G_{ij}^{o}(z - \Sigma_{ij}) \qquad (3.26)$$

where $G_{ij}^{(n)}(z)$ is the matrix element of the Green's operator for the self consistent n-cluster medium, $G_{ij}^{o}(z)$ is that corresponding to some chosen crystal Hamiltonian chosen as a

starting point and Σ_{ij} is the matrix of self energies determined, exact n-site clusters C_n can now be embedded in the following manner.

Let $\underline{H}^{(n)}$ be the self consistent Hamiltonian $\underline{H}^{(n)} = \sum_{i,j} \Sigma_{ij} \underline{T}_{ij}$ corresponding to the n-cluster CPA medium obtained. We wish to consider now a model Hamiltonian $\underline{H}^M$ which is exact over this cluster C_n while the rest of the system consists of $\underline{H}^{(n)}$, i.e.,

$$\begin{aligned} \underline{H}^M &= \sum_{i,j \notin C_n} H_{ij}^{(n)} + \sum_{i,j \in C_n} H_{ij}^{\text{exact}} \\ &= \sum_{i,j} H_{ij}^{(n)} + \sum_{i,j \in C_n} (H_{ij}^{\text{exact}} - H_{ij}^{(n)}) \\ &= \underline{H}^{(n)} + \underline{\delta H}^{(n)}, \quad \text{say} \end{aligned} \tag{3.27}$$

The difference Hamiltonian $\underline{\delta H}^{(n)}$ is finite only over the cluster C_n. The Green's function $\underline{G}^M$ corresponding to the $\underline{H}^M$ is,

$$\begin{aligned} \underline{G}^M &= (z\underline{I} - \underline{H}^M)^{-1} \\ &= (z\underline{I} - \underline{H}^{(n)} - \underline{\delta H}^{(n)})^{-1} \\ &= (\underline{I} - \underline{G}^{(n)} \quad \underline{\delta H}^{(n)})^{-1} \underline{G}^{(n)} \end{aligned} \tag{3.28}$$

equivalent to the usual Dyson equation. Each of $\underline{H}^{(n)}$, $\underline{G}^{(n)}$, $\underline{\delta H}^{(n)}$, $\underline{T}$ and $\underline{G}^M$ are n x n square matrices. The inversion of $(\underline{I} - \underline{G}^{(n)} \underline{\delta H}^{(n)})$ is facilitated by the fact that $\underline{\delta H}^{(n)}$ has non-zero elements only in the cluster subspace, so that the inversion reduces to that of a finite matrix.

By considering clusters of successively larger sizes, details of the environment implanted can be gradually increased, since $\underline{H}^M$ includes exact details of the interactions over the

cluster C_n, while it sees the rest of the medium effectively . Choosing a central site and its set of nearest neighbours, the density of states at the central site obtained from the corresponding number on the diagonal of $\underline{G}^M$ is clearly closer to that of the true Hamiltonian than the VCA or the 1-CPA.

Each configuration possible over a cluster considered can thus be dealt with to determine the density of states via the diagonal Green's function at the central site and eventually configurationally averaged Green's function determined. Particular features of the density of states thus obtained, e.g., peaks, can be identified as arising due to specific clusters. Further, some guesses about affinities may also be possible.

3.2 Application to III-V Semiconducting Alloys:

The above formalism for the n-CPA is now applied to the specific cases of binary substitutional alloys of III-V semiconductors GaAs, InAs, GaSb, InSb, GaP and InP. These form zinc-blende structures. The cations (Ga, In) and the anions (As, Sb, P) occupy an fcc sublattice each, relatively displaced by a fourth of the body diagonal of the smallest cubic unit cell. Each anion has around it as its nearest neighbours, four cations tetrahedrally arranged and vice versa. Fig. (3.3) shows the connectivity of a general zinc blende structure. Pairs of these semiconductors with a common cation or an anion mix in all concentrations. The sublattice of the common ion

is 'regular' or 'ordered' while that of the other ion is occupied randomly.

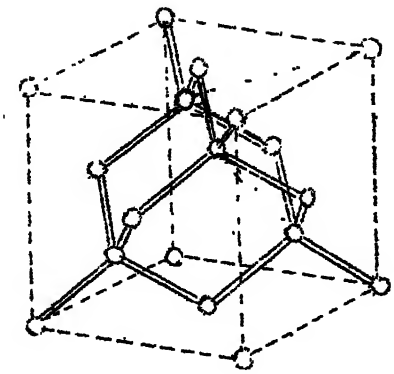

Fig. 3.3: Zinc blende crystal structure.

3.2.1 Bonding and Antibonding States as Valence and Conduction Bands:

Harrison et al (1973, 1974) have shown that bonding and other physical properties can be described well in the Bond Orbital Model (BOM) in such covalently bonded systems. The basis states are taken to be centred on bonds connecting nearest anion-cation pairs. The basis functions themselves are constructed from combinations of the sp^3 hybridised orbitals of adjacent atoms. The bonding and antibonding states resulting from these broaden into the valence and conduction bands respectively when these ions are immersed into the lattice of the solid.

In the BOM, the bonding functions alone are taken as the bases. In case the bonding and antibonding states are coupled significantly, the bonding bases is incomplete to describe even the valence band alone, as shown below.

Let $\underline{P}_V$ and $\underline{P}_C$ be the projection operators corresponding to the valence band (bonding states) and the conduction band (antibonding states) respectively and let the Hamiltonian $\underline{H}$ be partitioned into subspaces of these.

$$\underline{H} = \begin{bmatrix} \underline{H}^V & \underline{H}^{VC} \\ \underline{H}^{CV} & \underline{H}^C \end{bmatrix}$$

where,

$$\begin{aligned} \underline{H}^V &= \underline{P}_V \underline{H} \underline{P}_V , \\ \underline{H}^{VC} &= \underline{P}_V \underline{H} \underline{P}_C , \\ \underline{H}^{CV} &= \underline{P}_C \underline{H} \underline{P}_V \quad \text{and} \\ \underline{H}^C &= \underline{P}_C \underline{H} \underline{P}_C \end{aligned}$$

The Green's function determined in the subspace of valence orbitals only is approximate unless $\underline{H}^{VC}$ and $\underline{H}^{CV}$, the interactions between the valence and the conduction states subspaces are negligible, rendering the total Hamiltonian nearly block diagonal.

Using the theory of partitioned matrices (Bellman, 1960) the exact expression for the Green's operator corresponding to the valence band in terms of the partitioned submatrices of $\underline{H}$ is derived in the following.

Let $\underline{M}^{\underline{P}_y}$ denote the inverse of an operator $\underline{M}$ in the subspace y, then we are seeking,

$$\begin{aligned}\underline{G}^{(V)} &= \underline{P}_V \underline{G} \underline{P}_V \\ &= \underline{P}_V (z\underline{I} - \underline{H})^{-1} \underline{P}_V \\ &= (z\underline{I} - \underline{H})^{-\underline{P}_V} \\ &= (z\underline{I} - \underline{H}^V - \underline{H}^{VC} \tilde{\underline{G}}^{(C)} \underline{H}^{CV})^{-\underline{P}_V}\end{aligned}$$

in terms of the partitioned matrices, where $\tilde{\underline{G}}^{(C)} = (z\underline{I} - \underline{H}^C)^{-\underline{P}_C}$. If $\underline{H}^{VC}$ is small, we may to that order neglect the second term in the above expression. This would be true if the valence and conduction bands are well separated and there is little hybridisation. For the present computation, we confine ourselves to the bonding states only, ignore hybridisation and reserve the use of the above relation for a better calculation of the valence band for a future program.

3.2.2 The BOM Bases Set:

The basis set to be considered are thus the chemical bonding orbitals. To fix the notation (same as that used by Chen and Sher, 1978) let us use one of the fcc sublattices, say that of the anions as the reference lattice on which each lattice point is represented by a lattice vector $\vec{j}$. The four bond orbitals surrounding it may then be represented by $|\vec{j}\alpha\rangle$, $\alpha = 1,2,3,4$ centred at points specified by $\vec{j} + \vec{\tau}_\alpha$, where $\vec{\tau}_1 = (1, 1, 1)\, a$, $\vec{\tau}_2 = (-1, -1, 1)a$, $\vec{\tau}_3 = (-1, 1, -1)a$ and $\vec{\tau}_4 = (1, -1, -1)a$, where a = 1/8th of a, the edge of the primitive cubic unit cell, as shown in Fig.(3.4). The bond orbitals themselves are, of course, composed of symmetric linear

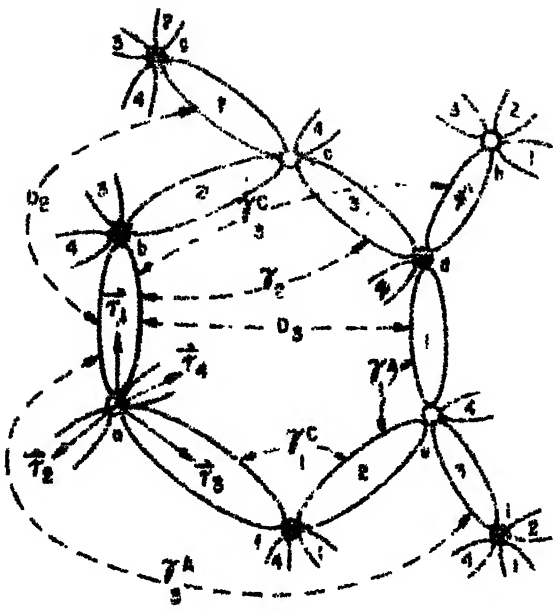

○ ANION

● CATION

a (0,0,0)

b (1/4,-1/4,1/4)

c (1/2,1/2,0)

d (1/4,3/4,1/4)

e (0,1/2,-1/2)

f (-1/4,1/4,-1/4)

g (3/4,3/4,1/4)

h (1/2,1,1/2)

i (-1/4,3/4,-3/4)

$\vec{T}_1$ (1/8,1/8,1/8)

$\vec{T}_2$ (1/8,-1/8,1/8)

$\vec{T}_3$ (-1/8,1/8,-1/8)

$\vec{T}_4$ (1/8,-1/8,-1/8)

coordinates are in units of a, the lattice constant of the fcc lattice

Fig. 3.4: Connectivities and coordinates in a flattened diagram for a zinc blende structure.

combinations of the hybridised atomic orbitals $|a\rangle$ and $|c\rangle$ centred at the anion and cation atomic sites respectively, i.e.

$$|\vec{j}\alpha\rangle = [|a\rangle + |c\rangle] \frac{1}{N_{ac}} = |ac\rangle, \text{ say}$$

where N_{ac} is the normalisation constant $\sqrt{2(1+S)}$, S being the orbital overlap $\langle a|c\rangle$ of neighbouring anion-cation pair, and

$$\begin{aligned} |a\rangle &= \frac{1}{2}|s_a\rangle + \frac{\sqrt{3}}{2}|p_a\rangle \\ |c\rangle &= \frac{1}{2}|s_c\rangle + \frac{\sqrt{3}}{2}|p_c\rangle \end{aligned} \qquad (3.29)$$

where $|s_a\rangle$ and $|p_a\rangle$ are the s and p orbitals on the anions while $|s_c\rangle$ and $|p_c\rangle$ are those on the cations. The p-orbitals are taken to be directed along the bond in the above expressions.

The Bloch basis functions can now be constructed from the bonding orbitals in the usual manner,

$$|\vec{k}\alpha\rangle = \frac{1}{\sqrt{N}} \sum_{\vec{j}} e^{i\vec{k}.(\vec{j}+\vec{\tau}_\alpha)} |\vec{j}\alpha\rangle \qquad (3.30)$$

where N is the total number of anions as cations in the crystal and $\vec{k}$ the wave vector within the Brilluoin Zone.

3.2.3 The BOM Hamiltonian and the Eigenvalue Spectrum.

The secular equation can, therefore, be written as,

$$\det|E\underline{I} - \underline{\underline{H}}^{\alpha\alpha}_{\vec{j}\vec{j}}| = 0 \qquad (3.31)$$

This in the k-space becomes

$$\det \mid E(\vec{k})\, \underline{I} - H^{\alpha\alpha}(\vec{k}) \mid = 0$$

where,

$$H^{\alpha\alpha'}(\vec{k}) = \sum_{j} \underset{\overrightarrow{0j}}{H^{\alpha\alpha'}} \exp\,[i\vec{k}.(\vec{j} + \vec{\tau}_{\alpha} - \vec{\tau}_{\alpha'})]$$

obtained by using the transformation of bases defined in (3.30). One of the site suffixes on the Hamiltonian in the real has been fixed as the origin without any loss of generality $\underset{\overrightarrow{00}}{H^{\alpha\alpha}}$ represents, for example a 4 x 4 matrix representing the energies and interactions between the four bonds originating from the anion site at the origin. In a similar manner, assigning non-zero lattice vector values to $\vec{j}$, interactions between other bonds can be seen to be involved.

Chen and Sher (1978) have shown that retaining interactions upto second nearest neighbour bonds is enough to obtain a band structure exhibiting all required features, and that including the third nearest neighbour interactions, alters the band structure insignificantly. Ignoring, therefore, interactions of further than second nearest parallel and non-parallel bonds, the distinct matrix elements of the Hamiltonian are e.g. of the kind $\underset{\overrightarrow{00}}{H^{12}}$, $\underset{\overrightarrow{0r_1}}{H^{12}}$, $\underset{\overrightarrow{0r_2}}{H^{11}}$, $\underset{\overrightarrow{0r_2}}{H^{12}}$ where $\vec{r}_1 = 2\,(\vec{\tau}_2 - \vec{\tau}_1)$ and $\vec{r}_2 = 2(\vec{\tau}_3 - \vec{\tau}_1)$ both symmetry translations of the fcc sublattices. These may be renamed H_1^A, H_1^C, H_2^P, H_2^{NP} for explicitness. $H_1^A(H_1^C)$ represents the interactions between first nearest neighbour bonds meeting at an anion (cation) site and H_2^P (H_2^{NP})

the interactions between second nearest neighbour parallel (non-parallel) bonds. Together with the diagonal bond energy say H_o, these form independent parameters describing the Hamiltonian, and correspond to $(\gamma_1^s + \gamma_1^a)$, $(\gamma_1^s - \gamma_1^a)$, D_2, γ_2 and D respectively in the work of Chen and Sher (1978), the k-dependent 4 x 4 Hamiltonian matrix under this approximation directly from Eq. (3.32) is, therefore,

$$H^{11} = H_o + 2H_2^P[\cos(2x+2y) + \cos(2x+2z) + \cos(2z+2y)]$$

$$H^{22} = H_o + 2H_2^P[\cos(2x+2y) + \cos(2y-2z) + \cos(2x-2z)]$$

$$H^{33} = H_o + 2H_2^P[\cos(2x-2y) + \cos(2y-2z) + \cos(2x+2z)]$$

$$H^{44} = H_o + 2H_2^P[\cos(2x-2y) + \cos(2y+2z) + \cos(2x-2z)]$$

$$H^{12} = 2\{H_1^s\cos(x+y) + 2H_2^{NP}\cos(x-y)\cos 2z\} - 2iH_1^a\sin(x+y)$$

$$H^{13} = 2\{H_1^s\cos(x+z) + 2H_2^{NP}\cos(x-z)\cos 2y\} - 2iH_1^a\sin(x+z)$$

$$H^{14} = 2\{H_1^s\cos(y+z) + 2H_2^{NP}\cos(y-z)\cos 2x\} - 2iH_1^a\sin(y+z)$$

$$H^{23} = 2\{H_1^s\cos(y-z) + 2H_2^{NP}\cos(y+z)\cos 2x\} + 2iH_1^a\sin(y-z)$$

$$H^{24} = 2\{H_1^s\cos(x-z) + 2H_2^{NP}\cos(x+z)\cos 2y\} + 2iH_1^a\sin(x-z)$$

$$H^{34} = 2\{H_1^s\cos(x-y) + 2H_2^{NP}\cos(x+y)\cos 2z\} + 2iH_1^a\sin(x-y)$$

where $H_1^s = (H_1^A + H_1^C)/2$ and $H_1^a = (H_1^A - H_1^C)/2$ and x, y, z symbolise $\frac{1}{4}k_x a$, $\frac{1}{4}k_y a$, $\frac{1}{4}k_z a$ respectively.

3.2.4 The Parameters

The values of the parameters in Table 3.1 have been obtained by conveniently fitting energy separations at specific symmetry points on the Brilluoin Zone, Γ , X,L,etc.

Table 3.1: Distinct matrix elements of the Hamiltonian used as parameters for the III-V semiconductors between nearest neighbour bonds and second nearest neighbour bonds.

Material	Parameter			
	H_1^s	H_1^a	H_2^P	H_2^{NP}
GaAs	-1.5187	- 0.4250	0.3406	- 0.1094
InAs	-1.3937	- 0.5125	0.3844	- 0.0656
GaSb	-1.2687	- 0.3750	0.3906	- 0.0594
InSb	-1.3500	- 0.3875	0.2937	- 0.0563
GaP	-1.3625	- 0.3250	0.3812	- 0.1188
InP	-1.3125	-0.4125	0.2625	- 0.0375

The parametrization approach employed is empirical. Also fitting with experimental data from different sources gives different results. Often variation in the values of a parameter obtained by fitting to different data for a given material is more than that over different materials. Chen and Sher eventually impose an energy dependent Lorentzian broadening and vary the parameters in order that the broadened

peaks thus obtained best resemble the experimental spectra obtained by Ley et al (1973).

The above procedure is somewhat arbitrary and its validity is also unclear. Despite this, the values of the parameters have been used for a preliminary cluster-CPA calculation. Results of these are presented in this chapter. Dissatisfaction with the above parametrization approach motivated an ab initio chemical pseudopotential calculation for the required parameters, starting with Herman-Skillman tables of self consistent Hartree-Fock atomic orbitals and potentials. The procedure for this calculation, comparison with the empirically obtained values and the results of the cluster-CPA calculation constitute the following chapter. The numbers shown in Table 3.1 are fitted with the experimental data by Chen and Sher (1978). However, if we fit to each experimental data, the numbers are different. For example, for GaAs, the difference in the parameters for the same material is more than that between different materials (Table 3.2).

3.2.5 Matrix Elements of the Green's Operator in the VCA and 1-CPA:

The alloys under consideration are of the kind $Ga_xIn_{1-x}As$ as a common cation alloy, and $GaAs_xP_{1-x}$ as an example of a common anion alloy. These alloy in all proportions and therefore x may anything between 0 and 1. Each of

Table 3.2: Parameters for Ga-As from experimental results as obtained by (i) Chelikowsky et al (1976), (ii) Ley et al (1973) and (iii) Eastman et al (1974) respectively.

Sl.No.	H_1^s	H_1^a	H_2^P	H_2^{NP}
(i)	-1.4437	-0.3750	0.3656	- 0.0344
(ii)	-1.6625	-0.4500	0.2437	- 0.0313
(iii)	-1.5000	-0.3875	0.4687	- 0.0563

Table 3.3: Bond lengths, bond energies and work functions for the III-V Semiconductors

	Bond Length (A^o)	Bond energy (eV)	Work function (eV)
GaAs	2.45	- 5.6687	5.5
InAs	2.61	- 4.7562	5.3
GaSb	2.65	- 4.7437	4.9
InSb	2.81	- 4.7625	4.8
GaP	2.36	- 5.1125	5.7
InP	2.54	- 4.5750	5.7

the six materials GaAs, InAs, GaSb, InSb, GaP and InP form the zinc-blende structure of nearly the same bond length (Table 3.3). We shall assume, therefore, that the interaction parameters corresponding to the pure materials are the same as those in the alloy.

Top of the valence band as the zero of the energy scale used by some authors is incorrect. The vacuum state must set the zero of the energy scale since that is the common state. Different work functions for the various materials (Table 3.3) also supports this view.

The VCA parameters are given by the average of those of the constituents, weighted by their respective concentrations. For dilute alloys, the parameters corresponding to the host are also good enough as a zeroeth approximation for the later CPA calculations, but in these cases, the virtual crystal is very nearly the host anyway.

Matrix elements of the Green's operator for the virtual crystal corresponding to the alloy are sought. An efficient method due to Chen (1977) called the 'Ray' Integration Technique

is employed for the purpose. Essentially a systematic $\vec{k}$-space integration over the Brilluoin Zone (BZ), the general method is described in Sec. A.1 of Appendix A. The 3-dimensional integration is reduced to far simpler one-dimensional integrations over thin tetrahedra into which the irreducible part of the BZ is divided. The method is fast and attractive for a machine calculation.

Fig.3.5 shows the density of states for pure InAs as obtained by the 'Ray' integration method. Band structure, i.e. energy eigenvalues along some standard symmetry directions of an fcc lattice is also shown for the same material.

In the form presented by Chen (1977) the method is applicable only to the calculation of functions whose integrands in the $\vec{k}$-integral bear the symmetry of the BZ. The diagonal Green's function can, therefore, be obtained by direct application of the method.

In Sec. A-2 of Appendix A, a generalisation of the method applicable also for functions, whose integrands do not reflect the symmetries of the BZ, is presented. The off-diagonal matrix elements of the Green's operator are in this class of functions and have been obtained by this generalized 'Ray' integration method.

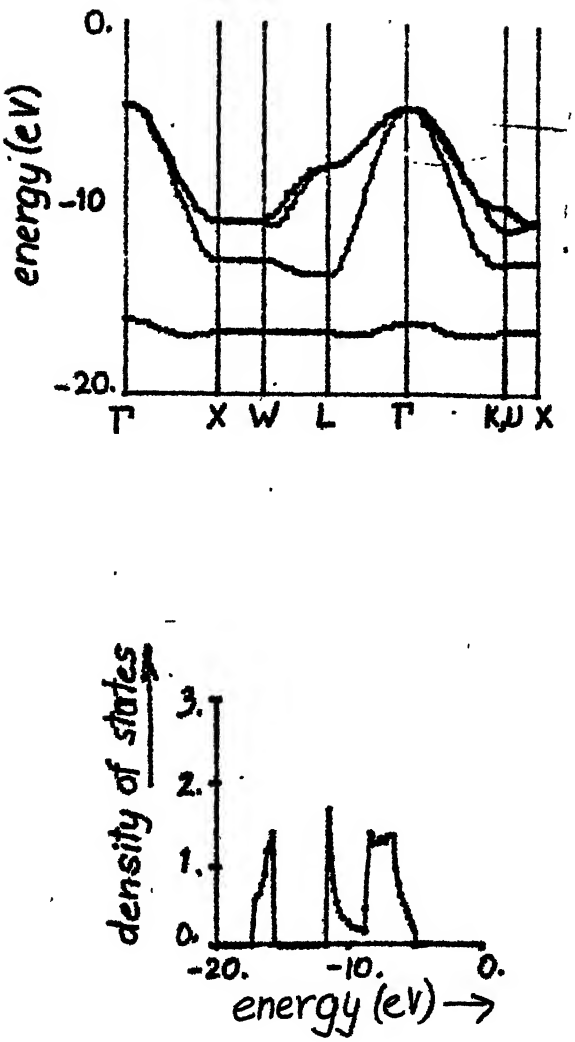

Fig. 3.5: Band structure of InAs and its density of states by 'Ray' integration technique

Ideally, a self-consistent calculation should be carried out. This has been stressed time and again by authors who deal with the coherent potential approximations. However, since the variation in the parameters H_1^A, H_1^C, H_2^P, H_2^{NP} is rather small as compared to that in the bond energy H_o over the various materials (Tables 3.1 and 3.3), cluster embedding is proposed to be carried out in the relatively easily obtained self consistent 1-CPA medium rather than the self consistent n-cluster-CPA medium. The use of a 1-CPA medium instead of the self consistent one, as is done by Kaplan and Gray (1976) leads to a narrower band width and distortion of the density of states near the band edges. The self consistent calculation on a single s-state on the diamond and bcc lattices has been recently done (Kumar, Mookerjee and Srivastava 1980, 1981 , Mookerjee and Srivastava, 1981). However, the full self consistent calculation on the diamond lattice with four sp^3 hybridised orbitals per site or the four bonds per pair of sites is still beyond the scope of the present work and will have to be left for later research. For the present cases under consideration, the corrections are expected to be small, but for other alloys with large off-diagonal disorders the effect of self consistency may be crucial. Under the above approximation, the self energy is a scalar, determined by solving self consistently eq. (2.4) reproduced here,

$$\frac{\varepsilon_A - \bar{\varepsilon} + \sigma}{1-(\varepsilon_A-\bar{\varepsilon}-\sigma)g(z-\sigma-\bar{\varepsilon})}\, C + \frac{\varepsilon_B - \bar{\varepsilon} - \sigma}{1-(\varepsilon_B-\bar{\varepsilon}-\sigma)\, g(z-\sigma-\bar{\varepsilon})}\,(1-C) = 0$$

The VCA diagonal Green's function is substituted as a zeroeth approximation and the quadratic equation in σ thus obtained is solved. The correct solution is chosen by checking that a) the chosen solution goes to zero as δ, the difference the bond energies of the constituent materials, goes to zer and b) that herglotz property is maintained. The Green's function is then calculated at $E - \sigma$ and substituted back into the above equation. The process is iterated until self consistent solution is obtained for a fixed value of energy. The energy parameter is spanned across the valence band.

Convergence is fast at all points except for those around sharp peaks in the VCA density of states. The real part of the self energy crosses a zero around these regions, and therefore the value of the self energy is taken to be the average of that at neighbouring points.

Fig. 3.6 shows the real and imaginary parts of the self energy, and the VCA and the 1-CPA diagonal Green's functions for $Ga_xIn_{1-x}As$ for $x = 0.1, 0.3, 0.5, 0.7, 0.9$.

3.2.6 Embedded Clusters:

Eq. (3.28) is now directly applied. A choice of the clusters considered is, of course, to be made at this stage.

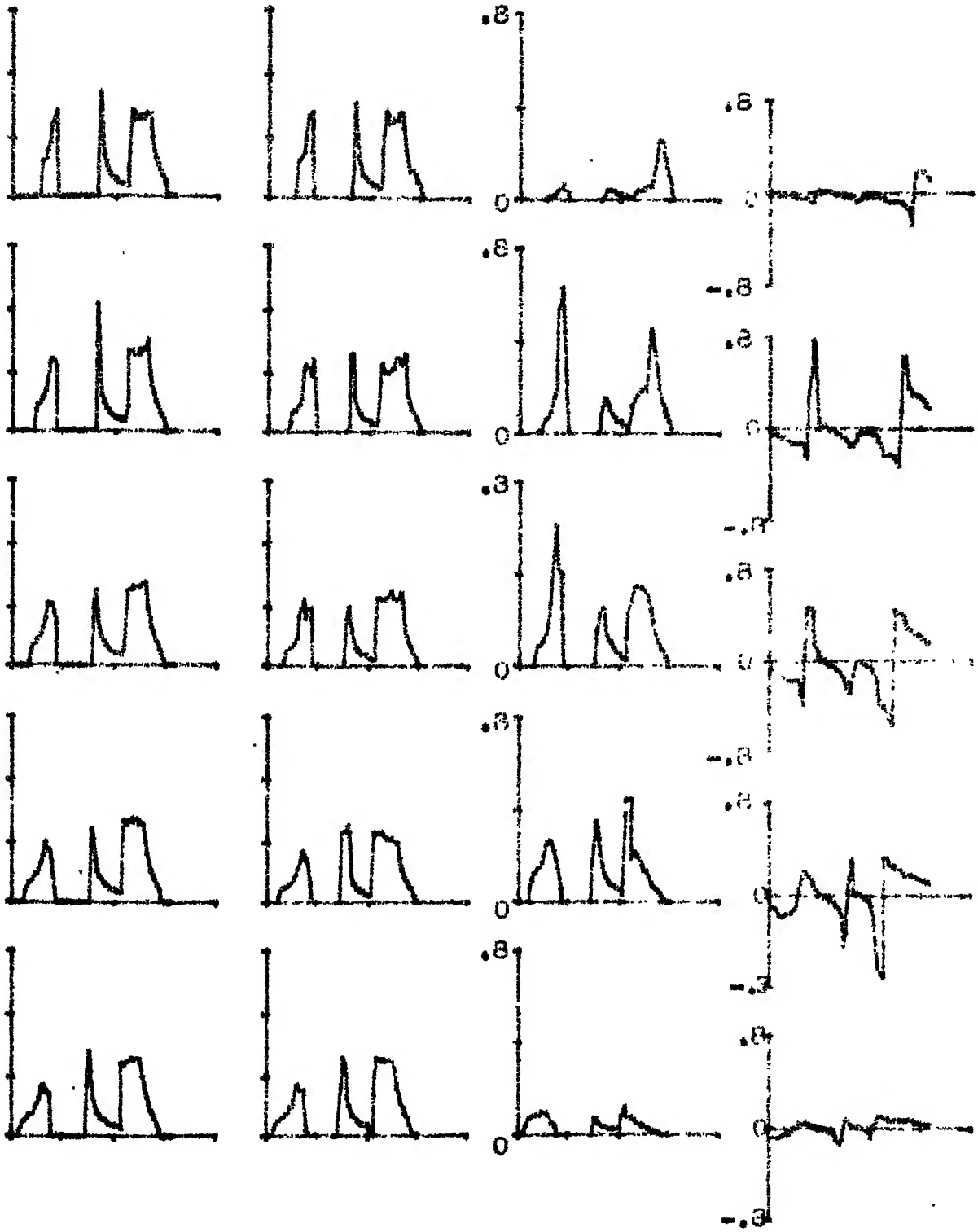

Fig. 3.6: (i) $-\mathrm{Im}\ G^{VCA}$ (ii) $-\mathrm{Im}\ G^{CPA}$ (iii) $-\mathrm{Im}\ \Sigma$ and (iv) $\mathrm{Re}\ \Sigma$ for the specific alloys $Ga_xIn_{1-x}As$ with $x = 0.1$, 0.3, 0.5, 0.7 and 0.9 obtained from the fitted parameters.

For a cluster of n sites, $\underline{G}^{m}$, $\underline{G}^{(n)}$, $\underline{H}^{(n)}$ and the unit matrix $\underline{I}$ involved in the equation are n x n matrices.

Figs. 3.7(a) to (e) show various distinct configurations of each cluster and the corresponding probabilities of occurrences are drawn in the following. Sites are indicated by small circles and bonds by lines connecting these sites. The alloyed ion is indicated by coloured circles. Sites are labelled for the specific alloys $Ga_xIn_{1-x}As$, in which the cation sites are alloyed and for which graphical results are presented subsequently. Exact clusters for any other alloy can easily be obtained from these diagrams.

The n x n difference Hamiltonian

$$\delta\underline{H}^{(n)} = \underline{H}^{exact} - \underline{H}^{(n)}$$

where $\underline{H}^{(n)}$ is the 1-CPA Hamiltonian as an approximation to the self-consistent n-CPA medium Hamiltonian. A particular cluster may consist completely of only one of the alloying constituents. In that case H_{ij}^{exact} simply consists of interactions between the i-th and the j-th bonds as in the unalloyed state. For example, for the alloy $Ga_xIn_{1-x}As$, one of the configurations of any cluster under consideration will consist of only Ga and As ions i.e. only Ga-As bonds. Depending on whether i,j are identical, nearest neighbour bonds parallel second nearest neighbour bonds, or whatever, the corresponding interaction parameter of pure Ga-As crystal would be substituted in H_{IJ}^{exact}.

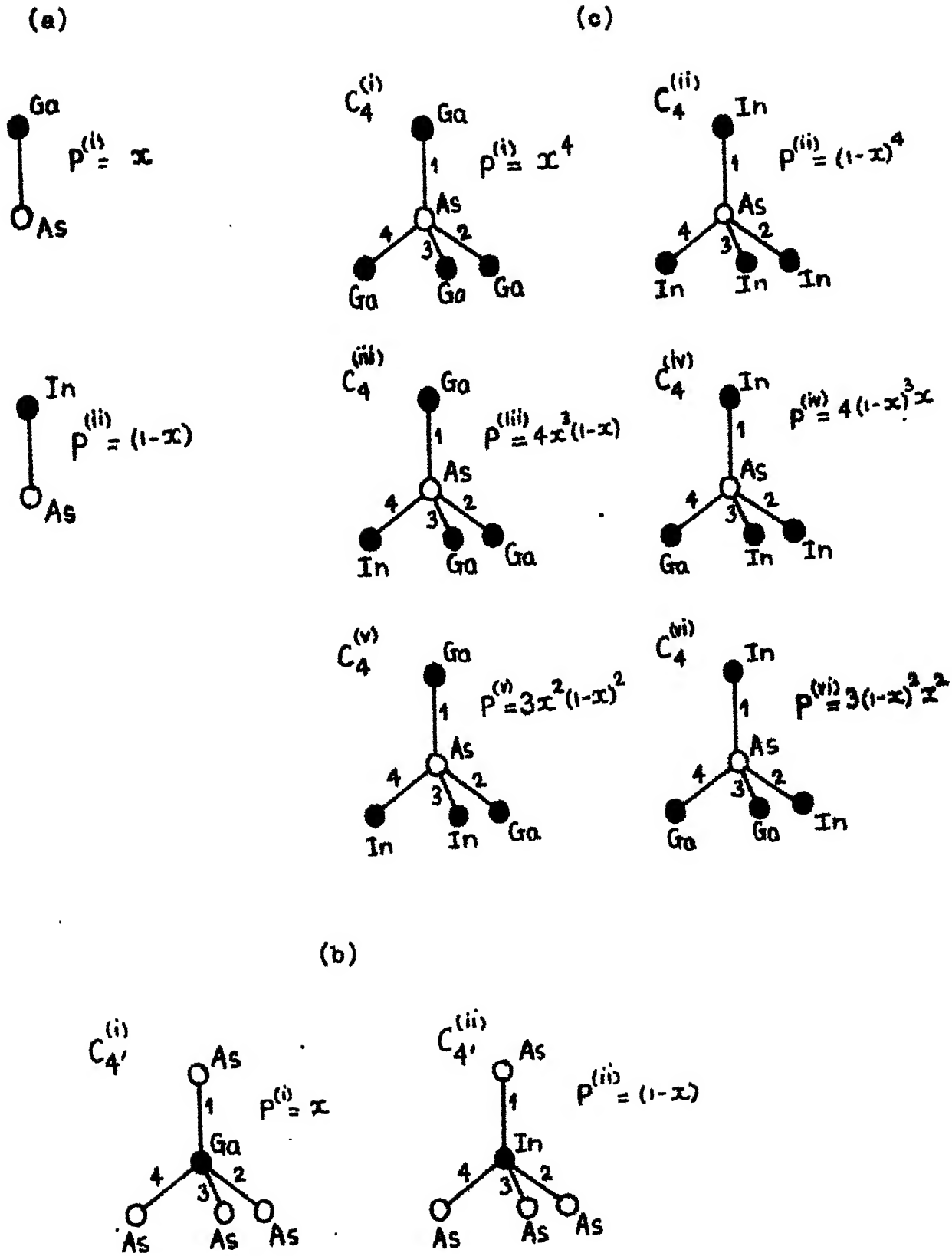

Fig. 3.7 (a), (b) and (c) continued.

$C_7^{(i)}$

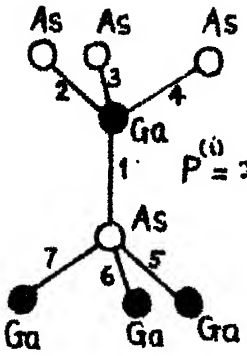

$P^{(i)} = x^4$

$C_7^{(ii)}$

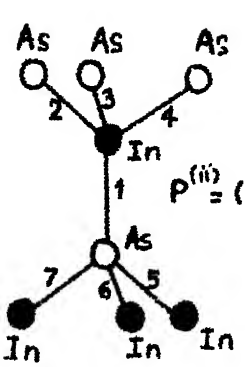

$P^{(ii)} = (1-x)^4$

$C_6^{(i)}$

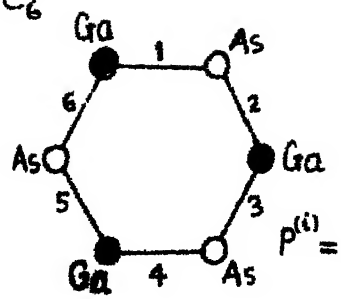

$P^{(i)} = x^3$

$C_7^{(iii)}$

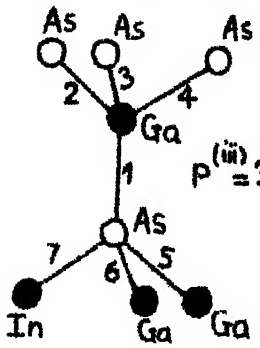

$P^{(iii)} = 3x^3(1-x)$

$C_7^{(iv)}$

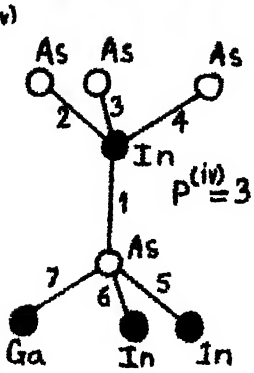

$P^{(iv)} = 3(1-x)^3x$

$C_6^{(ii)}$

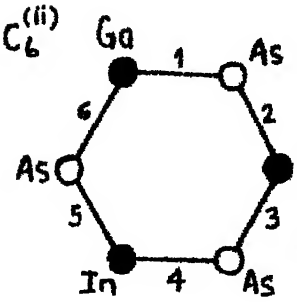

$P^{(ii)} = 3x^2(1-x)$

$C_7^{(v)}$

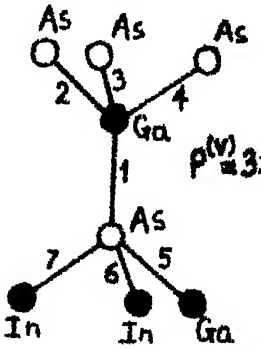

$P^{(v)} = 3x^2(1-x)^2$

$C_7^{(vi)}$

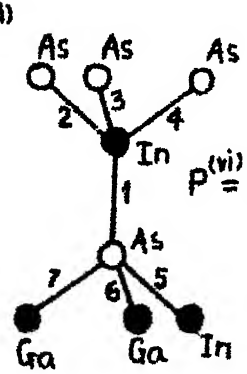

$P^{(vi)} = 3(1-x)^2x^2$

$C_6^{(iii)}$

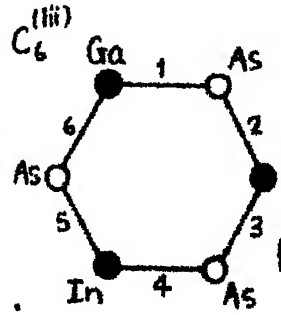

$P^{(iii)} = 3x(1-x)^2$

$C_7^{(vii)}$

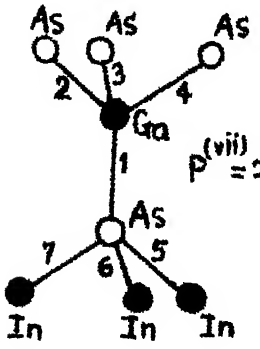

$P^{(vii)} = x(1-x)^3$

$C_7^{(viii)}$

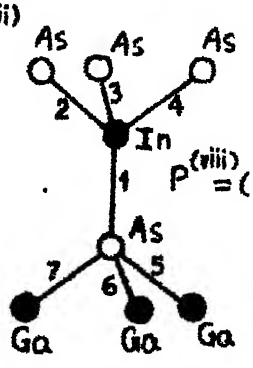

$P^{(viii)} = (1-x)x^3$

$C_6^{(iv)}$

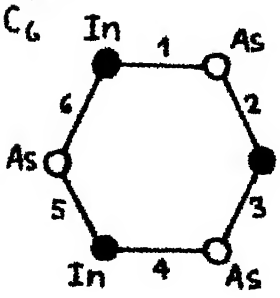

$P^{(iv)} = (1-x)^3$

The first term is vanishing because of the orthogonality of two different hybridised orbitals at the same site. The middle two terms would be identical in the unalloyed case due to the geometrical symmetry of the location of the orbitals involved. Hence this part of the expression is equivalent to the average of these corresponding to the pure cases. The last term is small compared with the middle two since it involves more distant orbitals. The approximation, therefore, involves the neglect of the variation in this term over the constituent materials, which is small anyway.

Various clusters considered are described in the following:

(a) For a one-bond cluster, only two distinct configurations are possible. The matrices become scalars and, therefore, the cluster Green's function $\underline{G}^{M}$ corresponding to each of the configurations $C_1^{(i)}$ and $C_1^{(iii)}$ shown in Fig. 3.7(a) are calculated directly using Eq. (3.28) and the weighted average of these is taken. Here $\underline{H}^{(n)}$ involves only the difference of the specific bond energies of the GaAs and the InAs bonds from the 1-CPA value. The 1-CPA Green's function is reproduced as is expected.

(b) A cluster of four bonds meeting at an alloyed site is now looked at. In case of $Ga_xIn_{1-x}As$, the central site is a cation site and there are again only two distinct configurations possibl

since only one alloyed site is involved in the cluster. These are indicated in Fig. 3.7 (b) with the four bonds numbered as shown, the 4 x 4 matrices are

$$\underline{H}^{exact} = \begin{bmatrix} H_0 & H_1^C & H_1^C & H_1^C \\ H_1^C & H_0 & H_1^C & H_1^C \\ H_1^C & H_1^C & H_0 & H_1^C \\ H_1^C & H_1^C & H_1^C & H_0 \end{bmatrix}, \quad \underline{G}^{(4)} = \begin{bmatrix} G_0 & G_1^C & G_1^C & G_1^C \\ G_1^C & G_0 & G_1^C & G_1^C \\ G_1^C & G_1^C & G_0 & G_1^C \\ G_1^C & G_1^C & G_1^C & G_0 \end{bmatrix}$$

where H_0 and H_1^C are the exact bond energy and the nearest neighbouring bond interaction parameter for bonds meeting at a cation site. G_0 and G_1^C are, in a similar notation, the diagonal and the appropriate off-diagonal matrix elements of the Green's operator in the bond basis, in the 1-CPA. $G^{(n)}$ is the same for the two configurations $C_1^{(i)}$ and $C_1^{(ii)}$ shown in Fig.3.7(b) while in $\underline{H}^{exact}$, appropriate numbers for the specific bonds and interactions are plugged in. Again, Eq. (3.28) is used to determine the diagonal Green's functions corresponding to each cluster and an average taken weighted by the probabilities x and (1-x) for the two clusters, to yield the configurationally averaged Green's function. The diagonal elements of $\langle\langle G^M \rangle\rangle$ so obtained are identical due to symmetry and correspond to the $\bar{G}$ sought.

(c) A four bond cluster in which the central site is the unalloyed site (the anion site in case of $Ga_xIn_{1-x}As$, for example) is considered next. Its specific configurations and

As a starting reference, a series of $Ga_x In_{1-x} As$ density of states per bond scaled by π in the VCA and the CPA are shown in Fig. 3.6 together with the real and imaginary parts (with the sign changed) of the diagonal CPA self energy Σ_o for various values of the concentration x indicated. The curves reveal an s-like band separated by a gap from a p-like band. The latter also is apparently made up of two separated peaks. These correspond to the second nearest neighbour parallel and non-parallel bond interactions. This is substantiated by the observation that the integral under the second peak is twice that under the first one.

As expected, the CPA rounds off the sharp peaks present in the VCA, lowers the δ-function like spikes and has small Σ_o at low concentrations of either constituent, increasing to a maximum at the 50-50 alloy.

Results of the density of states per bond scaled by π (that is, the imaginary parts of the diagonal Green's functions along the real axis with the sign reversed) for each configuration, and that averaged over these, for each of the clusters C_1, C_4, C_4', C_7 and C_6 described above (and shown pictorially in Fig. 3.7(a) to (e)) are shown graphically in Fig. 3.8 for the alloy $Ga_{0.1} In_{0.9} As$ and in Figs. 3.11 for the alloy $Ga_{0.5} In_{0.5} As$. The partial density of states corresponding to different clusters are important in that they indicate the way the effective medium spreads out the cluster eigen-energies

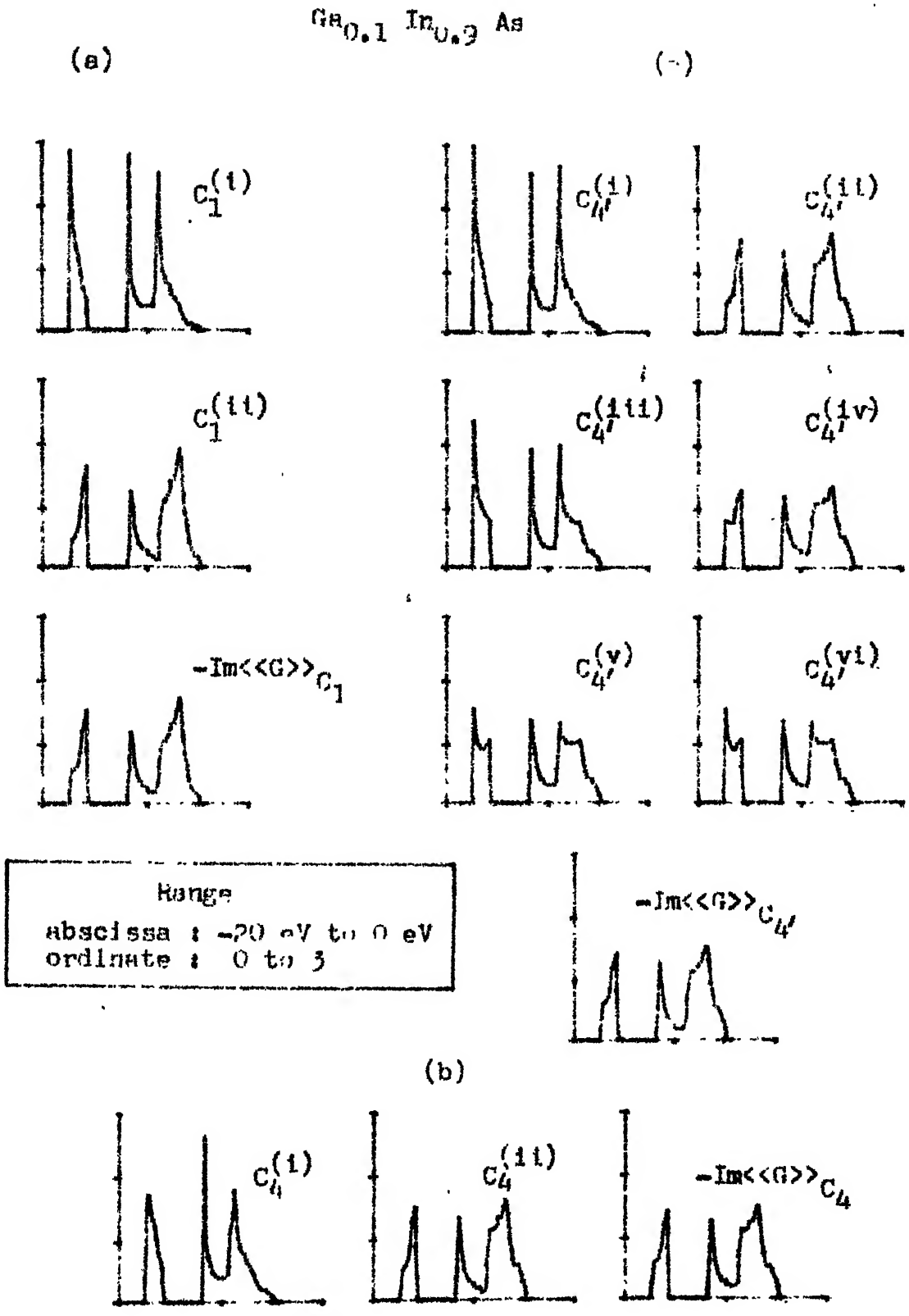

Fig. 3.3(a),(b) and (c) continued.

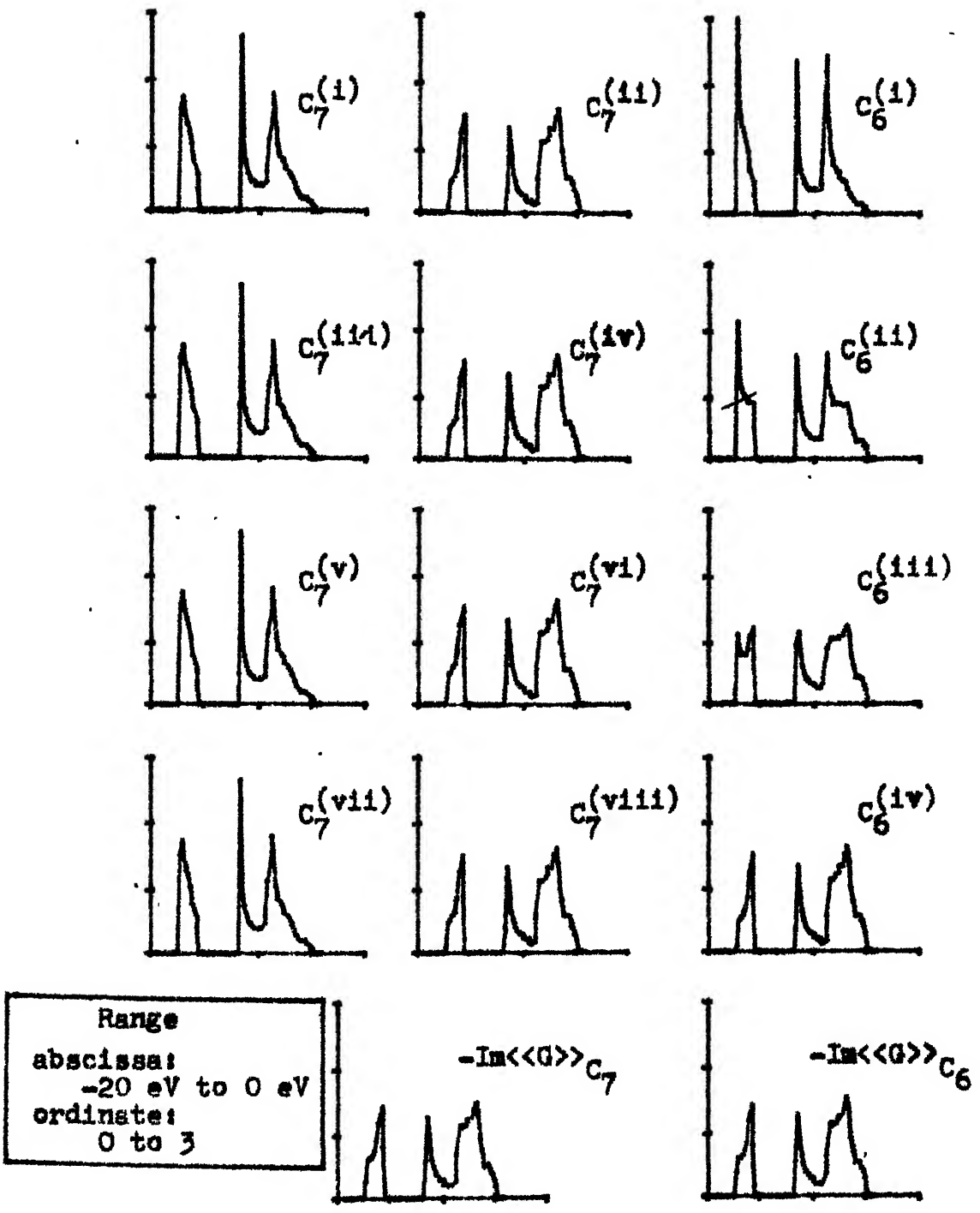

Fig. 3.8: Density of electron states per bond in units of x^{-1} ($-Im\ G$) for the alloy $Ga_{0.1}\ In_{0.9}As$ corresponding to each configuration (Fig. 3.7(a) to (e)) of the clusters (a) C_1 (b) C_4 (c) $C_{4'}$ (d) C_7 and (e) C_6 and those averaged over configurations of each cluster, using the fitted parameters.

$Ga_{0.1}\ In_{0.9}\ As$

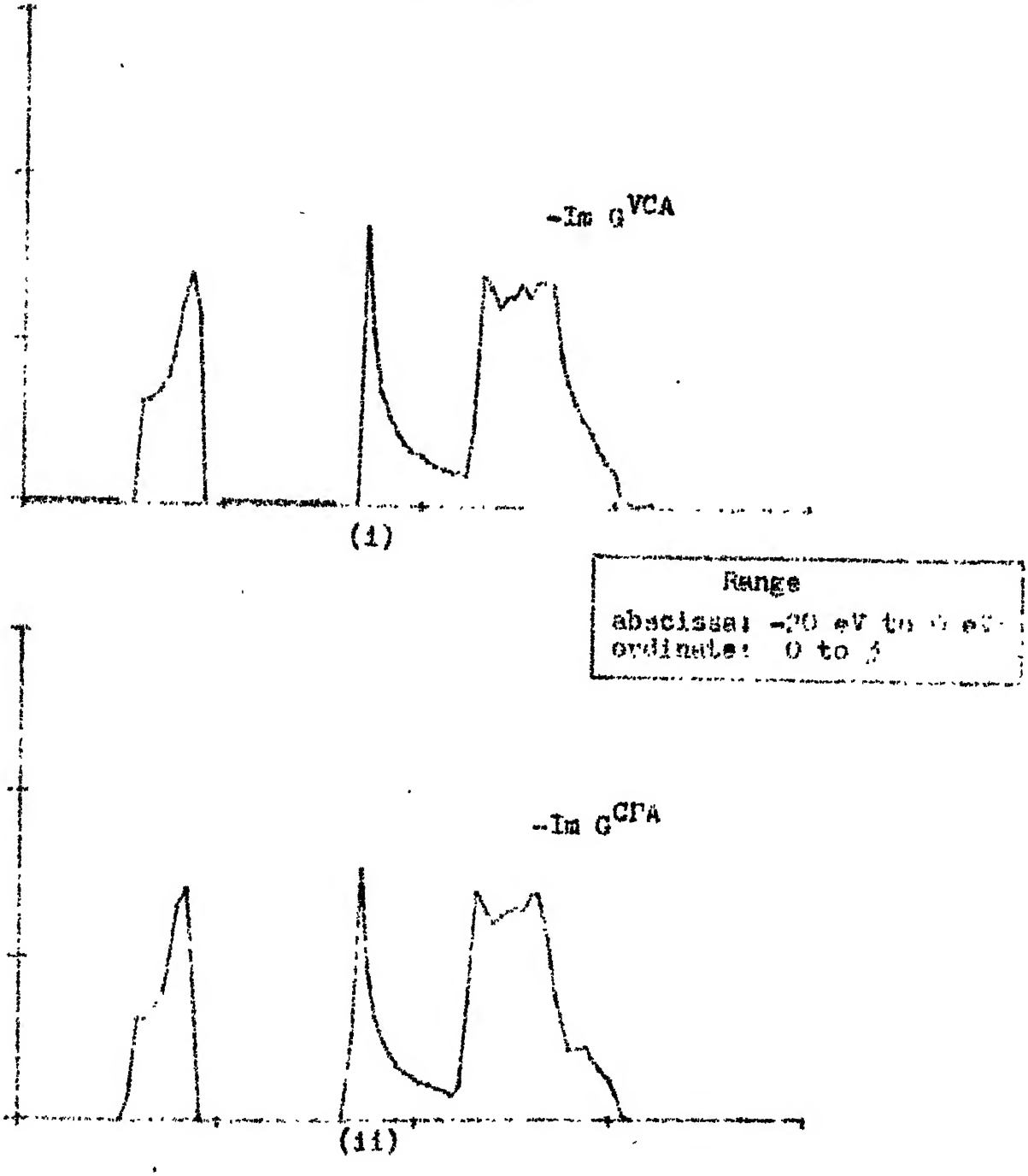

Fig. 3.9: (i) $-\mathrm{Im}\ G^{VCA}$ and (ii) $-\mathrm{Im}\ G^{CPA}$ for $Ga_{0.1}\ In_{0.9}\ As$ using the fitted parameters.

$Ga_{0.1}\ In_{0.9}\ As$

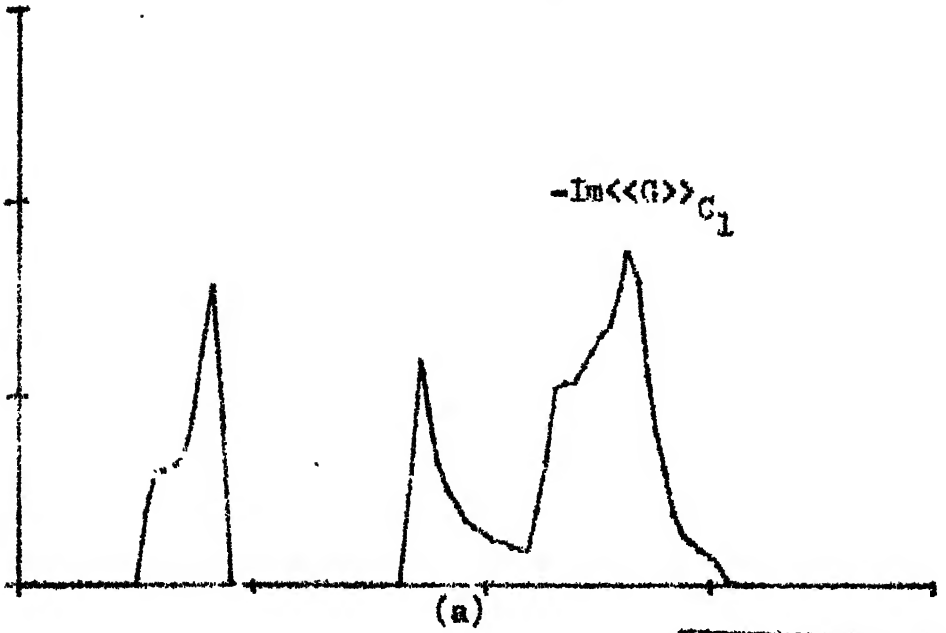

(a)

Range
abscissa: -20 eV to 0 eV
ordinate: 0 to 3

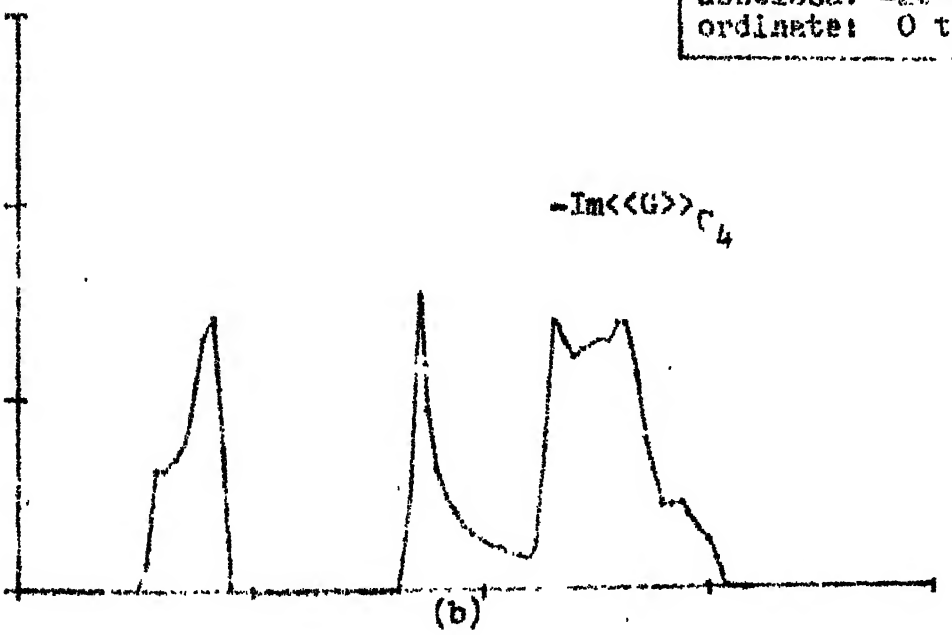

(b)

Fig. 3.10 (a) and (b) continued.

$Ga_{0.1}\ In_{0.9}\ As$

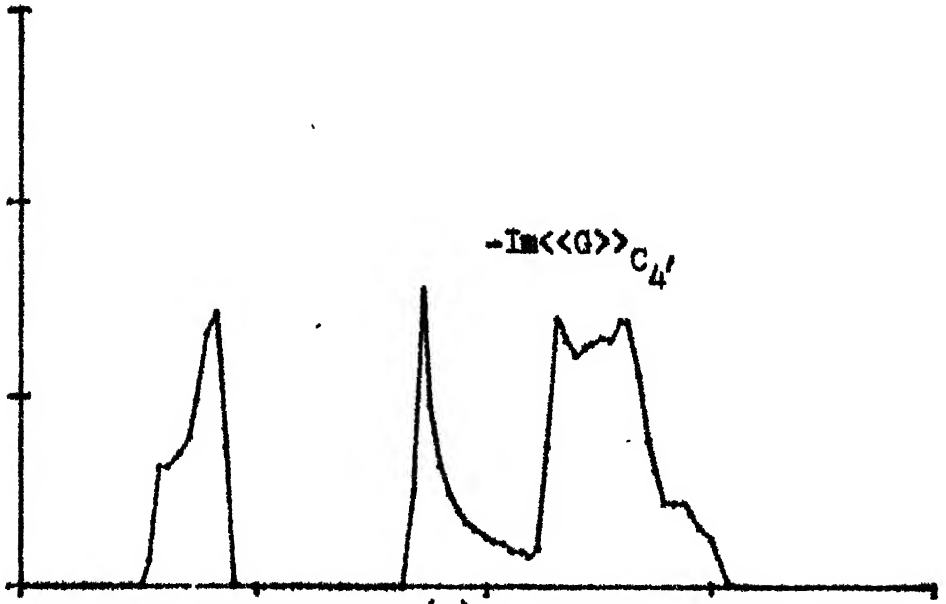

(c)

Range
abscissa: -20 eV to 0 eV
ordinate: 0 to 3

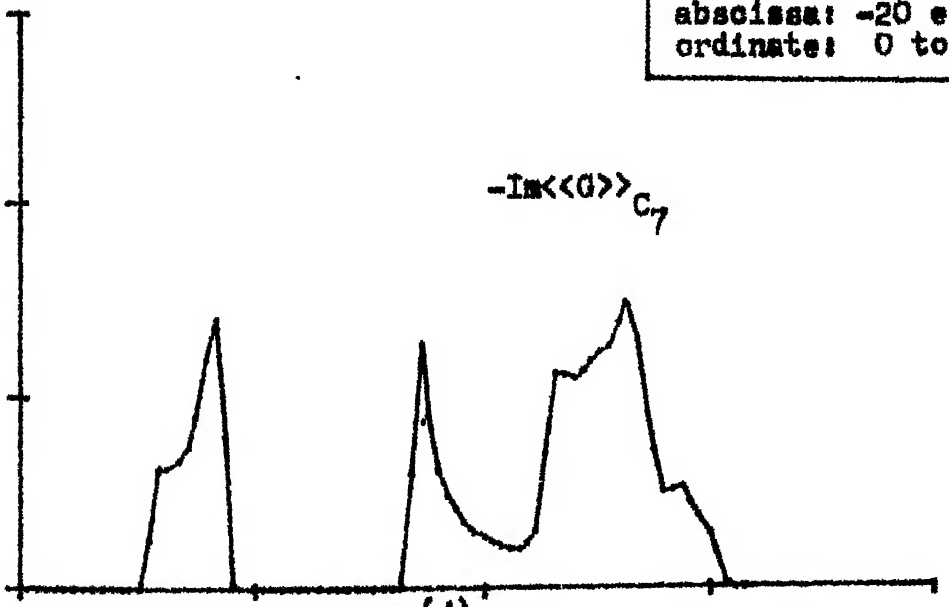

(d)

Fig. 3.10 (c) and (d) continued.

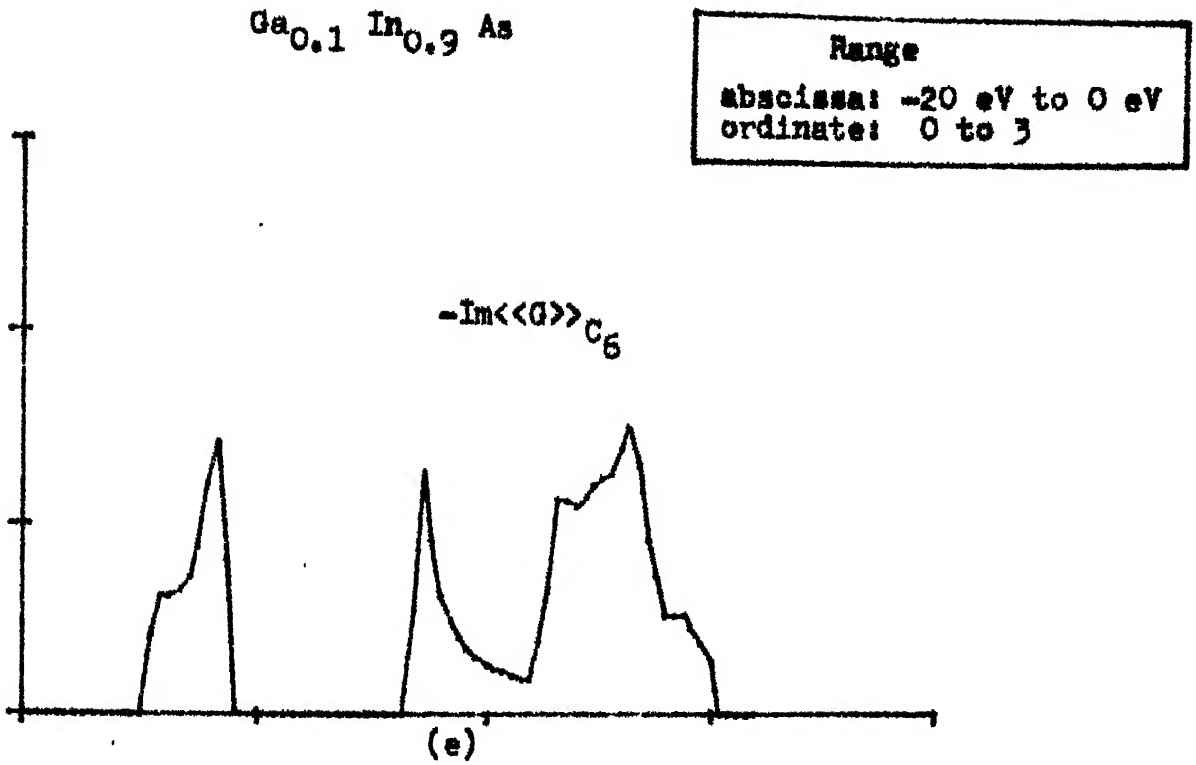

Fig. 3.10: (a) $-Im\langle\langle G\rangle\rangle_{C_1}$, (b) $-Im\langle\langle G\rangle\rangle_{C_4}$, (c) $-Im\langle\langle G\rangle\rangle_{C_4}$, (d) $-Im\langle\langle G\rangle\rangle_{C_7}$ and (e) $-Im\langle\langle G\rangle\rangle_{C_6}$ for $Ga_{0.1}\ In_{0.9}\ As$ using the fitted parameters.

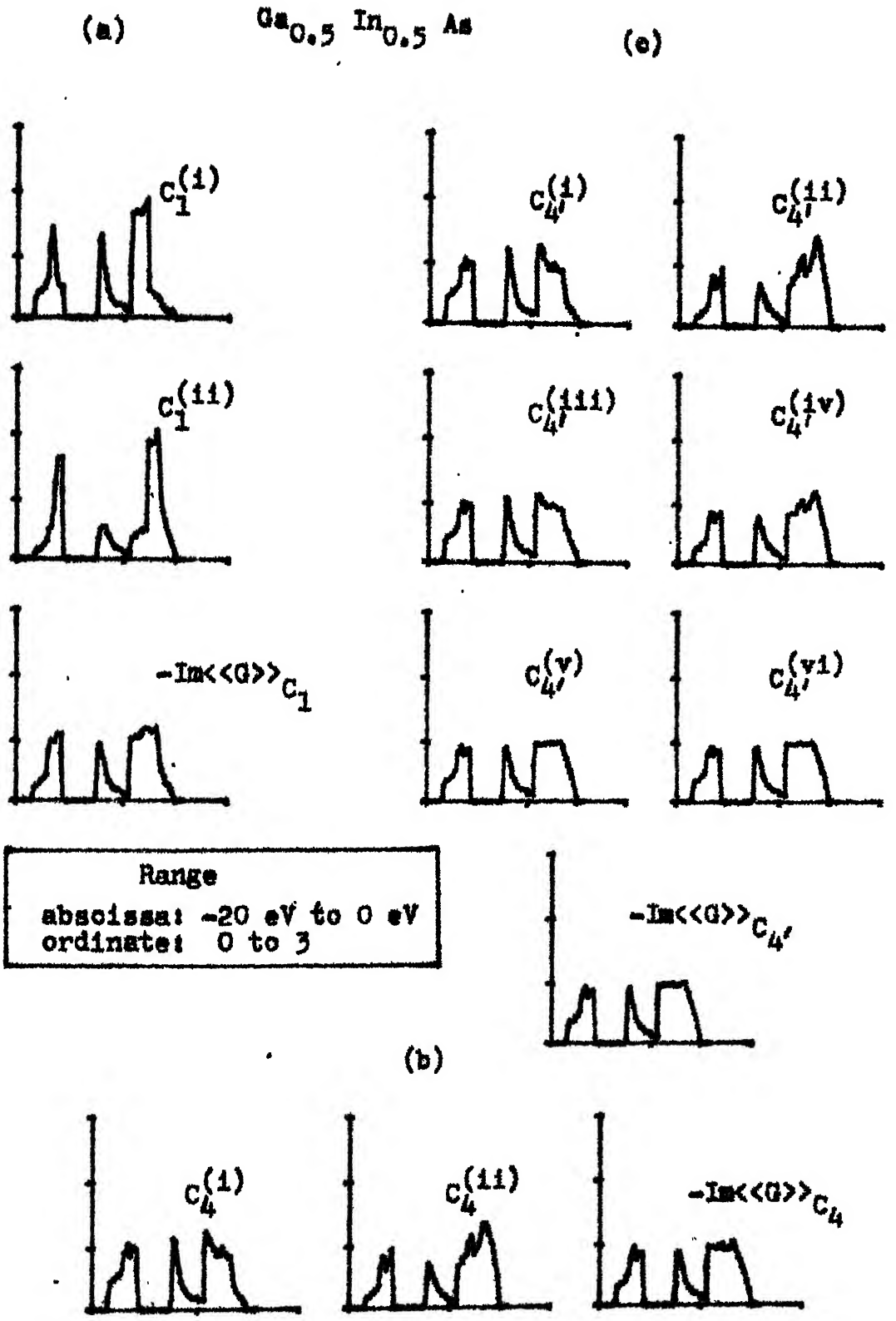

Fig. 3.11 (a), (b) and (c) continued.

$Ga_{0.5}\ In_{0.5}\ As$

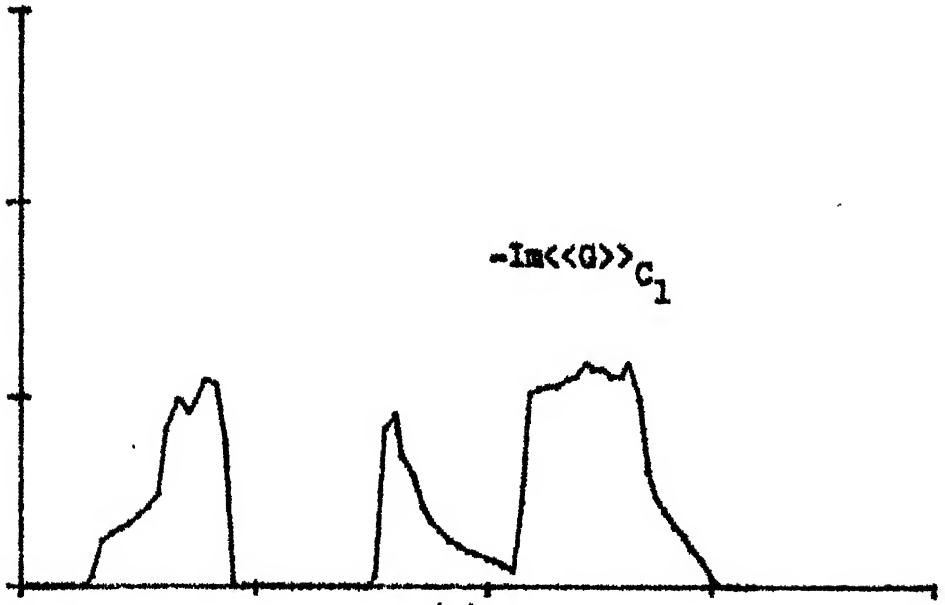

(a)

Range	
abscissa:	-20 eV to 0 eV
ordinate:	0 to 3

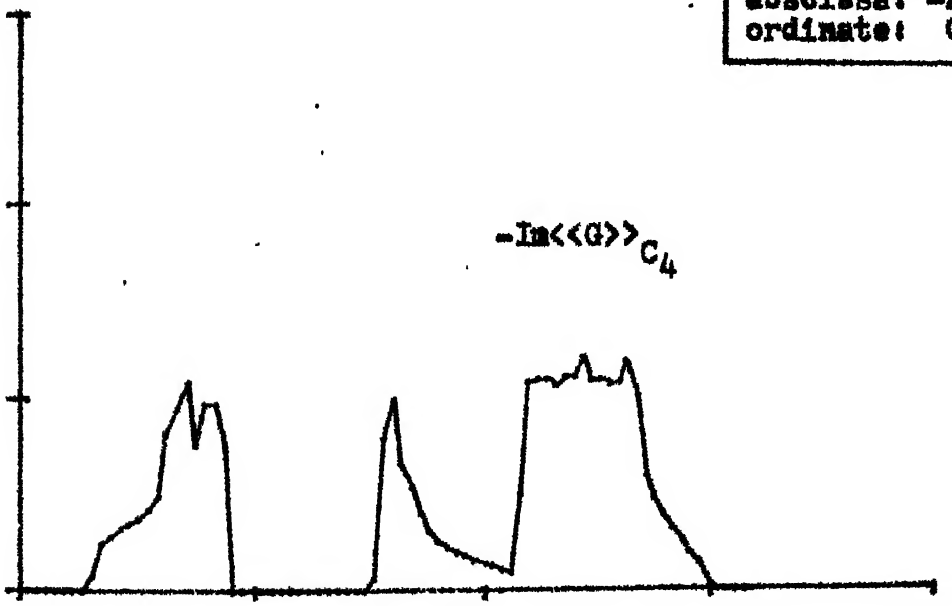

(b)

Fig. 3.13 (a) and (b) continued.

$Ga_{0.5}\ In_{0.5}\ As$

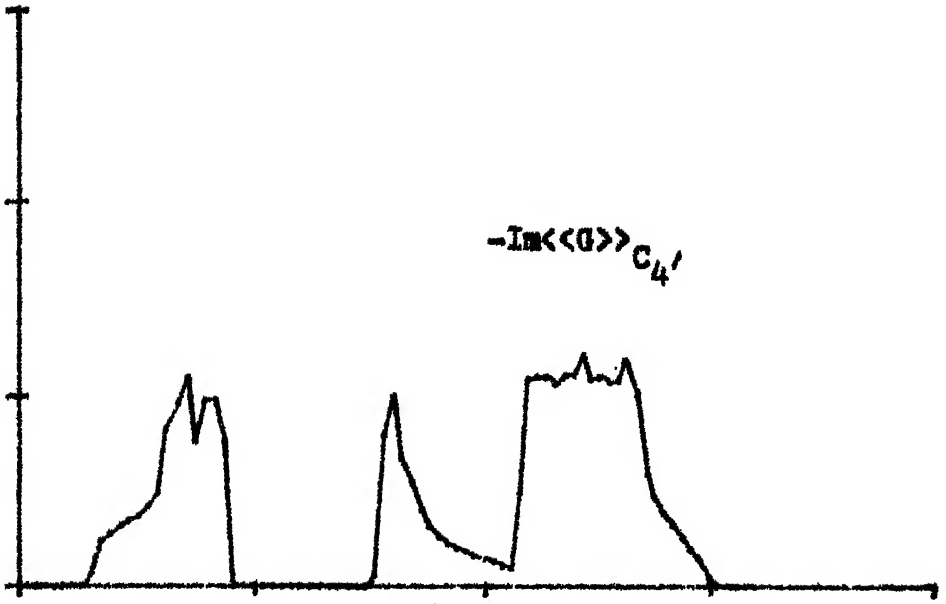

(c)

Range
abscissa: -20 eV to 0 eV
ordinate: 0 to 3

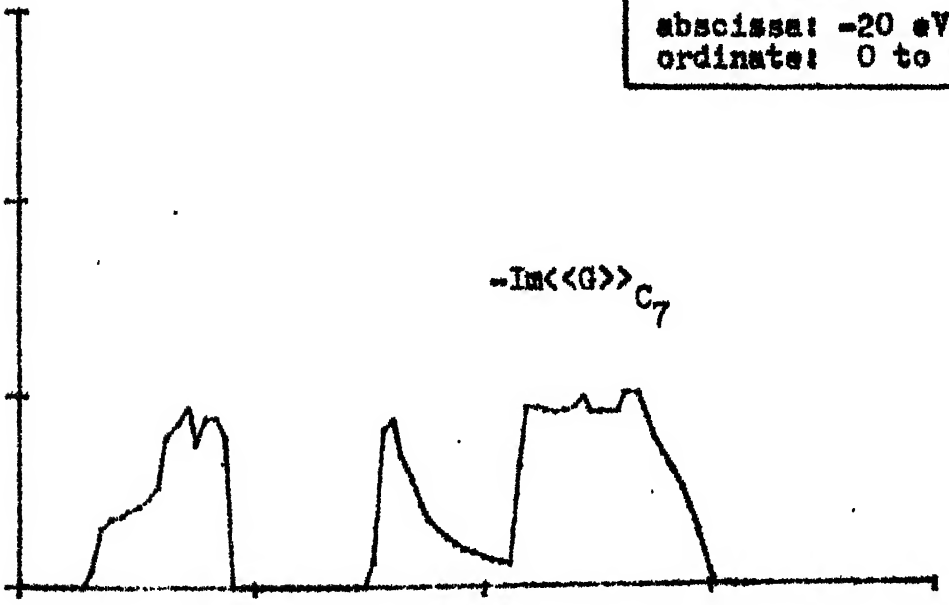

(d)

. Fig. 3.13 (c) and (d) continued.

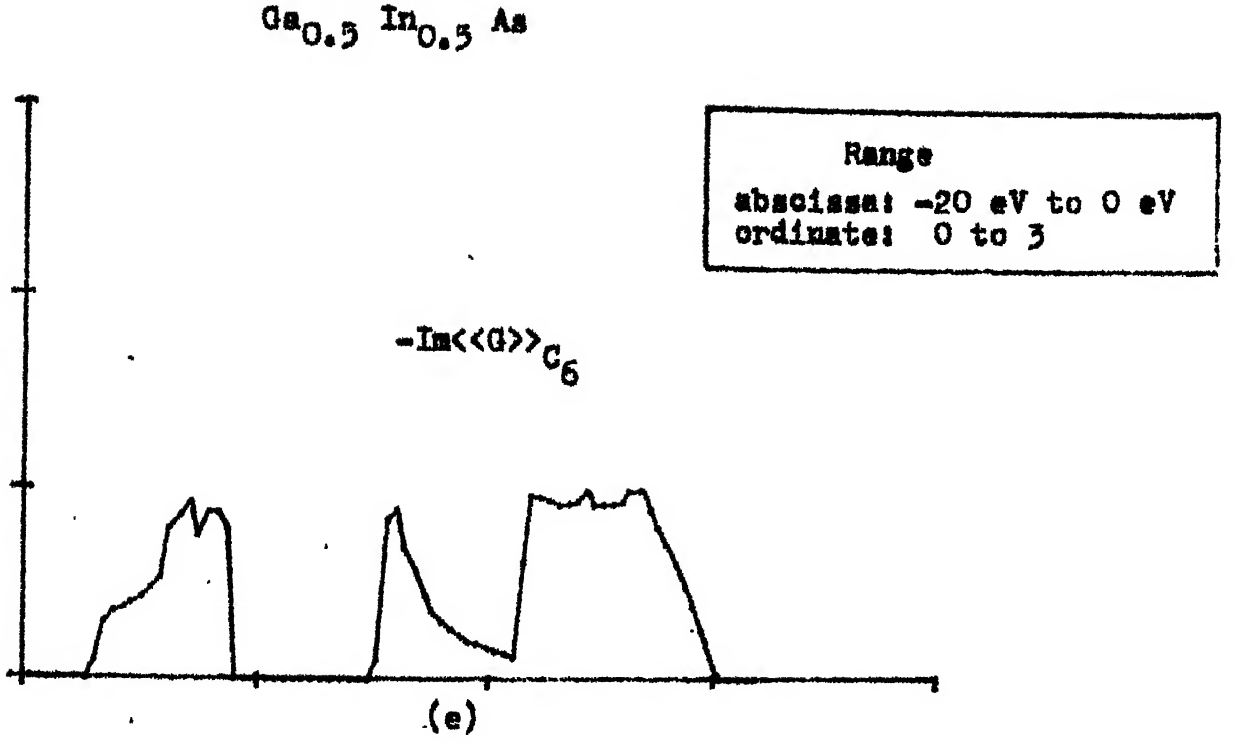

Fig. 3.13: (a) $-Im\langle\langle G\rangle\rangle_{C_1}$, (b) $-Im\langle\langle G\rangle\rangle_{C_4}$, (c) $-Im\langle\langle G\rangle\rangle_{C_{4'}}$, (d) $-Im\langle\langle G\rangle\rangle_{C_7}$ and (e) $-Im\langle\langle G\rangle\rangle_{C_6}$ for $Ga_{0.5}$ $In_{0.5}$ As using the fitted parameters.

when the latter are immersed in the former. The structure of those partial densities also indicate the cluster origin of the structure appearing in the averaged densities of states. For example, the enhancement of the peak at the top of the band in the 7-bond cluster CPA for $Ga_{0.1}$ $In_{0.9}$ As as compared to the 1-CPA and 4'-CPA can be attributed to the clusters $C_7^{(ii)}$ and $C_7^{(iv)}$ whose peaked structure at that energy contributes to this cluster property (See Fig. 3.8 and 3.10). The cluster effect is evident pronouncedly in each of the clusters consisting of either constituent of the alloyed ion only. Partial densities of states are also of interest in the calculation of the optical properties, particularly, the structure near the valence band top. In the absence of other calculations to compare with, it is necessary to generate these partial densities to account for the difference between the CPA and the cluster-CPA's.

Fig. 3.9 shows the VCA and CPA density of states on a larger scale for a more detailed examination. Fig. 3.10 (a) and (b) show that embedding single bond clusters is insufficient in case we want to describe these ternary alloys, while embedding the four bond cluster with the alloyed cation site at the central site, reproduces results resembling the 1-CPA very closely. C_4 is, therefore, the smallest unit embedded that is self consistent. Again, comparison of Fig. 3.10(b) and (c)

shows that in case of a four bond cluster, the one with the central site alloyed or disordered gives more information than with the unalloyed site at the center.

Fig. 3.10(c) and (d) compare the 4'-CPA and the 7-CPA. The 7-CPA involves embedding a central bond with its six nearest neighbours, and this can take into account variations in H_1^A and H_1^C and some of the second neighbour bond interaction. The significant clustering effects arise at the band top. This can be understood as due to the fact that only the states at the top of the band are relatively extended enough to sample the environment in detail. Lower lying states are localised and so do not sample the environment in detail.

Fig. 3.10(e) shows the result for a 6 bond ring cluster C_6 embedded in the medium. The results are comparable to the 7-CPA. The second near neighbour interactions are sampled but not completely. The cluster variations which give rise to the enhancement of the upper peak are also present here.

The Fig. 3.11 presents the partial densities of states for $Ga_{0.5}$ $In_{0.5}$ As. The cluster effect is less prominent now. This is to be expected as in model calculations (Kumar, Mookerjee and Srivastava, 1981). The partial densities also indicate that there are no highly probable peaked structures in these clusters. The CPA smooths out the VCA (Fig. 3.12) and

the cluster CPA's further introduce smoothening, lowering peaks and broadening out the density of states. There is again a perceptible filling up of states at the band top, if we compare Fig. 3.13(c) and (d) as we go from the 4'-CPA to the 7-CPA. The ring cluster (Fig. 3.13(e)) is as before, not very different from the 7-CPA. The clustering effect, though smaller than in case of $x = 0.1$, can be clearly seen to increase gradually as the size of the cluster is increased.

3.3 The Impurity Bands:

The appearance of impurity bands in a model calculation is a triumph for the 1-CPA. The n-CPA cluster embedding in a model calculation for a 90 - 10 alloy for $\delta = 1.0$ has been done by Mookerjee and Srivastava (1980) for the s-band. The graph (Fig. 3.14) clearly shows the extra lumps appearing. The cluster embedding in it is reported to broaden the band perceptibly.

3.4 Conclusions:

The n-cluster CPA formalism developed above is a refinement of the 1-CPA preserving essential physical properties of the configurationally averaged Green's function, gradual change in which is to be expected as the size of the cluster embedded is increased.

The application of the above formalism to the valence bands of III-V semi-conducting ternary alloys, indeed, shows

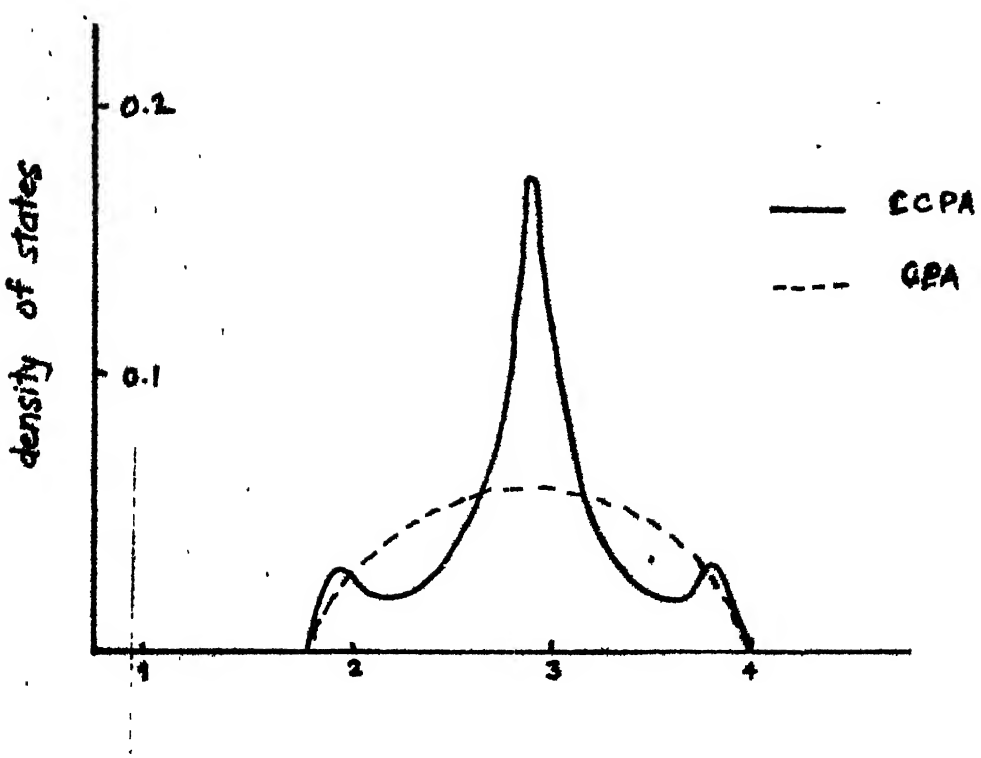

Fig. 3.14: Impurity band in the 1-CPA for the s-band in a model calculation on the diamond lattice.

the above. The cluster effects in these alloys is not dramatic. This is due to the fact that the variations in the diagonal energies are small compared with the "widening factor" $Z_1 H_1^s$, where H_1^s is the symmetric combination of the nearest neighbour bond interactions, H_1^A and H_1^C. Nevertheless, the effects are not negligible specially in dilute alloys. That the environment is not self consistent, is a drawback and may mask some further clustering effects, specially because of the off diagonal disorder. The self consistent problem could not be handled because of difficulties both in the formulation [specially in deciding the self-consistency condition in the cluster to the interior and surface atoms (Butler,(1973)] and in implementation of some of the proposed schemes, where the equations involved too many variables and seemed intractable. Yet even with the non-self consistent medium some features of clustering do show up. This in itself is the achievement of this work. Similar embedding in a non-selfconsistent media have been tried on model systems (Kaplan, and Gray, 1976, 1977, Kaplan et al 1980) and have shown that considerable amount of cluster structure does show up. However, it cannot be emphasized enough that eventually the self consistent solution should be obtained in future.

the six III-V semiconductors dealt with in the last chapter. The values of the parameters are compared with those obtained by parametric fitting.

Thereafter, in Sec. 4.4 the VCA and the 1-CPA medium calculations are carried out. Finally exact clusters are embedded and Green's functions corresponding to each specific cluster and that obtained after a configuration averaging over these clusters is done, are presented graphically for $Ga_xIn_{1-x}As$.

4.2 The General Chemical Pseudopotential Scheme:

The fact that simple metals have energy bands that are free electron like is surprising because the conduction states are required to be orthogonal to the core orbitals and must therefore be quite different from plane waves. The reason for this is that the Schrodinger equation for the conduction electrons can be transformed into a pseudo-Schrodinger equation which has the same conduction band eigenvalues as the original Hamiltonian but for which the wave functions are slowly varying in space and are nearly plane waves. Only for $\vec{k}$-vectors near Brilluoin Zone boundaries may these be combinations of degenerate plane waves. Clearly, there is no unique transformation that alone makes this possible. One such pseudopotential equation is the Austin et al form (1962)

$$T|\phi_{\vec{k}}\rangle + (V - \sum_{c} |\phi_c\rangle\langle\phi_c|V)\ |\phi_{\vec{k}}\rangle = E_{\vec{k}}|\phi_{\vec{k}}\rangle$$

The summation is over the core orbitals. Part of the potential V is cancelled by the core terms on each atom so that the net potential is weak. The eigenfunctions $|\phi_{\vec{k}}\rangle$ are thus little distorted from those of the kinetic energy operator T, i.e. the plane waves.

Similarly Anderson (1969) introduced a pseudopotential such that the pseudowavefunctions look localised and atomic like. The formulation justified Huckel's scheme for parametrization of molecular interaction in a fashion clearer than the usual procedure of making a unitary transformation to an orthogonal basis.

The aim of localised orbital theories is to present the exact band molecular orbitals $|\psi_i\rangle$ say, as linear combinations of orbitals $|\phi_\alpha\rangle$ localised at the atomic sites. In case the distortions due to neighbouring orbitals is small, this provides a chemical building block picture (Boys 1960, Boys, Foster 1960, Gilbert 1964) in which the wave functions of large molecular systems are built up from chemically invariant parts, which need not be calculated for each new system. Also, correlation effects can be conveniently studied in this basis. These ideas can be applied to crystals considering these to be very large molecular systems.

The Wannier functions as the basis set, are not suited for the above picture since the orthogonality constraint between those associated with different sites necessarily produces oscillations, more dispersed than the atomic functions. Also, the tails of the functions are rather sensitive to the environment. It is now clear that better sets of localised functions can be defined by employing the pseudopotential techniques (Adams 1961, 1962, 1971a, 1971b, 1971c, 1974, Gilbert 1964, Anderson 1968, 1969).

Consider a system made up of N atoms with a given self-consistent one-electron Hamiltonian H. In the isolated state these atoms have well defined energy levels ε_α° and eigenfunctions $|\phi_\alpha^\circ\rangle$ due to the free atom Hamiltonian H_a, such that

$$H_a|\phi_\alpha^\circ\rangle = \varepsilon_\alpha^\circ|\phi_\alpha^\circ\rangle \qquad (4.1)$$

When brought together to form a molecule or a lattice, these atomic orbitals overlap, and in the latter case, form bands, each containing exactly N states:

$$H|\psi_i\rangle = \varepsilon_i|\psi_i\rangle \qquad (4.2)$$

We are looking for a useful set of local orbitals $|\phi_\alpha\rangle$, linear combinations of which yield the $|\psi_i\rangle$ s. Clearly these span the same band space, hence,

$$|\phi_\alpha\rangle = P|\phi_\alpha\rangle \qquad (4.3)$$

where P is the projection operator on the band i.e.

$$P = \sum_{i=1}^{N} |\psi_i\rangle\langle\psi_i|$$

Using the properties of commutation with the Hamiltonian and idempotency of the projection operator, i.e.

$$PH = HP \qquad \text{and} \quad P^2 = P$$

Eq. (4.3) can be rewritten as

$$H|\phi_\alpha\rangle - PHP|\phi_\alpha\rangle = 0 \tag{4.4}$$

In order to define $|\phi_\alpha\rangle$ s uniquely, another condition must be incorporated. The most useful $|\phi_\alpha\rangle$ s will be those that resemble $|\phi_\alpha^o\rangle$ s most closely. To derive the $|\phi_\alpha\rangle$, we divide the total system into subsystems which may be atoms, ions, bonds etc, and constrain $|\phi_\alpha\rangle$ to satisfy H_a, the Hamiltonian associated with one such sub-system as well as possible within the permitted function subspace, i.e.

$$PH_aP|\phi_\alpha\rangle = \varepsilon_\alpha|\phi_\alpha\rangle \tag{4.5}$$

Within a single band, N nontrivial functions $|\phi_{\alpha j}\rangle$ will satisfy this Eq. (4.5), but only the lowest one $|\phi_{\alpha 1}\rangle$ $|\phi_\alpha\rangle$ will be localised and will correspond to the atomic like orbitals of H_a (Bullett, SSP, Vol. 35). Adding Eqs. (4.4) and (4.5), we obtain, the Adam's equation,

$$H|\phi_\alpha\rangle - P(H-H_a)|\phi_\alpha\rangle = \varepsilon_\alpha|\phi_\alpha\rangle$$

or
$$H_a|\phi_\alpha\rangle + \{U_a - PU_aP\}|\phi_\alpha\rangle = \varepsilon_\alpha|\phi_\alpha\rangle \tag{4.6}$$

where $U_a \equiv H-Ha$, is the perturbation to the cell Hamiltonian due to the rest of the system.

This is the determining equation for $|\phi_\alpha\rangle$ and shows why the environment may often have little effect on the original localised orbitals of Eq. (4.1) since the perturbation itself is reduced by projecting out all ot it which acts within the band. The residual screened interaction $U_a - PU_aP$ can most often be treated by standard perturbation theory by an iterative procedure to obtain self consistent orbitals $|\phi_\alpha\rangle$ starting from $|\phi^o_\alpha\rangle$. However, Anderson points out in his work (1969), that whenever the scheme is applied, no attempt to solve for the exact eigenfunctions is required, that these can be found or exist in principle is all that is necessary.

It may be noticed that the localised orbitals corresponding to different cells are determined by different Hamiltonians in general, and there is no orthogonality relation between them.

The pseudopotential equation introduced by Anderson is obtained by simplifying the projection operator P to P_b involving projections only on the local states and

$$U_a = \sum_{b \neq a} V_b^{(a)}$$

where $V_b^{(a)}$ is the perturbation due to cell labelled by b. Then using the properties $PP_b = P_b$ and $P|\phi_\alpha\rangle = |\phi_\alpha\rangle$, Eq.(4.6) becomes,

$$H_a|\phi_\alpha\rangle + \sum_{b\neq a} \{V_b^{(a)} - |\phi_\beta\rangle\langle\phi_\beta|V_b^{(a)}\}|\phi_\alpha\rangle = \varepsilon_\alpha|\phi_\alpha\rangle$$

i.e. $$H|\phi_\alpha\rangle = \varepsilon_\alpha|\phi_\alpha\rangle + \sum |\phi_\beta\rangle\langle\phi_\beta|V_b^{(a)}|\phi_a\rangle \qquad (4.7)$$

Anderson applied this to the case of the π-orbitals of benzene and showed that the cancellation is so complete that the self-consistent solutions are very close to the unperturbed atomic orbitals.

The molecular orbitals are given by linearly combining these self consistently obtained orbitals, i.e.

$$|\psi_i\rangle = \sum_\alpha C_{\alpha i}|\phi_\alpha\rangle \qquad (4.8)$$

The usual secular equation determining the eigenvalues would then be

$$\det |H - ES| = 0 \qquad (4.9)$$

where S is the overlap matrix, not a unit matrix since the basis is not orthogonal. A far more efficient and convenient method which takes full advantage of the form of the Eq.(4.7) would be to rewrite it as,

$$H|\phi_\alpha\rangle = \sum_\beta |\phi_\beta\rangle D_{\beta\alpha} \qquad (4.10)$$

where $D_{\alpha\alpha} = \varepsilon_\alpha$ and $D_{\beta\alpha} = \langle\phi_\beta|V_b^{(a)}|\phi_\alpha\rangle$ for $b \neq a$, and substitute this in the Schrodinger equation to give

$$\begin{aligned} H|\psi_i\rangle &= \sum_\alpha C_{\alpha i} H|\phi_\alpha\rangle \\ &= \sum_\alpha \sum_\beta C_{\alpha i} |\phi_\beta\rangle D_{\beta\alpha} \\ &+ \varepsilon_i \sum_\alpha C_{\alpha i} |\phi_\alpha\rangle \end{aligned}$$

Now linear independence of the orbitals on different sites alone implies that the coefficient of every $|\phi_\alpha\rangle$ must vanish. Hence the secular equation becomes simply

$$\det |D_{\alpha\beta} - E_i \delta_{\alpha\beta}| = 0 \qquad (4.11)$$

It may be noticed that orthogonality of the bases is not demanded, nor does the overlap matrix appear in the expression. Further, the off-diagonal matrix elements $D_{\alpha\beta}$ contain only the localised operator $V_b^{(a)}$ which is relatively insensitive to modification by the neighbouring cells.

The price, of course, is paid by the non-hermiticity, in general, of the pseudo-Hamiltonian matrix obtained since $\langle\phi_\beta|V_b^{(a)}|\phi_\alpha\rangle$ and $\langle\phi_\alpha|V_a^{(b)}|\phi_\beta\rangle$ may not be alike unless each cell is the same and is placed in the same environment. In fact, from Eq. (4.10)

$$D = S^{-1} H$$

and therefore, D will be Hermitian if and only if the Hermitian matrices S and H commute. This will be so when every orbital environment is identical so that these are diagonalisable simultaneously. Yet, no imaginary components should arise in the eigenvalues since Eq. (4.11) is trivially related to the Hermitian form in Eq. (4.9).

Premultiplying Eq. (4.6) by $\langle\phi_\alpha|$ we obtain,

$$\varepsilon_\alpha = \langle\phi_\alpha|H_a|\phi_\alpha\rangle + \sum_{b\neq a} (\langle\phi_\alpha|V_b^{(a)}|\phi_\alpha\rangle - \langle\phi_\alpha|\phi_\beta\rangle\langle\phi_\beta|V_b^{(a)}|\phi_\alpha\rangle)$$

In case the unperturbed orbitals $|\phi_\alpha^o\rangle$ are not very different from the self-consistently obtained orbitals $|\phi_\alpha\rangle$ from Eq.(4.6) the former can be substituted for the latter in the above Eq. (4.12) to yield

$$\varepsilon_\alpha = \varepsilon_\alpha^o + \sum_{b\neq a} (\langle\phi_\alpha^o|V_b^{(a)}|\phi_\alpha^o\rangle - \langle\phi_\alpha^o|\phi_\beta^o\rangle\langle\phi_\beta^o|V_b^{(b)}|\phi_\alpha^o\rangle) \tag{4.13}$$

giving the orbital energy ε_α in the bonded state in terms of that corresponding to the unperturbed state and a first order correction. The correction consists of the first order perturbative term lessened by the orbital overlap times the interactive term.

In case the bases chosen consists of the bond orbitals, an effective bond Hamiltonian H_{ac} associated to a bond orbital $|ac\rangle$ needs to be defined such that

$$H_{ac}|ac\rangle = \varepsilon_b|ac\rangle \tag{4.14}$$

where ε_b is the bond energy and the bond orbital $|ac\rangle$ consists of the site orbitals $|a\rangle$ and $|c\rangle$ on the bonding atomic sites i.e.,

$$|ac\rangle = \frac{1}{N_{ac}}(|a\rangle + |c\rangle) \tag{4.15}$$

where N_{ac} is the normalisation constant = $2(1+S)$, $S = \langle a,c\rangle$, the overlap. The orbitals $|a\rangle$ and $|c\rangle$, in case of diamond and zinc blende structures are the sp^3 hybridised orbitals. Now writing

$$H_{ac} = T + V_{ac}$$

4.3 Application to III-IV Semiconductors:

Just as before, interaction terms upto second nearest neighbouring bonds are retained, this time of the pseudo-Hamiltonian. The pseudopotential interaction terms to be calculated are those, between adjacent bonds with a cation or an anion site in common and the second nearest neighbour parallel and the non parallel bonds. A direct volume integration is carried out in a 'Wigner-Seitz' cell defined around a bond. This consists of a three dimensional space such that every point in it is closer to the centre of this bond than the centre of any other.

Fixing the origin of the coordinate system on the centre of the bond, and the z-axis along the bond in one direction, coordinates of the centres of the neighbouring bonds and those of the sites involved are determined. A grid is assigned to the spherical coordinates (r, θ, ϕ) such that the three dimensions of the curvilinear volume elements so obtained are comparable. These are then considered in successively larger spherical shells. The distances of these from the atomic sites concerned are used to determine the values of the atomic potentials and the radial parts of the s- and the p-orbitals from Hermann-Skillman tables of these for the cations Ga, In and the anions As, Sb, P. Since these are tabulated at discrete points, linear extrapolation is carried out between near points. The '$\cos\theta$' factor for the p-orbital wave functions corresponding

to each site is determined by a scalar product of appropriate unit vectors. Volume elements are then considered one by one. In case the considered one is closer to the centre of the bond and origin of the polar coordinate system than any other bond centre, the contributions in it to the integrands for the parameters is accumulated. Besides the matrix elements between the nearest neighbour bonds meeting at an anion and a cation, which are symmetric, both kinds of each of those between second nearest neighbouring parallel and non-parallel bonds are calculated. In a self-evident notation, these are D_1^A, D_1^C, $D_2^{P(A)}$, $D_2^{NP(A)}$, $D_2^{P(C)}$ and $D_2^{NP(C)}$ corresponding to $\langle 1|D|2\rangle$, $\langle 1|D|3\rangle$, $\langle 1|D|4\rangle$, $\langle 1|D|5\rangle$, $\langle 1|D|6\rangle$ and $\langle 1|D|7\rangle$ respectively with the bonds numbered as shown in Fig. 4.1. The procedure ensures integration only over the Wigner-Seitz cell around the bond without going into the details of its geometry.

The bond potentials for Ga-As along the bond and along lines parallel to it in the plane containing a neighbouring bond at either end are shown in Fig. 4.2.

The values of the six parameters $D_1^s = (D_1^A + D_1^C)/2$, $D_1^a = (D_1^A - D_1^C)/2$, $D_2^{P(A)}$, $D_2^{P(C)}$, $D_2^{NP(A)}$ and $D_2^{NP(C)}$ computed above for the six III-V semiconducting materials considered in the last chapter are tabulated in Table 4.1, along with the corresponding parametrically fitted values for comparison.

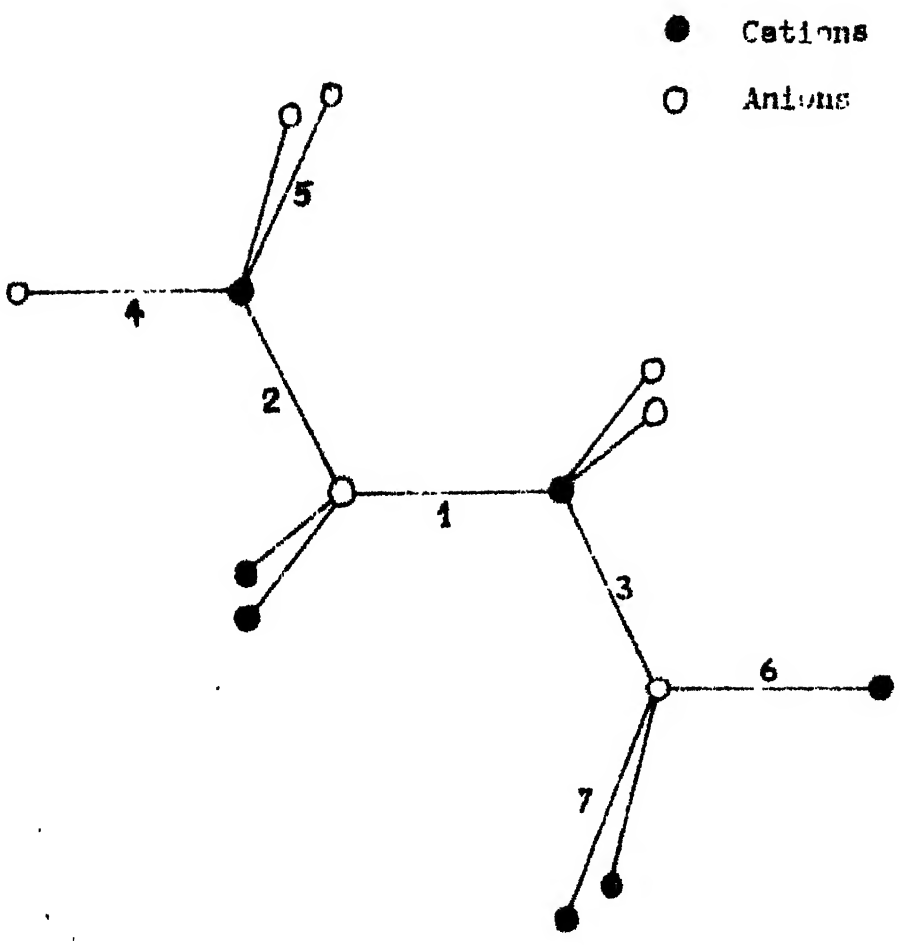

Fig. 4.1: The neighbourhood of a bond for III-V Semiconductors.

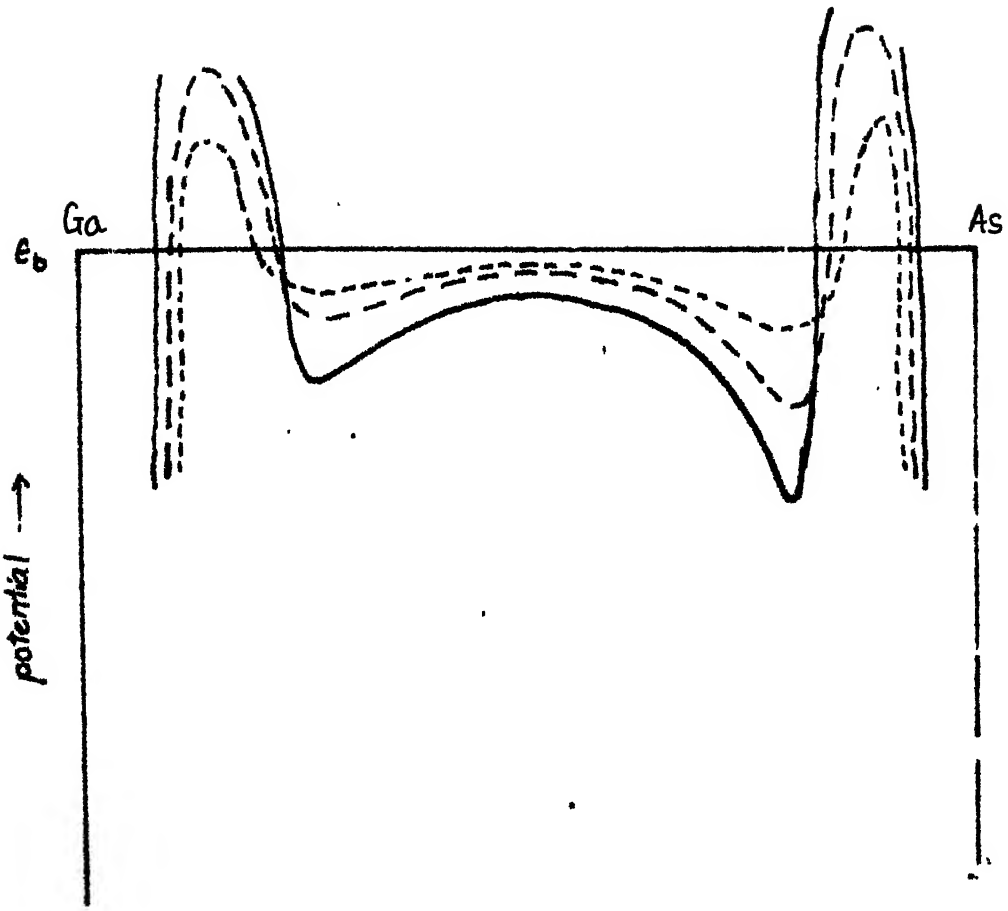

along bond

displaced by 0.1 of bond length

displaced by 0.2 of bond length

Fig. 4.2: Bond potentials for GaAs along the bond and along lines parallel to the bond at a distance 0.1 and 0.2 of the bond length, in the plane containing a neighbouring atom at either end.

Table 4.1: Comparison of Parameters Obtained by Chemical Bond Pseudopotential with those Obtained by Fitting.

P : Pseudopotential F : Fitting

		D_1^s	D_1^a	$D_2^{P(A)}$	$D_2^{P(C)}$	$D_2^{NP(A)}$	$D_2^{NP(C)}$
GaAs	P	-1.4192	-0.2801	0.5291	-0.2945	-0.0878	0.0968
	F	-1.5187	-0.4250	0.3406		-0.1094	
InAs	P	-1.2482	-0.3108	0.4570	0.2163	0.1189	-0.0916
	F	-1.3937	-0.5125	0.3844		-0.0656	
GaSb	P	-0.8963	0.0421	0.3716	0.2324	-0.0258	-0.0256
	F	-1.2687	-0.3750	0.3906		-0.0594	
InSb	P	-0.7960	-0.0324	0.2397	0.1571	-0.0455	0.0049
	F	-1.3500	-0.3875	0.2937		-0.0563	
GaP	P	-0.5863	0.2030	0.1197	-0.0457	0.1620	-0.0288
	F	-1.3625	-0.3250	0.3812		-0.1188	
InP	P	-0.7393	0.0525	0.1440	0.2098	-0.0747	-0.0589
	F	-1.3125	-0.4125	0.2625		-0.0375	

The parameter that essentially gives the 'spread' to the bands is the symmetric combination $D_1^s = (D_1^A + D_1^C)/2$. The values obtained from chemical bond pseudopotentials are smaller than the corresponding fitted parametric values. Otherwise there is no other systematic trend. The parameter $D_1^a = \frac{1}{2}(D_1^A - D_1^C)$, which measures the asymmetry between the cation and anion composing the III-V semiconductor, is obtained of different signs for different materials. This feature is to be expected but is absent in the values tested by Chen and Sher.

If interactions upto first nearest neighbouring bonds only were retained, the sign of D_1^a would not alter the eigenvalue spectrum (See Sec.3.2.5) but when interactions between mere distant bonds are taken into account, the sign of H_1^a becomes important. Since the pseudo Hamiltonian is non-hermitian, the matrix elements between second nearest neighbouring parallel and non-parallel bonds each are of the two kinds. For the purpose of the calculation, the symmetric combinations $D_2^{P(s)}$ and $D_2^{NP(s)}$ are used to define an approximate hermitian Hamiltonian, and the eigenvalue spectrum evaluated therefrom.

Fig. 4.3 shows the band structures and the density of states of GaAs and InAs as obtained by using the fitted parameters and those obtained from chemical bond pseudopotential parameters.

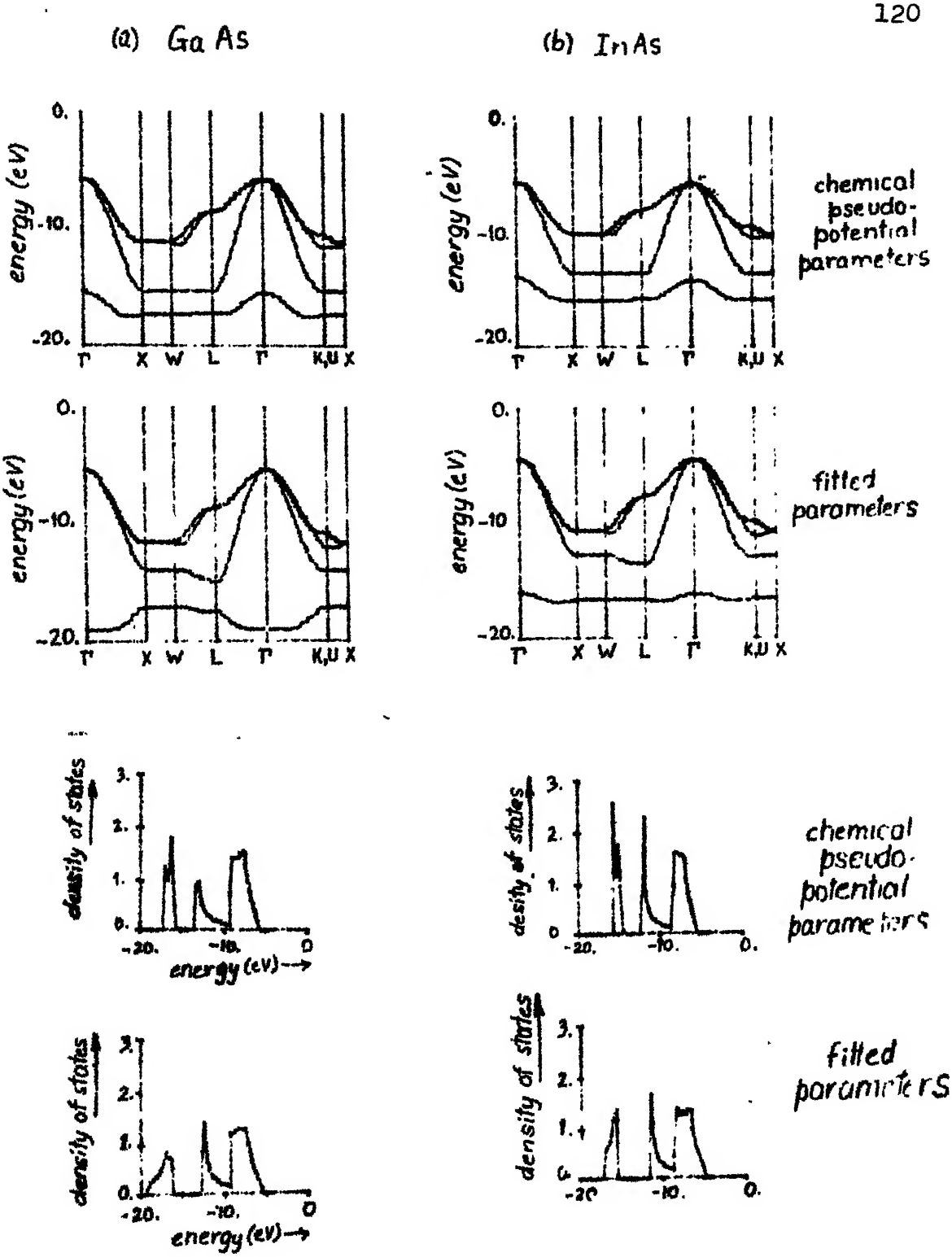

Fig. 4.3: Band structures and density of states per bond in units of π^{-1} for (a) GaAs and (b) InAs from (i) Chemical pseudopotential parameters and (ii) the fitted parameters.

The principal difference is in the lower s-like band. In the LΓK and XΓX sectors the branch is convex towards Γ in the fitted parameters, but concave in the chemical pseudopotential method, giving rise to (a) a much diminished gap between the s-like and p-like states, and (b) a contraction of the total band width. The upper branches are not very dissimilar.

It must be emphasized, as in Bullett (1975) that the chemical pseudopotential method, at least in the relatively crude, non-selfconsistent calculation is quantitatively inferior to the fitted parameters. But it is a starting point of an ab initio derivation of the energy spectrum, taking into account the non-orthogonality of the basis. This is an important factor, in case there are a variety of different experimental results and we are not sure which we should select for our fitting.

4.4 CCPA Calculation Using the Chemical Bond Pseudopotential Parameters:

The cluster-CPA calculation has been made again, now using the chemical bond pseudopotential parameters. The VCA and the 1-CPA density of states per bond times π and $-\mathrm{Im}\,\Sigma$ and $\mathrm{Re}\,\Sigma$ along the real Z axis for $Ga_x\,In_{1-x}\,As$ for $x = 0.1$, 0.3, 0.5, 0.7, 0.9 are shown in Fig. 4.4. The one bond cluster C_1, the four bond clusters C_4 and $C_{4'}$ with one and

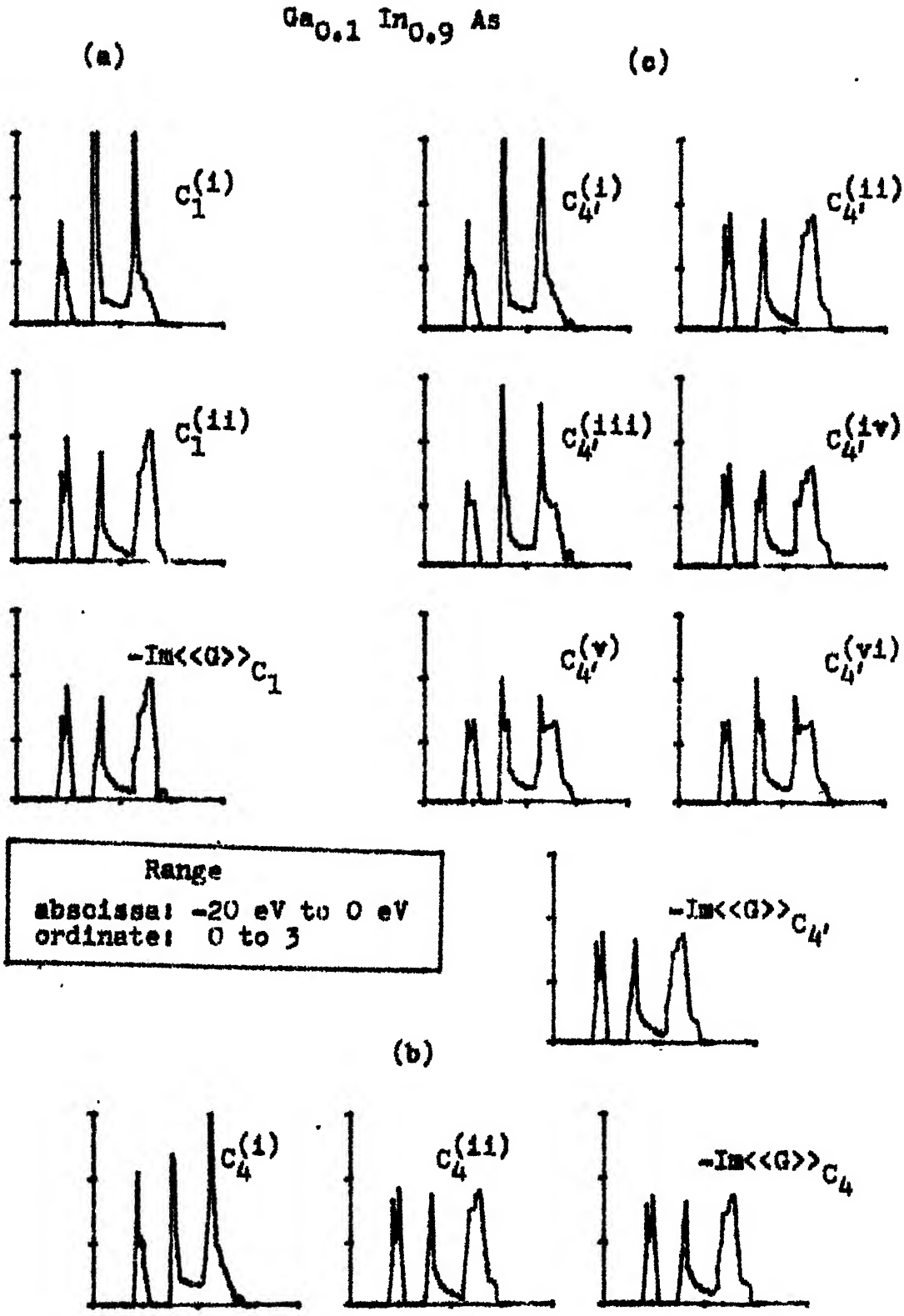

Fig. 4.3 (a), (b) and (c) continued.

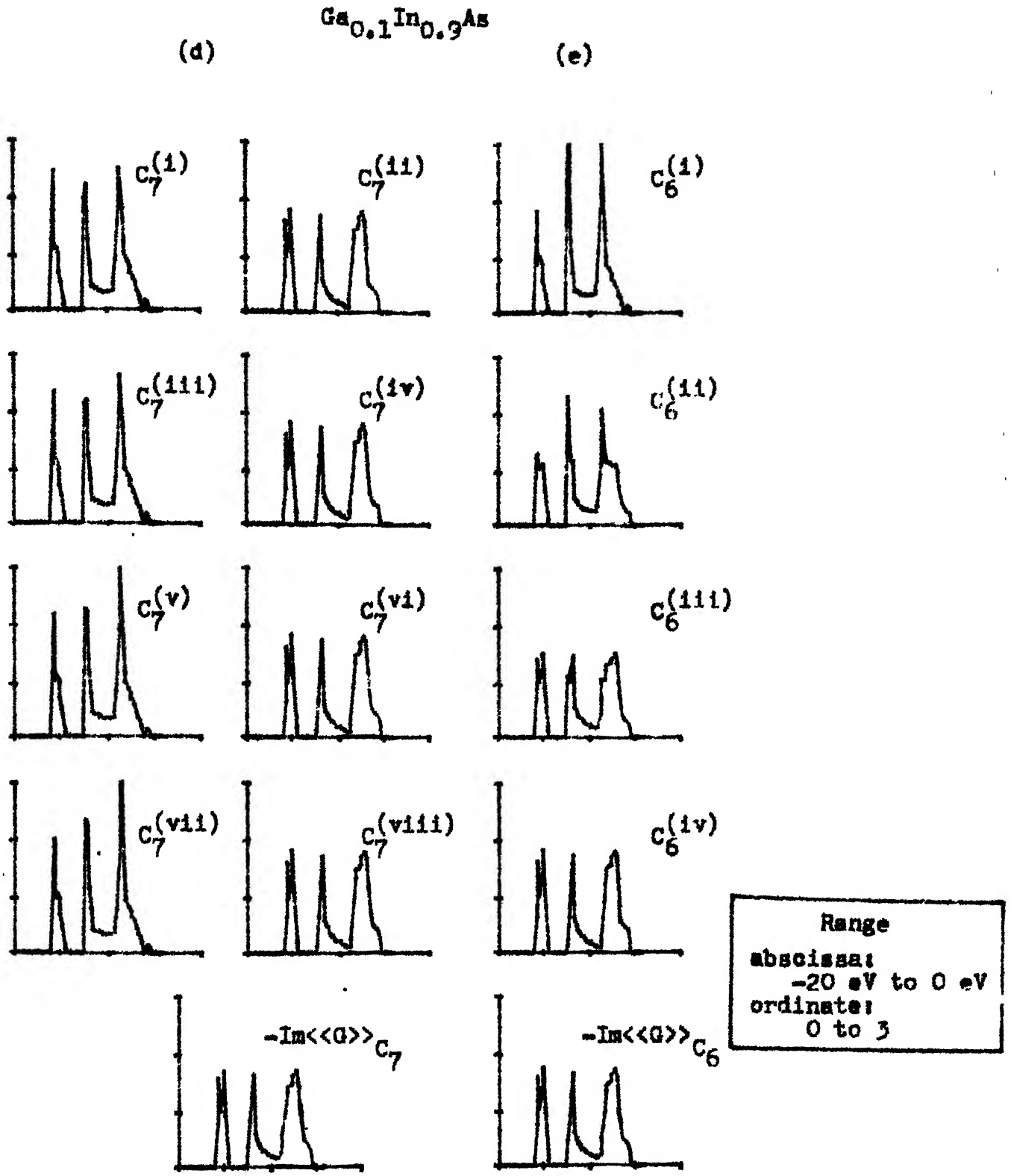

g. 4.5: Density of electron states per bond in units of π^{-1} (-Im G) for the alloy $Ga_{0.1}$ $In_{0.9}$ As corresponding to each configuration (Fig. 3.7(a) to (e)) of the clusters (a) C_1 (b) C_4 (c) C_4, (d) C_7 and (e) C_6 and those averaged over configurations of each cluster, using

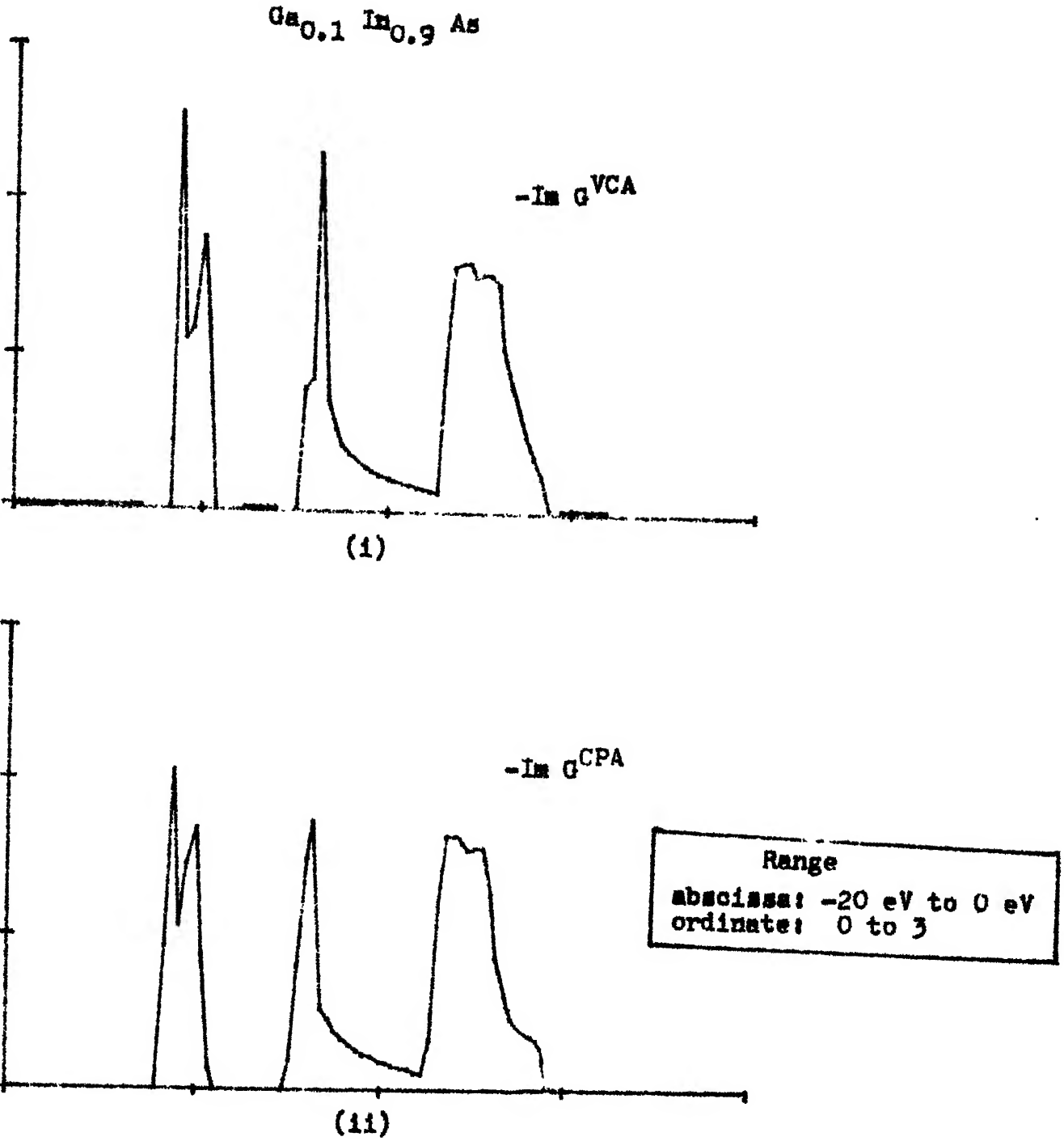

Fig. 4.6: (i) $-Im\ G^{VCA}$ and (ii) $-Im\ G^{CPA}$ for $Ga_{0.1}$ $In_{0.9}$ As using chemical bond pseudopotential parameters.

$Ga_{0.1}\ In_{0.9}\ As$

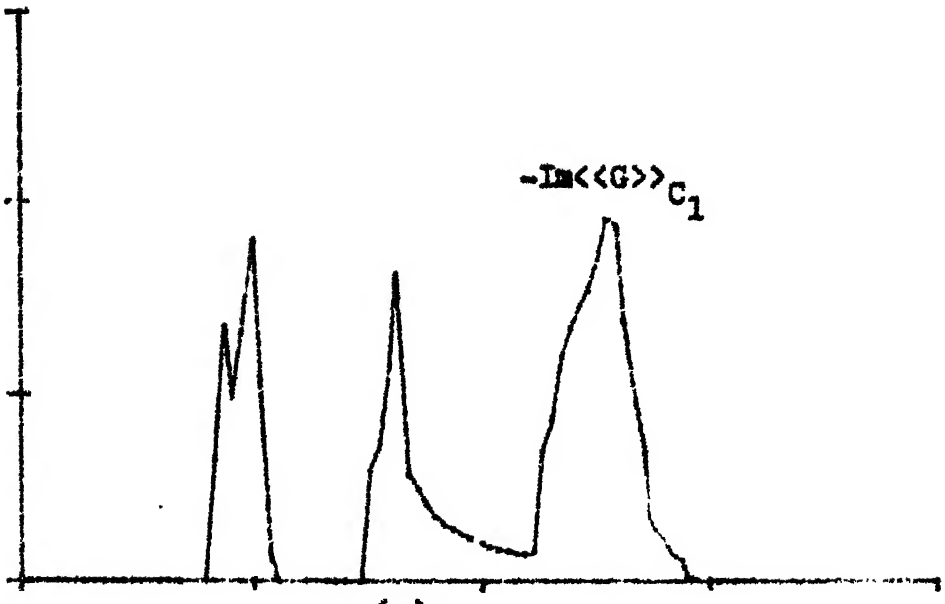

(a)

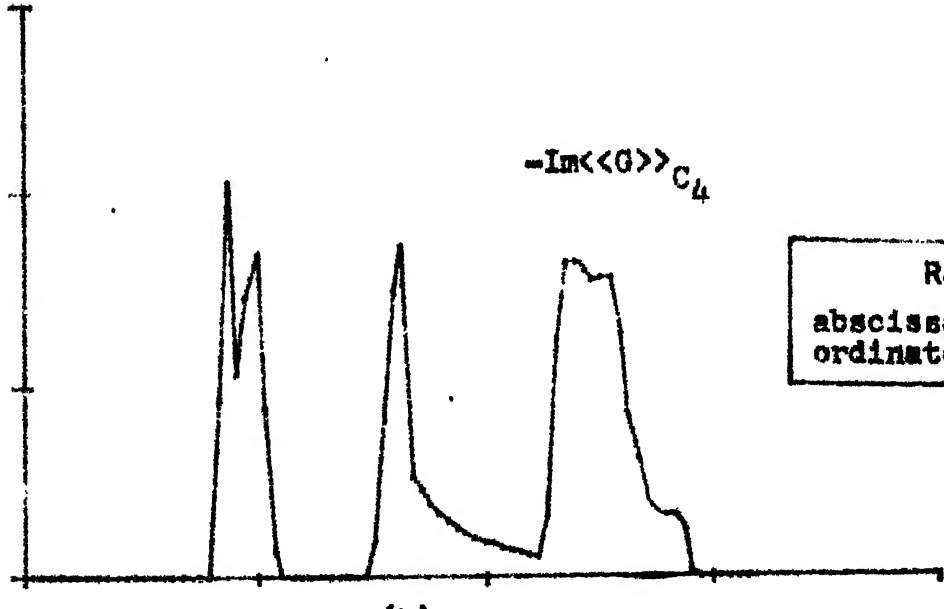

Range
abscissa: -20 eV to 0 eV
ordinate: 0 to 3

(b)

Fig. 4.7 (a) and (b) continued.

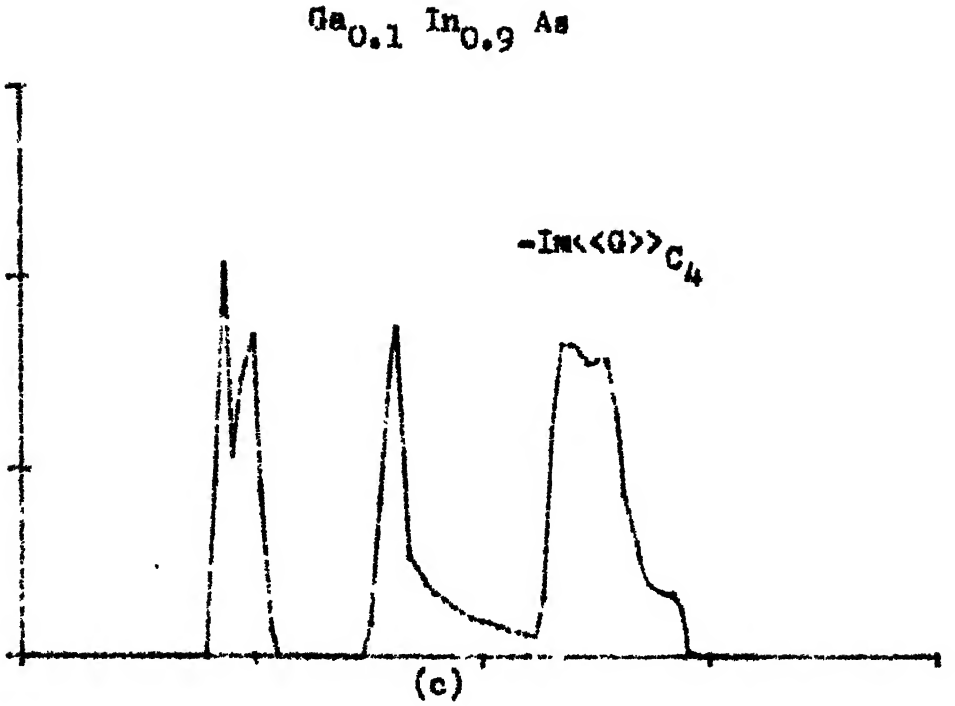

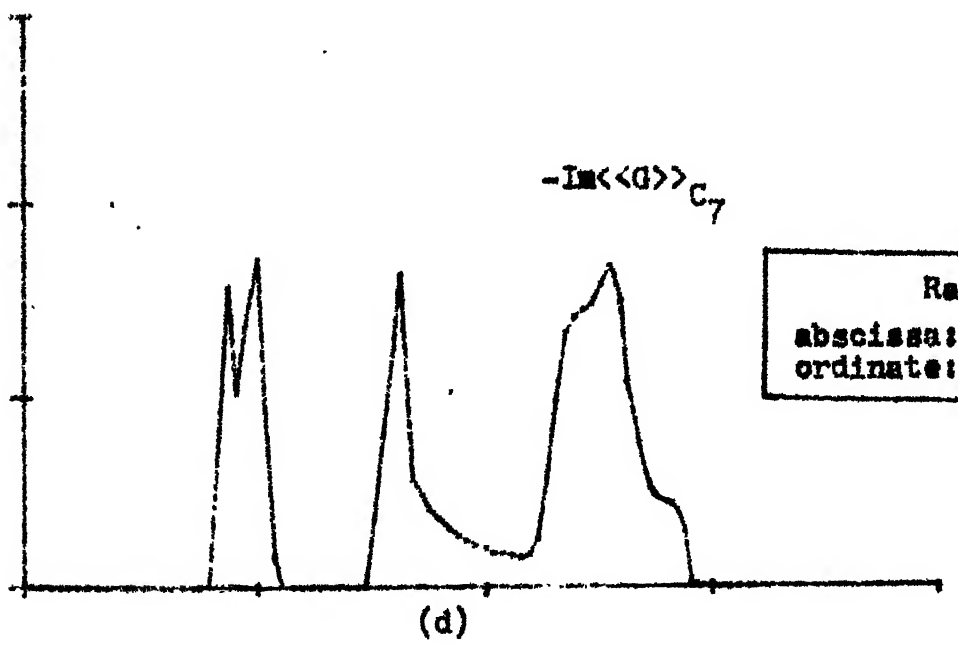

Fig. 4.7 (c) and (d) continued.

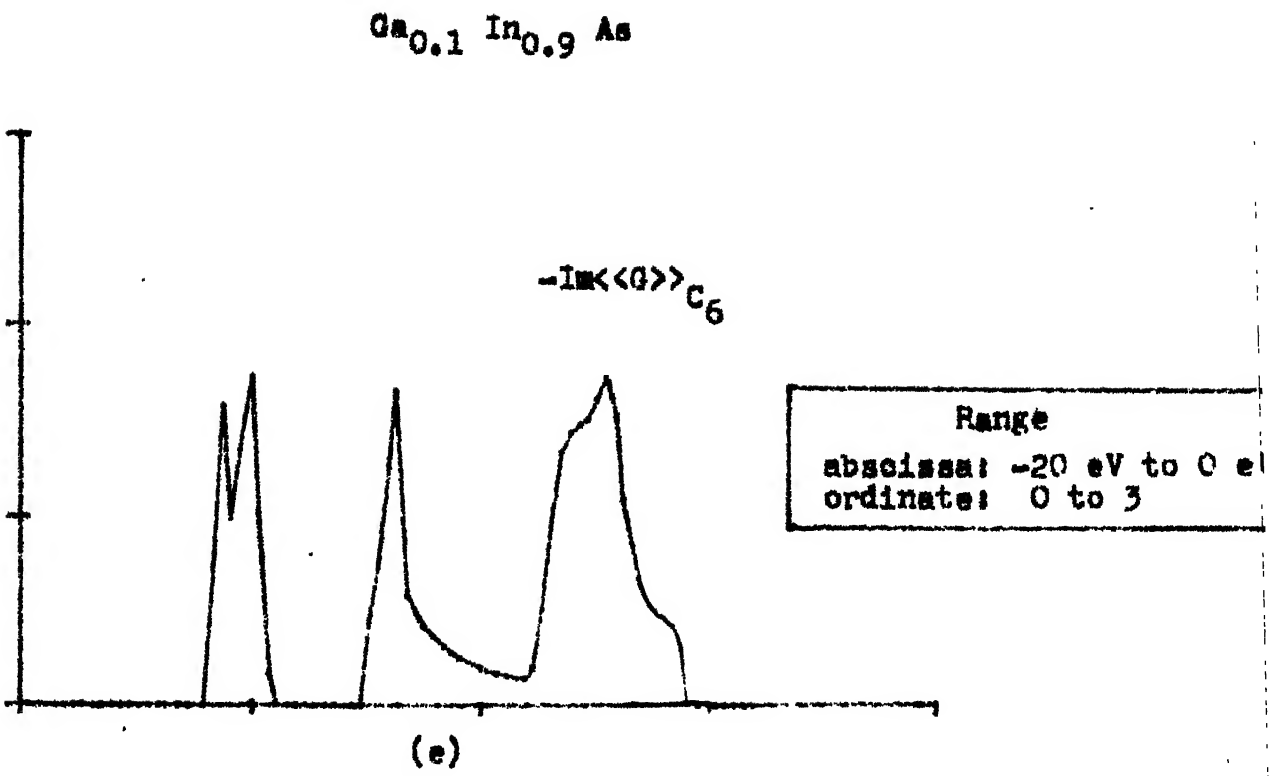

Fig. 4.7: (a) $-Im\langle\langle G\rangle\rangle_{C_1}$, (b) $-Im\langle\langle G\rangle\rangle_{C_4}$, (c) $-Im\langle\langle G\rangle\rangle_{C_4}$, (d) $-Im\langle\langle G\rangle\rangle_{C_7}$ and (e) $-Im\langle\langle G\rangle\rangle_{C_6}$ for $Ga_{0.1}$ $In_{0.9}As$ using chemical bond pseudopotential parameters.

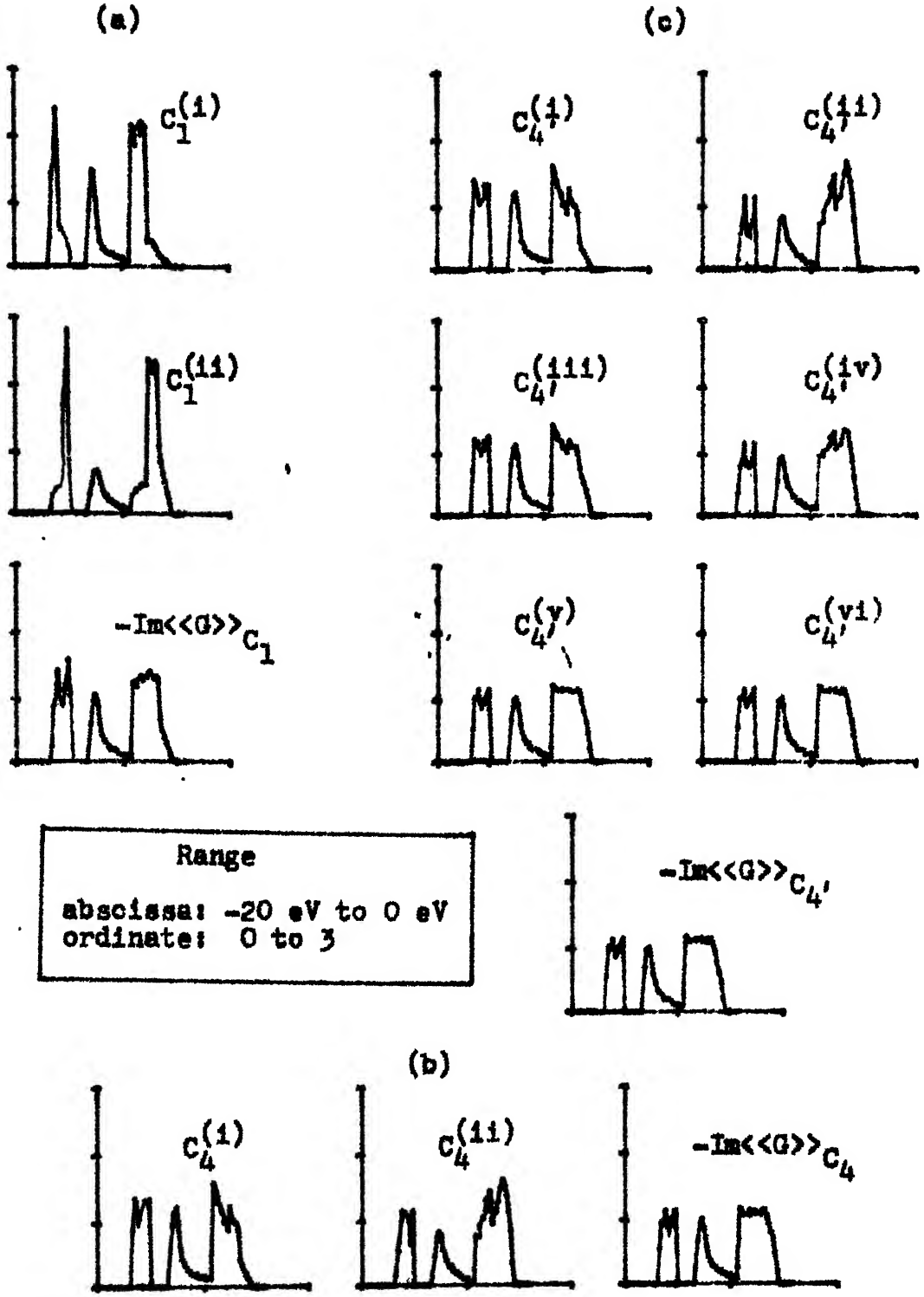

Fig. 4.8 (a), (b) and (c) continued.

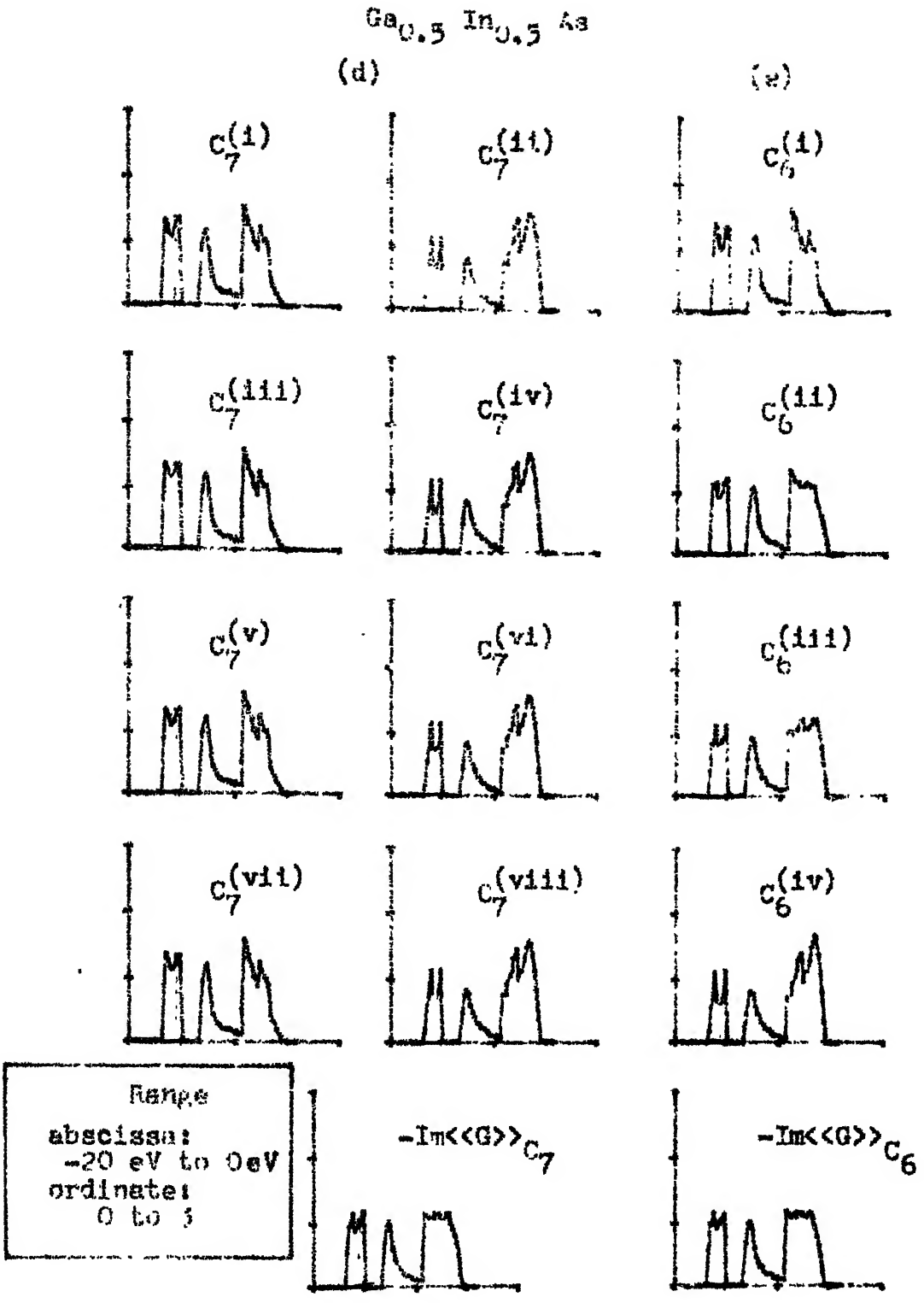

Fig. 4.3: Density of electron states per bond in units of π^{-1} ($-Im\ G$) for the alloy $Ga_{0.5}$ $In_{0.5}$ As corresponding to each configuration (Fig. 3.7(a) to (e)) of the clusters (a) C_1 (b) C_4 (c) C_4' (d) C_7 and (e) C_6 and those averaged over configurations of each cluster, using

$Ga_{0.5}\ In_{0.5}\ As$

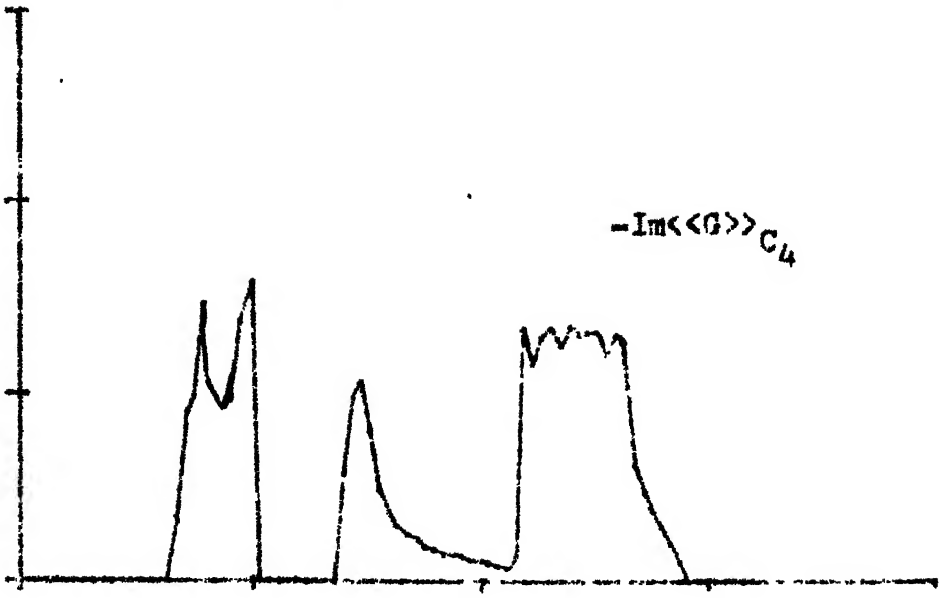

(c)

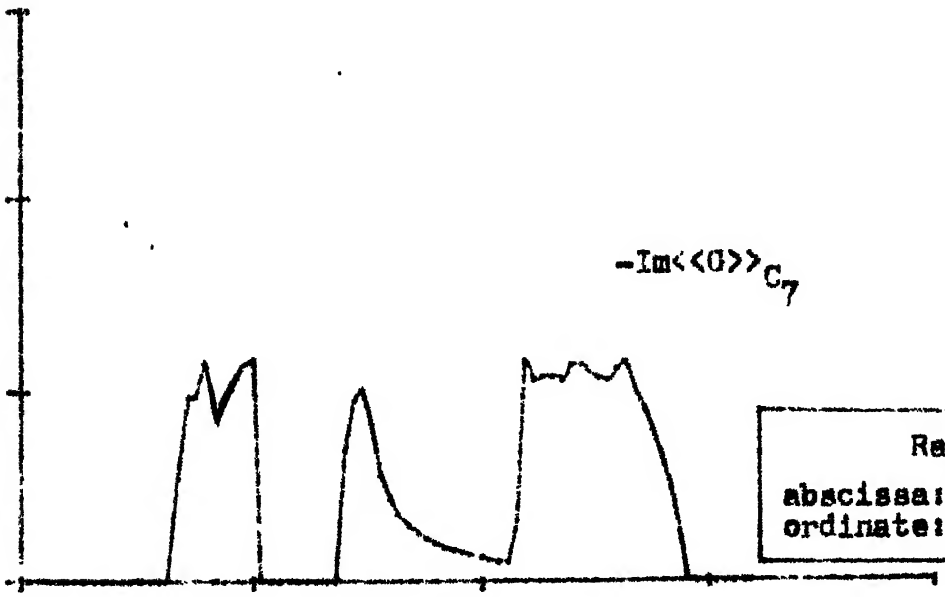

(d)

Fig. 4.10 (c) and (d) continued.

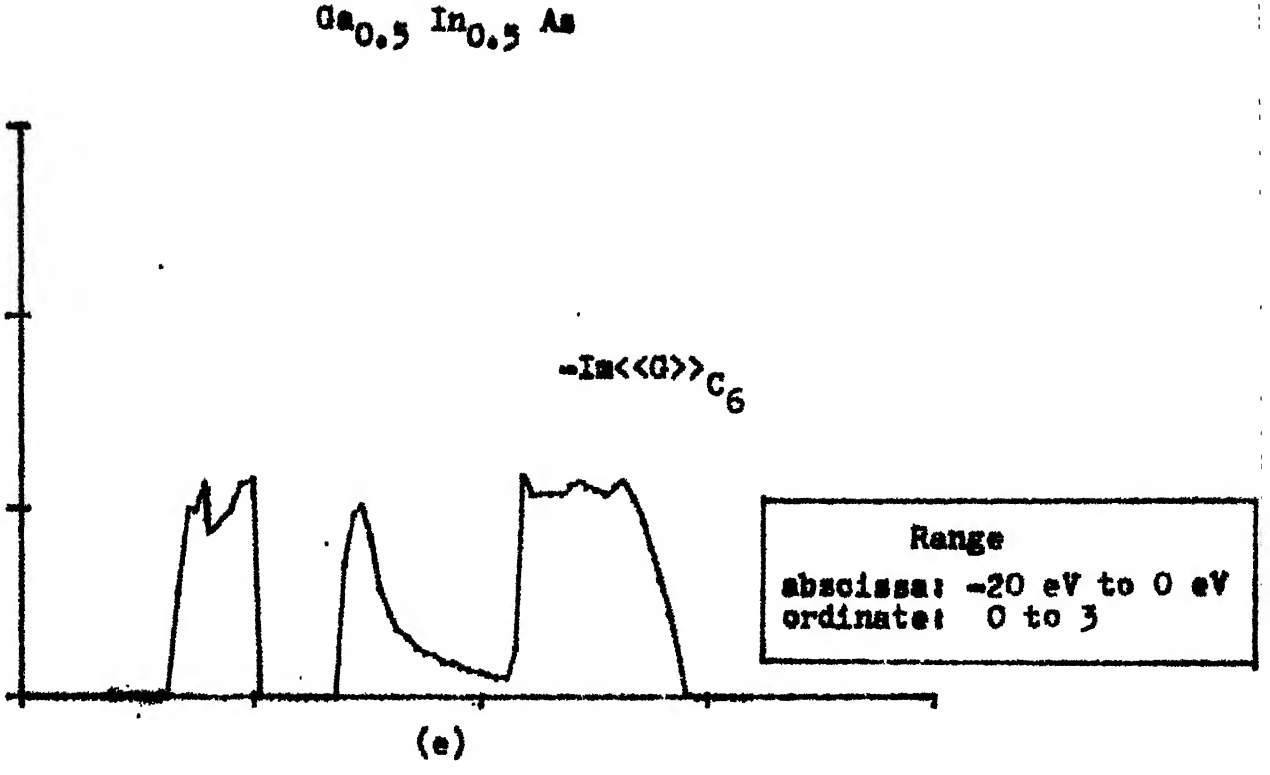

Fig. 4.10: (a) $-Im\langle\langle G\rangle\rangle_{C_1}$, (b) $-Im\langle\langle G\rangle\rangle_{C_4}$, (c) $-Im\langle\langle G\rangle\rangle_{C_4}$, (d) $-Im\langle\langle G\rangle\rangle_{C_7}$ and (e) $-Im\langle\langle G\rangle\rangle_{C_6}$ for $Ga_{0.5}$ $In_{0.5}$ As using chemical bond pseudopotential parameters.

4.5 Conclusions:

In conclusion it must be said that despite the simplicity of the definition of the bond pseudopotentials, the "Wigner trick" and the free atom self-consistent orbital wave functions and potential functions used, the results are highly satisfactory. The main achievement being that arbitrariness involved in a parametric fitting with experimental results, which considerably differ among themselves, has been by-passed. The only parameter used in the application of the chemical pseudopotential scheme above that has its source in experimental results is the bond energy with respect to the vacuum state. The part of this which is the work function, is a parameter obtained very easily by a simple experimental set-up for the photoelectric effect. Hence its value is reliable. The "bond energy" is a parameter that enters every local chemical bonding behaviour of atoms and is, therefore, well known.

CHAPTER V

LOCALISATION

5.1 Introduction:

The question of the nature of electron states in a disordered system is now tackled. Unlike the extended Bloch-type wave functions in crystals or ordered systems in general, Anderson (1958) first demonstrated the presence of non-diffusive ie localised electronic states. For a simple tight-binding model Hamiltonian with diagonal disorder and nearest-neighbour interactions only (now known as the Anderson Hamiltonian) he considered the evolution of an electron initially in one of the tight-binding basis states. In case of an ordered system, the electron would eventually diffuse over the entire system and the amplitude of the final state at the original site would become vanishingly small. He showed that for some minimum degree of disorder (measured, say, by the width of the probability distribution of the random members on the diagonal of the Hamiltonian matrix), the amplitude at the site of origin becomes definitely (i.e. with probability = 1) finite. After some controversy over this work of Anderson (Ziman 1969, Lloyd 1969, Brouers 1970) localisability became an established fact (Thouless 1970, Anderson 1970, Mott 1970). For various models of one-

dimensional systems, Ishii (1973) has shown that any finite amount of disorder makes all the states localised.

On making a more detailed examination, Mott (1967, 1968) introduced the idea of sharp mobility edges separating the localised and the extended states in the bands, and showed plausibly, that as disorder is increased, these mobility edges move into the bands, until these meet. He termed this the Anderson transition , i.e. when all states become localised. The same picture was also later arrived at by Cohen, Fritsche and Ovshinsky (1969) in their model for amorphous semi-conducting alloys. Now known as the Mott-CFO model, it is consistent with Lifshitz's (1964) arguments concluding that for mild disorder, band edges tail and a finite portion of the band near the edges consists of localised states.

Economou and coworkers (1970a, 1970b, 1972) define a "localisation function"to locate the mobility edges and obtain the above movement of the mobility edge with increase of disorder.

In this chapter a delocalisation criterion for the electronic states based on the size of the localisation domain in introduced and discussed. An averaged localisation length is obtained. Results are presented for weak disorder. Near the mobility edges, these are soluble, while near the band edge, numerical computation is required.

Mookerjee (1975) has examined the localisation criterion of Abou-Chacra et al (1973) and pointed out that the criterion involved quantities like $\langle|a_i(E)|\rangle$ where $a_i(E)$ are the tight binding amplitudes of the localised wave function $\psi(E, \vec{r})$ at the site $\vec{r}_i$. It was also indicated that a better criterion should rather involve quantities of the kind $\langle|a_i(E)|^2\rangle$ since it is these that are related to physical probabilities. In the localised regime, this implies the study of averaged size of the domain over which the wave function is localised. This is related to the 'localisation length'. Such a study would have two-fold significance: firstly, we take as our delocalisation criterion, the probabilistic divergence of the localisation domain, and thus determine the mobility edge E_c as a function of the disorder parameter. This study has already been reported by Kumar et al (1975) for the weak disorder limit. We shall also indicate the analysis in the case when disorder is larger, leading to Anderson transition. Secondly, in the localised regime, we can look at the behaviour of the averaged size of the localisation domain and the way in which it diverges as $E \to E_c$. The size of a localised state is an important parameter that enters expressions for various physical properties, for instance, phonon-assisted hopping conduction. (Austin and Mott 1969). This calculation of the averaged inverse size of the localisation domain will form the bulk

of this present work. We shall present results for the weak disorder limit.

5.2 Preliminary Formulation:

Let us follow Anderson (1958) in conducting a hypothetical experiment. Suppose at $t = 0$, we place an electron at the site r_o and look at the probability it is there at $t \to \infty$. This probability

$$P_o = \int_{-\infty}^{+\infty} dE \lim_{\eta \to 0^+} \frac{\eta}{\pi} |G_{00}(E + i\eta)|^2 \qquad (5.1)$$

$G_{00}(Z)$ is a representation of the resolvent $(ZI - H)^{-1}$ of the Anderson Hamiltonian $\underline{H} = \sum_i \varepsilon_i \underline{P}_i + \sum_{i,j} \underline{V}_{ij} \underline{T}_{ij}$ and can be expressed as a Feenberg perturbation series (Feenberg 1948),

$$G_{00}(Z) = \sum_{n=1}^{\infty} \sum_{Q_n} V_{0i_1} G^{(0)}_{i_1 i_1} V_{i_1 i_2} G^{(0,i_1)}_{i_2 i_2} \cdots G^{(0,i_1,\ldots i_{n-1})}_{i_n i_n} V_{i_n 0} \qquad (5.2)$$

where Q_n are all non-intersecting paths of length n starting and ending at $\vec{r}_o$. Subscripted index indicates that the vertex is deleted and the Green's function is calculated on the resulting subgraph.

We may now introduce the Cayley Tree Approximation (CTA) in two ways. Graphically, we may think of it as delinking all closed non-intersecting paths, i.e. ignoring contributions of all such paths to Green's function. As an example, in the exact lattice, there was a contribution $V_{01}\, G_{11}^{(0)}\, V_{12}\, G_{00}^{(01)}\, V_{23}\, G_{33}^{(012)}\, V_{30}$ as shown in Fig. (5.1). On delinking, such a contribution is absent.

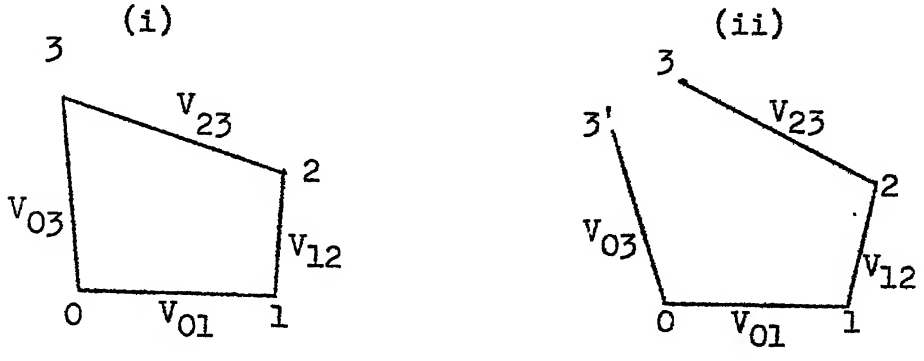

Closed 'path' Delinked 'path'

Fig. 5.1: An example of a 'path' (i) in the exact lattice and (ii) in the Cayley Tree Approximation, obtained by delinking.

A study of Eqn. (5.2) shows that apart from the $n = 1$ and $n = 2$ terms, all the rest comes from such closed non-intersecting paths. Equivalently, the CTA may be thought of as truncating the Feenberg series after $n = 2$. The latter view has been taken by Abou Chacra et.al. (1973). The first view point perhaps gives some insight into the electron diffusion experiment. An electron on a Cayley

Suppose K is the connectivity of our Cayley tree. Then the self energies have the following simple relationships.

$$\sigma_0(Z) = \sum_{j\varepsilon N_0}^{(K+1)} \frac{V^2}{Z-\varepsilon_j-\sigma_j(Z)} ,$$

$$\sigma_j(Z) = \sum_{k\varepsilon N_j}^{(K)} \frac{V^2}{Z-\varepsilon_k-\sigma_k(Z)} \qquad (5.4)$$

If $Z = E + i\eta$ $(\eta > 0)$ and $\sigma_j = E_j + i\Delta_j$,

$$E_j(Z) = \sum_{k\varepsilon N_j} \frac{V^2(E-\varepsilon_k-E_k)}{(E-\varepsilon_k-E_k)^2 + (\eta+\Delta_k)^2} , \text{ and}$$

$$\Delta_j(Z) = \sum_{k\varepsilon N_j} \frac{V^2(\eta + \Delta_k)}{(E-\varepsilon_k-E_k)^2 + (\eta + \Delta_k)^2}$$

Now let $\eta \to 0^+$. In the localised regime, $\Delta_j/\eta \to l_j$ and $\Delta_k \to 0$, except on a set of points of measure zero. If we replace all equalities with almost equality (almost $\equiv$ except on a set of points of measure zero), then

$$E_j = \sum_{k\varepsilon N_j} \frac{V^2}{(E-\varepsilon_k-E_k)} \qquad (5.5a)$$

$$l_j = \sum_{k\varepsilon N_j} \frac{V^2(1+l_k)}{(E-\varepsilon_k-E_k)^2} \qquad (5.5b)$$

Note that while $-\infty < E_j < \infty$, $0 < l_j < \infty$ because of herglotzicity of $\sigma(Z)$. Assume now that E's and l's on

either side of the equation have identical distributions, and make the substitution

$$X = \frac{V^2}{x} , \qquad Y = \frac{V^2 y}{x^2}$$

where, $E - \varepsilon_k - E_k = x$

$$l + l_k = y$$

which implies that $f(x) = E-\varepsilon_k-x = E_k$, and

$$g(y) = y-l = l_k$$

Now, if $G(x, y)$ is the probability density of x, y and $F(E_k, l_k)$ is that of E_k, l_k, then

$$G(x, y) = \int_{-\infty}^{+\infty} d\varepsilon_k \int_{-\infty}^{+\infty} dE_k \int_{0}^{\infty} dl_k \, F(E_k, l_k)$$

$$\delta[E_k - f(x)] \, \delta[l_k - g\, y)] \, p(\varepsilon_k)$$

$$= \int_{-\infty}^{+\infty} d\varepsilon_k \, F(E-\varepsilon_k-x;\, y-1) \, p(\varepsilon_k)$$

So, $$G(X, Y) = \int_{-\infty}^{+\infty} d\varepsilon_k \, F\left(E-\varepsilon_k - \frac{V^2}{X}, \frac{YV^2}{X^2} - 1\right) \frac{V^4}{X^4} \, p(\varepsilon_k)$$

Then (5.5a) and (5.5b) give,

$$\tilde{F}(k, s) = [G(k,s)]^K \quad \text{and}$$

$$\tilde{F}_0(k, s) = [G(k,s)]^{K+1} \tag{5.6}$$

that is,

$$\tilde{F}_0(k,s) = [\tilde{F}(k,s)]^{(K+1)/K}$$

where $\tilde{F}(k, s)$, $\tilde{F}_0(k, s)$ and $G(k, s)$ are the Fourier-Laplace transforms of $F(E_j, l_j)$, $F_0(E_0, l_0)$ and $G(X, Y)$ respectively. These yield the integral equation,

$$\tilde{F}(k, s) = \{ \frac{1}{2\pi} \int_{-\infty}^{+\infty} dx \int_{-\infty}^{+\infty} dk' \, \tilde{p}(k') \, \tilde{F}(k', \frac{sV^2}{x^2}) \exp [-ik'(E-x) - \frac{ikV^2}{x} - \frac{sV^2}{x^2}] \}^K \qquad (5.7)$$

where $\tilde{p}(k)$ is the Fourier transform of $p(\varepsilon)$.

We shall attempt a solution of the type,

$$\tilde{F}(k, s) = \tilde{f}(k, \{x_r\}) \, \tilde{P}(s, \{x_r\}) \qquad (5.8)$$

Here $\{x_r\}$ denotes a set of parameters describing the probability density of E_j. We note that the probability density of E_j can be obtained directly from (5.5a). It is not affected by the probability density of l_j which is why we have kept $\tilde{f}(k)$ independent of the parameters describing $P(l_j)$. On the other hand, the variables l_j and E_j are dependent. So $P(l_j)$ can be affected by the probability density of E_j. This is the assumption involved in writing $\tilde{F}(k, s)$ as in (5.8). The assumption does not imply the statistical independence of E_j and l_j. It is an approximation none-the-less. Examine the particular form taken for $\tilde{F}(k,s)$,

$$\tilde{F}(k, s) = \tilde{f}(k) \, \tilde{P}(s) \qquad (5.9)$$

for $p(k) = e^{-\gamma \mathrm{sgn}(k)\, k}$

try $\tilde{f}(k) = \exp\left[-iZ_r k - Z_i\, s(k)\, k\right]$

$\tilde{P}(s) = \exp\left[-as - bs^{\alpha}\right], \quad a > 0, \quad 0 < \alpha < 1$

as a solution. It is clear from the solution that a, α, b are functions of Z_i, Z_r. However, we are also assuming here a and b to be independent of k. Eventually we need only a(k =0), b (k = 0) but a(k), b(k) will satisfy integral equations similar to AAT equations (Abou Chacra et.al. 1973) for which a full knowledge of a(k), b(k) for all k's is required, in order to solve for a(k = 0), b(k = 0). The exact import of this approximation is still unclear. However, it is not as drastic as assuming E_j, l_j to be completely statistically independent, neither is it the severe upper limit approximation.

Suppose $p(\varepsilon_k)$ has a Cauchy distribution $\dfrac{\gamma/\pi}{\varepsilon_k^2 + \gamma^2}$ and try the solution,

$$\tilde{f}(k) = e^{-iZ_r k - Z_i\, \mathrm{sgn}\,(k)\, k}$$

then (7) gives for s = 0,

$$e^{iZ_r k - Z_i \mathrm{sgn}(k) k} = \left[\frac{1}{2\pi} \int_{-\infty}^{+\infty} dx \int_{-\infty}^{+\infty} dk' \exp\left(-ikV^2/x\right) \exp\left[-\ \mathrm{sgn}\,(k') - iZ_r - Z_i\, \mathrm{sgn}(k') + i(E-x)\right] k'\right]^K$$

$$= \{\frac{1}{2\pi} \int_{-\infty}^{+\infty} dx \; \frac{2(\gamma + Z_i)}{(E-Z_r-x)^2 + (\gamma+Z_i)^2}$$

$$\exp\,[-ikV^2/x]\}^K$$

Therefore,

$$Z_r + iZ_i = \frac{KV^2}{(E - Z_r) - i(\gamma + Z_i)} \tag{5.10}$$

Again, for k = 0 (5.7) gives

$$\tilde{P}(s) = \{ \int_{-\infty}^{+\infty} \frac{(\gamma+Z_i)/\pi}{(E-Z_r-x)^2 + (\gamma+Z_i)^2} \; \tilde{P}\,(\frac{sV^2}{x^2})$$

$$\exp\,(-\frac{sV^2}{x^2})\}^K \tag{5.11}$$

If $\tilde{F}_0(k, s) = \tilde{f}_0(k)\,\tilde{P}_0(s)$, then from (5.6)

$$\tilde{f}_0(k) = [\tilde{f}(k)]^{(K+1)/K}$$

and

$$\tilde{P}_0(s) = [\tilde{P}(s)]^{(K+1)/K}$$

Because of the factor $\exp\,(-\frac{sV^2}{x^2})$, the integral in (5.11) cannot be carried out in the usual manner. If we want to study the case for any value of the disorder parameter then $\tilde{P}(s)$ must be numerically solved from (5.11) and then $\tilde{P}_0(s)$ obtained from (5.12).

5.4 The Weak Disorder Limit:

If $(\gamma + Z_i) \ll 1$, then

$$\frac{(\gamma+Z_i)/\pi}{(E-Z_r-x)^2 + (\gamma+Z_i)^2} \simeq \delta(E-Z_r-x) + O(\gamma^2)$$

Neglecting the subsequent terms is equivalent to evaluating the integral in (5.11) by the steepest descents approximation. In this approximation, (5.11) reduces to

$$\tilde{P}(s) = \exp\left(-\frac{KSV^2}{(E-Z_r)^2}\right)\left\{\tilde{P}\left[\frac{SV^2}{(E-Z_r)^2}\right]\right\}^K \qquad (5.13)$$

Let,

$$\tilde{P}(s) = e^{-as}\,\tilde{Q}(s)$$

substituting this in (5.13), we have

$$a = \frac{KV^2}{(E-Z_r)^2 - KV^2} \qquad (5.14)$$

if

$$\tilde{Q}(s) = \left\{\tilde{Q}\left[\frac{SV^2}{(E-Z_r)^2}\right]\right\}^K \qquad (5.15)$$

If $Q(x)$ is the Laplace inverse of $\tilde{Q}(s)$, then (5.15) shows that it must be a stable, infinitely divisible distribution (Gredenko and Kolmogorov, 1954). Further, since we must have $Q(x) = 0$ for $x < 0$, an approximate form for $Q(s)$ is $\exp\left(-s^\alpha \operatorname{Sec}\frac{\pi\alpha}{2}\right)$, $0 < \alpha < 1$.

Substituting this in (5.15) we obtain,

$$(E - Z_r)^{2\alpha} = KV^{2\alpha}$$

therefore,

$$\alpha = \frac{1}{2}\,\frac{\ln K}{\ln\left(\frac{E-Z_r}{V}\right)} \qquad (5.16)$$

Hence (5.12) gives,

$$\tilde{P}_0(s) = \exp\left[-a_0 s - \frac{K+1}{K}\left(\text{Sec}\,\frac{\pi\alpha}{2}\right) s^{\alpha}\right],$$

$$a_0 = \frac{K+1}{K}\, a$$

The required probability density of L then is

$$P_0(y) = Q_0\,(y - a_0)$$

where,

$$Q_0(y) = \frac{1}{2\pi i}\int_{\lambda-i\infty}^{\lambda+i\infty} \exp\left[ys - \frac{K+1}{K}\,\text{Sec}\,\frac{\pi\alpha}{2}\, s^{\alpha}\right] ds \qquad (5.17)$$

Once $Q_0(y)$ is known from here, we can calculate,

$$\langle L^{-1}\rangle = \int_0^{\infty} \frac{1}{1+y}\, Q_0\,(y - a_0)\, dy$$

$$= \int_0^{\infty} \frac{1}{y+a_0+1}\, Q_0(y)\, dy \qquad (5.18)$$

Equations (5.10) and (5.14) give the mobility edge. If $a \to \infty$, since $P_0(y) = 0$ for $y < a$, the domain size diverges in probability. This happens as,

$$(E_c - Z_r)^2 = KV^2$$

which, for $\gamma \ll 1$ gives,

$$E_c = 2\,K\,V - (\sqrt{}KV)^{1/3}\,\gamma^{1/3} \text{ (Kumar et al, 1975)}$$

Thus $E_c \to E_b$ as $\gamma \to 0$, correctly, as opposed to the AAT limit. The new criterion involving $\langle |a_i(E)|^2 \rangle$ has the edge over the other.

Let us examine the form $\tilde{Q}_0(s) = \exp\left[-\frac{K+1}{K} \operatorname{Sec} \frac{\pi\alpha}{2}\, s^{\alpha}\right]$

(i) Since $\alpha < 1$, $-\frac{dQ_0(s)}{ds} = \alpha \frac{K+1}{K} s^{\alpha-1} Q_0(s) \operatorname{Sec} \frac{\pi\alpha}{2}$ as $s \to 0$, since $\alpha < 1$. That is, the average $\int_0^{\infty} y\, Q_0(y)\, dy$ does not exist, as remarked before. However $\langle 1/L \rangle$ exists and that is why we usually speak in terms of $\langle 1/L \rangle^{-1}$ rather than $\langle L \rangle$.

(ii) If $Q_0'(y)$ is the inverse Laplace transform of $Q_0'(s) = e^{-s^{\alpha}}$, $Q_0'(y)$ and $Q_0(y)$ have the same form except that the x-axis is scaled by a factor $(\frac{K+1}{K} \operatorname{Sec} \frac{\pi\alpha}{2})^{1/\alpha}$. This is apparent from (5.17) by changing the variable s to $(\frac{K}{K+1} \cos \frac{\pi\alpha}{2})^{1/\alpha} s'$. It is, therefore, enough to invert $e^{-s^{\alpha}}$ and then simply scale the inverse.

$$\langle L^{-1} \rangle = \int_{a_0}^{\infty} \frac{1}{y(\frac{K+1}{K} \operatorname{Sec} \frac{\pi\alpha}{2})^{1/\alpha} + a_0 + 1} Q_0'(y)\, dy \qquad (5.19)$$

Some $Q_0'(y)$ for E not very near E_c are shown in Fig. 5.2. They have similar shapes, reminiscent of Pearson curves. They are non-zero for positive arguments and have long tails. As $E \to E_c$, the curves peak near 1.0 and become narrow, but retain the tails caused by $0 < \alpha < 1$, although here the tails fall off faster.

(iii) When E is very near E_c, α becomes almost 1, and the $Q_0(y) \sim \delta(y-1)$, or, equivalently,

Fig. 5.3 shows the averaged inverse localisation length in the localised regime ($E_c < E < E_B$) for a very weakly disordered system, specified by $\Gamma = 0.01$. The points near E_c are evaluated from Eq. (5.20) while those near E_B are evaluated from Eq. (5.18) by integration. The linear divergence of the localisation domain E_c marks the sharp transition to extended Bloch type states in the interior of the band.

The mobility edges act as a band edge for transport properties depending upon mobile electrons in extended states. Gaps as measured by optical and electrical experiments do not tally for this reason. Phonon assisted hopping conduction (Austin, Mott 1969) is possible in the energy range $E_C < E < E_B$. This is distinguished from that due to extended electrons by the temperature dependence of the conductivity.

5.4 Conclusions:

A quantitative estimate of the averaged localisation length for weak disorder has been achieved. The linear divergence as the mobility edge is approached, is obtained as expected. Also, the mobility edge is located numerically.

In generalisating to strong disorders we are faced with a very difficult mathematical problem. The δ-function approximation to the Lorenzian has to be dropped and the non-linear integral equation cannot be reduced to a non-linear

algebraic one. The mathematics of the solution of such non-linear equations is still in an embroycnic stage. This led us directly into the interest in non-linear problems reported in Appendix C . However, that problem is a much simpler one and although it yields some insight is insufficient for the localisation solution.

CHAPTER VI

CONCLUDING REMARKS

The development of the theory of alloys beyond the 1-CPA is significant, even though in the cases of III-V semiconducting ternary alloys, to which it has been applied, the additional features obtained are not very large. But the path is paved for application to alloys of materials so widely different in mass, potentials and bond lengths that the VCA or even the 1-CPA are not satisfactory. The n-cluster CPA density of states for each specific cluster can be very useful in determining affinities by comparing the configurationally averaged density of states with the experimental one and identifying some configuration or configurations required in more or less than statistical properties, for a good agreement.

In conclusion, we may sum up the achievements of this work.

1) Formulation of a cluster extension of the coherent potential approximation for alloys which is (a) herglotz at all energies, concentrations and degrees of disorder, and (b) tractable for realistic calculations.

CHAPTER VI

CONCLUDING REMARKS

The development of the theory of alloys beyond the 1-CPA is significant, even though in the cases of III-V semiconducting ternary alloys, to which it has been applied, the additional features obtained are not very large. But the path is paved for application to alloys of materials so widely different in mass, potentials and bond lengths that the VCA or even the 1-CPA are not satisfactory. The n-cluste CPA density of states for each specific cluster can be very useful in determining affinities by comparing the configurationally averaged density of states with the experimental one and identifying some configuration or configurations required in more or less than statistical properties, for a good agreement.

In conclusion, we may sum up the achievements of this work.

1) Formulation of a cluster extension of the coherent potential approximation for alloys which is (a) herglotz at all energies, concentrations and degrees of disorder, and (b) tractable for realistic calculations.

2) Chemical pseudopotential determination for the electronic structure of the pure materials and the alloy.

3) Application of the above formulations to a series of III-V ternary alloys.

4) Formulation of a localisation criteria based on the averaged localisation length, and determination of this parameter in a weak disorder limit on a Cayley tree.

5) Eigenvalue and eigen-functions are calculation for the quartic anharmonic oscillator in all regimes of anharmonicity (k - α plane). The accuracies of these is restricted only by the machine precision. The method evolved is fast even in those regimes where previous calculations have been done.

Several refinements and extensions over the calculation presented in this thesis suggest themselves. Some of the immediate ones are the following:

1. Band structures of the III-V semiconductors show no dispersion along the Z and X axes of the Brillouin Zone even if the third nearest neighbour interactions in the Bond Orbital Model are included (Chen and Sher 1978). This may be overcome if the complete non-hermitian pseudopotential Hamiltonian matrix is solved for eigenvalues rather than the approximate hermitian matrix. The antisymmetric combinations of the somewhat different interactions between second and also the third nearest neighbouring parallel and non-parallel bonds

each, must be included. As pointed out in Sec. 4.2, the eigenvalues of the non-hermitian pseudo-Hamiltonian must still be real since these are the same as those corresponding to those of the true Hamiltonian by definition (See Eqs.4.9 and 4.11).

2. The evaluation of the n-cluster n-CPA self consistent medium which was by-passed for application to the III-V semiconducting alloys must be carried out. However, the size of graphs in the full augmented space increasesvery rapidly. For a cluster of n-sites, the size of graphs to be considered are 2^{n+1}-gon. Also, the number of distinct self energy functions corresponding to each distinct matrix element of the Hamiltonian, and hence the number of equations to be solved simultaneously for self consistency increases, making the process tedious. A 2-CPA self-consistent calculation has, however, been reported since (Kumar, Mookerjee, Srivastava 1980).

3. The pseudopotential scheme can be used beyond Anderson's approximation to include the effect of the core orbitals. Of course, finally the more localised pseudopotential wave functions and eigenvalues must be determined self consistently, although the use of the free atom orbitals and potentials together with the truncation involved in the "Wigner trick" is a good starting approximation.

4. Just as the bonding orbitals have been used for evalu ing the Green's functions for the valence bands, the anti-bonding orbitals, in principle, determine the conduction banc However, a scheme similar to the BOM is not expected to reproduce the conduction band. The conduction band states are necessarily more extended and hence interactions between rather distant bonds are required to be included.

The effect of the conduction band on the valence band can, however, be studied by incorporating an approximate Green's function corresponding to the subspace of the conduction states, e.g. in a free electron model (See Sec. 3.2.1). This is expected to alter essentially the top of the band again, since these states are the nearest to the conduction states on an energy scale. It may be interesting to compare the effect of the cluster-environment with that due to coupling with conduction states, since both seem to alter the top of the valence band, important for all transport properties.

5. The variation of the bond length has also been neglected. In the pseudopotential scheme, the interactions can be re-calculated at the inter-atomic distances corresponding to specific alloys. In this way, the approximation made for Ga-As-In kind of near neighbour bond interactions can also be refined. This involves the calculation of somewhat more number of interaction parameters, but it is nonetheless tractable.

6. The study of cluster effects in case of widely different constituent materials showing a separated impurity band in the 1-CPA, can also be made in a model calculation.

7. The calculation of averaged inverse localisation length for large disorder has been attempted, but the difficulties with the mathematical formulation are enormous. The case of weak disorder becomes tractable essentially because of the δ-function approximation to a highly peaked Lorenzian. As soon as this approximation is dropped, the already complicated integral equation becomes very difficult to handle.

8. The quantum anharmonic oscillator dealt with in Appendix C (Banerjee, 1976, Banerjee et al, 1978) has, since the work was published, made the solution to many other perturbative problems that are divergent but asymptotic possible. The difference equation method, in which scaling of the bases is easily incorporated, is thus more powerful than believed until now. Besides the eigenvalues and eigenfunctions, all moments between any two levels can be obtained starting with only the first one as input to an appropriate moment recurssion relation (Banerjee 1977). At higher values of the energy level quantum number, the WKB approximation can be shown to preserve the scale (Banerjee 1978a). The method has been extended to study a general inharmonic oscillator (Banerjee 1978b), in which case a rescaling of the perturbation series has been

Bishop, A.R., Mookerjee, A. (1974) J. Phys. C7 2165.

Borland (1963) Phys. Rev. A274 529.

Boys, S.F. (1960) Rev. Mod. Phys. 32 296.

Boys, S.F., Forster, J.M. (1960), Rev. Mod. Phys. 32, 300.

Brovers, F. (1970) J. Non Cryst. Solids 4, 428.

Bullett, D.W. (1975) J. Phys. C8 2695.

Butler W.H. (1973) Phys. Rev. B8 4499.

Chelikowsky, J.R. and Cohen, M.L. (1976) Phys. Rev. B14 556.

Chen, A.B. (1977) Phys. Rev. B16 3291.

Chen, A.B. and Sher, A. (1978) Phys.Rev. B17 4726.

Cohen, M.H., Fritzsche, H., Ovshinsky, S.R. (1969) Phys. Rev. Lett 22 1065.

Cyrot-Lackmann, F. (1970) J. Phys. Paris Suppl. C1 67.
(1972) J. Phys. C5 300.
(1974) J. Physique 35 C4-104.

Cyrot-Lackmann, F. and Ducastelle, F. (1971) Phys. Rev. Lett 27 429.

Cyrot-Lackmann, F., Desjonqueres, M.C. and Gaspard, J. (1974) J. Phys. C7 925.

Cyrot-Lackmann, F., and Gaspard, J. (1974) J. Phys. C7 1829.

Dean, P. (1972) Rev. Mod. Phys. 44 127.

Diehl, H.W., Leath, P.L. (1979a) Phys. Rev. B19 596.
(1979b) Phys. Rev. B19 879.

Ducastelle, F. (1971) J. Phys. C4 L75.

Eastman, D.E., Grobman, W.D., Freeoof, J.L. and Erbudak,M.(197 Phys. Rev. B9 3473.

Economou, E.N., Cohen, M.H. (1970) Phys. Rev. Lett 25 1445.
(1971) Phys. Rev. B4 396.
(1972) Phys. Rev. B5 2931.

Economou, E.N., Kirkpatrick, S., Cohen, M.H., and Eggarter, T.P. (1970) Phys. Rev. Lett 25 520.

Edwards, J.T., Thouless, D.J. (1972) J. Phys. C5, 807.

Elliott , R.J., Krumhausl, J.A., Leath, P.L. (1974) Rev. Mod. Phys. 46 465.

Feenberg, E. (1948) Phys. Rev. 74 206.

Gilbert, T.L. (1964), Molecular Orbitals in Chemistry, Physics and Biology, Ed.Pullman and Lowdin (New York, Acad. Press).

Gredenko, B.V., Kolomogorov, A.N. (1954) Limit Distributions for Sums of Independent Random Variables, pp. 102, Addison Wesley, Cambridge.

Harrison,W.A. (1973) Phys. Rev. B8 4487.

Harrison,W.A. and Ciraci S. (1974) Phys. Rev. B10 1516.

Haydock, R. (1972) Ph.D. Thesis, Univ. of Cambridge.

Haydock, R., Heine, V. and Kelley, M.J.
(1972) J. Phys. C5 2848.
(1975) J. Phys. C8 2591.

Herman, F., Skillman,S. (1963), Atomic Structure Calculations, Prentice Hall Inc. New Jersey.

Hill, H. and Matthias (1968) Phys. Rev. 168 464.

Ishu, K. (1973) Prog. of Theor. Phys. Suppl. No. 53, 77.

Kadanoff, L.P. and Baym G. (1962) Quantum Statistical Mechanics, (Benjamin, N.Y.).

Kaplan, T. Gray, L.J. (1976) Phys. Rev. B14 3462.
(1977) Phys. Rev. B15 3260.

Kaplan, T., Leath, P.L., Gray, L.J., Diehl,H.W. (1980) Phys. Rev. B21 4230.

Kirkpatrick, S., Velicky, B., and Ehrenreich,H. (1970) Phys. Rev. B1 3250.

Kirkpatrick, S., Velicky, B., Ehrenreich, H. and Lang, N.D. (1969) J. Appl. Phys. 40 1283.

Kumar, N., Heinrichs, J., Kumar, A.A. (1975) Solid State Comm. 17 541.

Kumar, V., Joshi, S.K. (1978) Ind. J. of Phys. Comm. Vol. Part II.

Kumar, V.,Mookerjee, A., Srivastava, V.K. (1980) ICTP preprint IC /80/42.

Ley, L., Pollak, R.A., McFreely, F.R., Kowalczyk, S.P. and Shirley, A. (1973) Phys. Rev. B9 600.

Lifshitz, I.M. (1964) Adv. Phys. 13 483.

Lloyd, P. (1969) J. Phy. C2 1717.

Love, J.C., Obenshain, F.E. and Gzyzek, G. (1971) Phys. Rev. B3 2827.

Matsubara, T. and Kaneyoshi, T. (1966) Prog. Theor. Phys. 36 695.

Matsubara, T. and Toyozawa, Y. (1961) Prog. Theor. Phys. 26 7

Mookerjee, A. (1973a) J.Phys. C6 L 205.
(1973b) J. Phys.C6 1340.
(1975a) J.Phys. C8 29.
(1975b) J.Phys. C8 1524
(1975c) Pramāna 5 118.
(1979) Disordered Systems, Hindustan Pub. Corpn. (India).

Mott, N.F. (1967) Adv. Phys. 16 49.
(1968) Phil. Mag. 17 1259.
(1970) Phil. Mag. 22 7.

Mott, N.F. and Jones, H.(1979) Theory of Metals and Alloys, (Oxford, London).

Muller-Hartmann, E. (1973) Solid State Comm. 12 1269.

Ovshinsky, S.R. (1968) Phys. Rev.Lett. 21 20 1450-53.

Payton, D.N. and Visscher, W.M. (1967) Phys.Rev.154 802.

Schwartz, L.M., Siggia, E. (1972) Phys. Rev. B5 383.

Thouless, D.J. (1970) J. Phys. C3, 1559.

Vander Rest, J., Gautier, F. and Brouers, F. (1975a)
(1975a) J.Phys. F5 2283.
(1975b) J.Phys. F5 995.

Van Vleck, J.H. (1953) Rev. Mod. Phys. 25 220.

Wanger, L.F. and Spicer, W.E. (1974) Phys. Rev. B9 1512.

Yonezawa, F. and Matsubara, T. (1966a) Prog. Theor.Phys. 35 357.
(1966b) Prog. Theor.Phys. 35 759.

Yonezawa, F. (1968a) Prog. Theor. Phys. 39 1076.
(1968b) Prog. Theor. Phys. 40 734.

Ziman, J.M. (1969) J. Phys.C2 1230.

APPENDIX A

GENERALISED 'RAY' INTEGRATION TECHNIQUE AND APPLICATIONS

The 'Ray' Integration method developed by Chen (1977) determines essentially the diagonal Green's function via the density of states function. A general spectral function F(E) is of the form

$$F(E^+) = R(E) - i\pi I(E) = \int_{BBZ} d^3k \frac{f(\vec{k})}{[E^+ - E(\vec{k})]}$$

where E^+ means that the function is to be evaluated by including an infinitesimally small imaginary part in E, and $E(\vec{k})$ is the band structure. For $f(\vec{k}) = 1$, I(E) reduces to the density states:

$$I(E) = \int_{BZ} d^3k \; [E - E(\vec{k})]$$

since,

$$\lim_{\varepsilon \to 0} \frac{1}{E + i\varepsilon} = \frac{1}{E} - i\pi\delta(E)$$

where E and ε are real. When $f(\vec{k}) = 1$, or more generally, when it is invariant under the symmetry transformations of the Brillouin Zone (BZ), it is clearly sufficient to integrate over the Irreducible part of the Brilluoin Zone (IBZ), i.e., that part of the BZ which, through the application of these transformations, reproduces the complete BZ. For those spectral functions for which $f(\vec{k})$ does not reflect all the symmetries of

the BZ, as is the case with the off diagonal matrix elements of the Green's operator required for the CCPA, the method as described by Chen is not directly applicable. For such spectral functions, a generalisation of the method has been developed which does not necessitate integration over the complete BZ. This is described in this Appendix after a brief description of Chen's procedures recapitulated for the sake of completion.

A.2 Chen's Ray Integration Method:

First, the IBZ is decomposed into one or more tetrahedra as triangular prisms. Consider now, one such tetrahedron ΓABC defined by the three vectors $\vec{q}_1$, $\vec{q}_2$, $\vec{q}_3$ (Fig. A.1). Any point P inside it is identified by a $\vec{k}$ vector.

$$\vec{k} = \alpha\vec{q}_1 + \alpha\beta\vec{q}_2 + \alpha\beta\,\vec{q}_3$$

where $\alpha = \Gamma A'/\Gamma A$, $\beta = A'L/A'B'$ and $\gamma = LP/LM$, each parameter ranging from 0 to 1 to scan the tetrahedron completely. A'B'C' is a plane parallel to ABC passing through P and LM is parallel to B'C! Points corresponding to constant values of α describe planes parallel to ABC. Constant γ planes are all hinged at the edge ΓA and vary from ΓAB to ΓAC. Similarly, constant β planes all pass through Γ and span the tetrahedron from ΓBC to ΓA, cutting the face ABC at a line parallel to BC. $\beta = 0$ corresponds to the line ΓA. Along any line starting from called a 'ray' by Chen, β and γ are constant, while α goes from

0 to 1. This is the advantage of the above manner of parameterisation since it facilitates the use of one-dimensional interpolation procedures, e.g. by calculation $E(\alpha_i)$ on a reasonable grid $\{\alpha_i\}$ along some fixed 'ray', interpolation by say, Lagrangian formula.

$$E(\alpha) = \sum_i L_i(\alpha)\, E(\alpha_i)$$

can be used, where $L_i(\alpha)$ are interpolation coefficients depending on the order of the interpolation rule.

The tetrahedron is, therefore, further divided into thin tetrahedra (TT) as shown (Fig. A.2). Let $I_i(E)$ be the result of integration over the i-th TT. Then,

$$I(E) = \sum_i I_i(E) = \sum_i \int d\Omega_i\, dk\, k^2\, f(\vec{k})\ \delta(E-E(\vec{k}))$$

If the TT are thin enough, angular dependence can be approximated as constant, and,

$$I_i(E) \sim \Delta\Omega_i \int dk_i\, k_i^2\, f(k_i)\, \delta(E-E(k_i))$$

$$= \Delta\Omega_i \sum_r f(k_r) \left[\frac{dE(k_i)}{dk_i}\Big|_{k_i=k_r} \right]^{-1}$$

where, $\Delta\Omega_i$: solid angle element of the i-th TT,

k_i : is along the axes of the i-th TT,

k_r : root of the equation $E-E(k_r) = 0$

and the summation is over various roots of the same. If k_t is the length of the axes and $k_i = dk_t$, then,

$$\Delta\Omega_i = \Delta\vec{S}_i \cdot \vec{k}_t / k_t^3$$

$$= 3V\,(\Delta S_i/S)/k_t^3$$

$$= 3V\delta_i/k_t^3$$

where V is the volume of the whole tetrahedron, $\delta_i = \Delta S_i/S$, ΔS_i being the area at the end of the TT and S the area of ABC. Then,

$$I_i(E) = 3V_i \sum_r f(\alpha_r)\,\alpha_r^2 \left[\frac{dE(\alpha)}{d\alpha}\Big|_{\alpha=\alpha_r}\right]^{-1} \qquad (A.1)$$

where $\alpha_r = k_r/k_t$.

The method can thus be summarised in the following:

(1) Divide each tetrahedron into thin enough TT's specified by β_i and γ_i corresponding to their axes, i.e. line joining to the median of the triangular face on the base, (ii) Determine, $E(\alpha)$ at a few points $\{\alpha_i\}$, say n in number along the axes of each, including one at the tip Γ and one at the BZ surface, (iii) Fix the energy value E at which the value of the imaginary part of the spectral function is to be determined, (iv) Use an n-point interpolation formula, say Lagrange's, to evaluate the values of α_r at which the value of E, if at all, is hit by say, Newton-Raphson technique, in each TT, considering all of these one by one. (v) Determine the slope $dE(\alpha)/d\alpha$ at these points by calculating $E(\alpha)$ at points $\Delta\alpha/2$ around α_r s and dividing by $\Delta\alpha$, choosing $\Delta\alpha$ to be small enough, (vi) Evaluate $I_i(E)$ as in

contributions in each IBZ,-like portion of the BZ is to be evaluated. As shown in the following, these contributions can be obtained by the use of the symmetries of the BZ, without having to solve the eigenvalue equation again.

Suppose a point $\vec{k} = (k_x, k_y, k_z)$ has been located in the IBZ at which the value E is hit in the n-th band, that is $E = \varepsilon_n(\vec{k})$, then, corresponding points in the six similar IB Zones (three of opposite parity) in the quadrant $x > 0$, $y > 0$, $z > 0$, are obtained by permuting the components of $\vec{k}$ in all possible ways, i.e. the six points are described by coordinate sets $X(k_x, k_y, k_z)$, (k_x, k_z, k_y), (k_y, k_x, k_z), (k_z, k_y, k_x), $(k_y\ k_z, k_x)$ and (k_z, k_x, k_y). Changing signs of k_x, k_y and k_z takes one to the octant described by $x < 0$, $y < 0$, $z < 0$ and permutations of these gives corresponding points in the six IB Zones in that octant. Similarly, changing signs of one or two components at a time and permuting each such set, the rest of the six octants are scanned. This identifies the 48 points in the BZ at which the value E is crossed, corresponding to the point (k_x, k_y, k_z) located in the IBZ actually scanned.

Writing the point $\vec{k}$ as a 3 x 1 column matrix $\begin{bmatrix} k_x \\ k_y \\ k_z \end{bmatrix}$ each of the above transformations can be written as a 3 x 3 matrix which when postmultiplied with the column matrix yield another column

matrix representing the corresponding point in one other IBZ. For example, the matrix,

$$S_{xy} = \begin{bmatrix} 0 & 1 & 0 \\ 1 & 0 & 0 \\ 0 & 0 & 1 \end{bmatrix}$$

interchanges the values of x and y components of $\vec{k}$. Similarly S_{yz} and S_{xz} are defined. Together with the products $S_{xy}S_{yz}$, $S_{xy}S_{xz}$ and the identity operator, these form a six-membered group under the matrix multiplication operation. That is, products of any number of these in any order yield a matrix identical with some member. The product is, in general, non-commutative and the group is isomorphic to the symmetric group S_z.

Further defining the operator $S_{-x} = \begin{bmatrix} -1 & 0 & 0 \\ 0 & 1 & 0 \\ 0 & 0 & 1 \end{bmatrix}$ which changes the sign of the x component only, and similarly, S_{-y}, S_{-z}, their products between themselves and those with the six defined above, cover all the 48 parts of the BZ similar to IBZ. These 48 matrices also constitute a group as can easily be checked.

The Hamiltonian from Eq. (3.32) is given by a 4 x 4 matrix at each $\vec{k}$

$$H^{\alpha\alpha'}(\vec{k}) = \sum_{\vec{r}} H^{\alpha\alpha'}_{\vec{r}\vec{0}} \left[\exp \dot{x}\{i\vec{k}.(\vec{r} + \vec{\tau}_{\alpha} - \vec{\tau}_{\alpha'})\}\right] \quad (A.3)$$

where $\alpha\alpha'$ are bond orientation indices and the sum is over vectors connecting sites in the same fcc sublattice. It will now be shown that applications of any of the transformations described above, amounts to renaming these indices α, α'.

Writing the column matrix corresponding to the point $\vec{k}$ as $\underline{K}$ and the displacement vector $\vec{R} = (\vec{r} + \vec{\tau}_\alpha - \vec{\tau}_\alpha)$, as $\underline{R}$,

$$\vec{k}.\vec{R} = \underline{K}^T\underline{R}$$

If $\underline{K}' = \underline{S}\,\underline{K}$, where $\underline{S}$ is one of the 3 x 3 transformation matrices, then,

$$\begin{aligned} \vec{k}'.\,\vec{R} &= (\underline{S}\,\underline{K})^T\,\underline{R} \\ &= \underline{K}^T\underline{S}^T\underline{R} \\ &= \underline{K}^T\,(\underline{S}^{-1}\underline{R}) \\ &= \underline{K}^T\,(\underline{S}'\,\underline{R}) \end{aligned}$$

where $\underline{S}^{-1} = \underline{S}'$ is necessarily some other member of the set of transformation matrices since these form a group.

Hence it is required to simply look at the way the symmetry operations take terms of the kind $(\vec{r} + \vec{\tau}_\alpha - \vec{\tau}_{\alpha'})$ to those corresponding to different α s and α s. This depends on the way $\vec{\tau}_\alpha$ and $\vec{\tau}_{\alpha'}$ are defined. Once these are known, the appropriate numbers are put into the Eq. (A.2) corresponding to each of the IB Zones and summation carried out.

A simplification is possible by noticing that changing $\vec{k}$ to $-\vec{k}$ takes $H(\vec{k})$ to its complex conjugate (Ref. Fig. A.3).

Since,

$$H\phi = E\phi$$

implies

$$H^* \phi^* = E\phi^*$$

E being real, the eigenvectors of $H^*(\vec{k})$ or $H(-\vec{k})$ are complex conjugates of those of $H(\vec{k})$ at the same $\vec{k}$. Therefore, the integrands in the BZ integrations for the complex conjugates under this transformations $\vec{k} \rightarrow -\vec{k}$. Twice the real part may thus be retained and integrations carried out over carefully chosen 24 IB Zones.

From Eq. (A.3) or from the explicit form in Eq. (3.32) and the $\vec{\tau}_\alpha$ s defined in Sec.3.2.2, the six permutations of xyz amount to the following rearrangements of the bond indices:

xyz	1234	zxy	1342
yxz	1243	yzx	1423
xzy	1324	zyx	1432

Also,

-x y z	4231
x-y z	3214
x y-z	2134

where x, y, z symbolise the components of the $\vec{k}$-vectors. Six permutations of these are again obtained by keeping the first index fixed and permuting the other three as above. Those corresponding to (-x, -y, z), (-x, y, -z), (x,-y,-z) and (-x, -y, -z) and permutations of each of these are clearly

obtained by changing the overall signs are taken care of by retaining twice the real part of the integrands, as mentioned above.

The required Green's functions for the CCPA calculation are.

G_{00} : Diagonal element; $\vec{r} = 0$, $\alpha = \alpha' = 1$, say

G^{A}_{01} : Across adjacent bonds meeting at an anion; $\vec{r} = 0$, $\alpha = 1$, $\alpha' = 2$

G^{C}_{01} : Across adjacent bonds meeting at a cation; $\vec{r} = 0$, $\alpha = 2$, $\alpha' = 1$,

G^{P}_{02} : Across second nearest neighbour parallel bonds; $\vec{r} = \vec{r}_1$, $\alpha = \alpha' = 1$,

G^{NP}_{02} : Across second nearest neighbour non-parallel bonds $\vec{r} = \vec{r}_1$, $\alpha = 1$, $\alpha' = 2$.

where $\vec{r}_1$ is the fcc sublattice nearest neighbour displacement vector, and required parameters in the exponent in the integrands are indicated. For G^{C}_{01} the exponent is the same as that for G^{A}_{01} except that α and α' are interchanged. This distinguishes these. Explicitly stating, if the integrand is looked at as a product of two complex factors $C_1 = e^{-i\vec{k}.\vec{R}}$ and $C_2 = \phi(\vec{k}n\alpha)\phi^*(\vec{k}n\alpha')$ then those corresponding to G^{A}_{01} and G^{C}_{01} have distinct terms like $C_1 C_2^*$ and $C_1 C_2$ respectively.

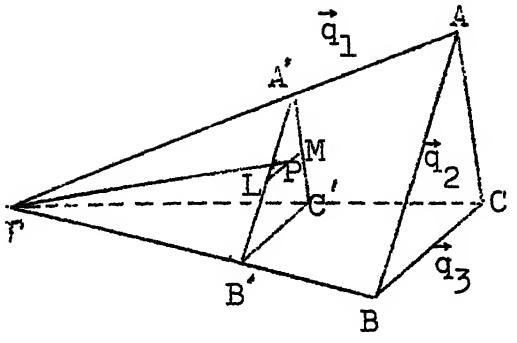

Fig. A.1: A tetrahedral part of Brillouin Zone.

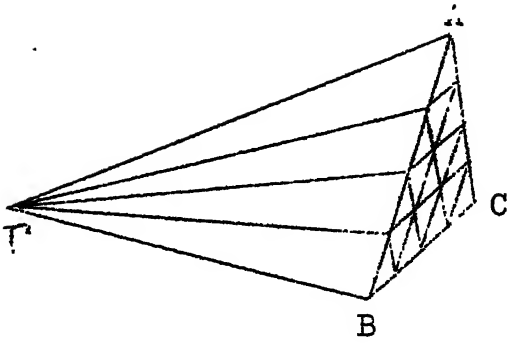

Fig. A.2: Division of a tetrahedron into thin tetrahedra (TT).

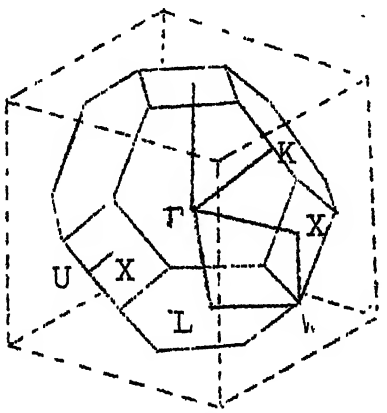

Fig.A.3: Brillouin Zone of an fcc lattice showing some symmetry points.

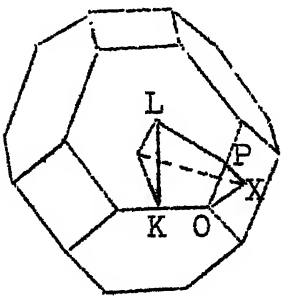

Fig. A.4: Irreducible part of the Brillouin Zone (IBZ) of an fcc lattice.

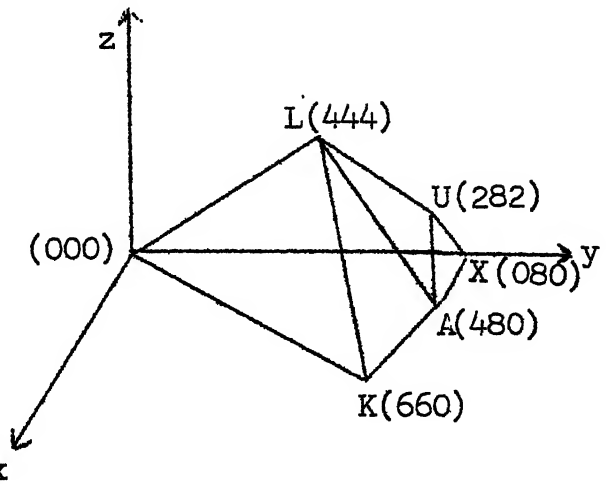

Fig. A.5: The Irreducible part of the Brillouin Zone of the fcc lattice and its division into three tetrahedra. Coordinates shown are in the units of $\pi/16a$, where a is the edge of the direct fcc lattice cubic unit cell.

APPENDIX B

INVERSE LAPLACE TRANSFORMS BY COMPLEX CONTOUR INTEGRATION

The required inverse Laplace transform is,

$$Q'(y) = \frac{1}{2\pi i} \int_{-i\infty}^{+i\infty} e^{ys-s^{\alpha}} \, ds$$

Considering the complex integral over the closed curve of Fig. B.1, we obtain,

$$Q'(y) = \frac{1}{\pi} \int_{0}^{\infty} e^{-ys-s^{\alpha}\text{Cos } \pi\alpha} \text{ Sin } (s^{\alpha} \text{ Sin } \pi\alpha) \, ds$$

Since $\frac{1}{2} < \alpha < 1$, for any finite y, however small, exp (-ys) eventually (large s) decreases more rapidly than exp ($-s^{\alpha}$ Cos $\pi\alpha$) increases. These form the envelope of the oscillations due to the factor Sin (s^{α} Sin $\pi\alpha$). The distance between two successive zeros of the integrand decreases as s increases, making the oscillations very rapid for large s. These zeros can be evenly spaced by the following substitution.

s^{α} Sin $\pi\alpha$ = t, when

$$Q'(y) = \frac{1}{\pi \alpha \left(\text{Sin } \frac{\pi\alpha}{2}\right)^{1/\alpha}} \int \exp \left[-t \text{ Cos } \pi\alpha - \frac{yt^{\alpha}}{\left(\text{Sin } \frac{\pi\alpha}{2}\right)^{1/\alpha}}\right] t^{(1/\alpha)-1} \text{ Sin } t \, dt$$

$$= \frac{1}{\pi\alpha \left(\text{Sin } \frac{\pi\alpha}{2}\right)^{1/\alpha}} \sum_{n=0}^{\infty} I_n(y)$$

where,

$$I_n(y) = \int_{n\pi}^{(n+1)\pi} \exp\left[-t \text{ Cos } \pi\alpha - \frac{yt^{\alpha}}{\left(\text{Sin } \frac{\pi\alpha}{2}\right)^{1/\alpha}}\right] t^{(1/\alpha)-1} \text{ Sin } t \, dt$$

These integrals are calculated numerically by the Gaussian integration technique. Fig. 5.2 shows plots of unnormalised probability functions $Q'(y)$'s for various E's near the band edge. These fall off to 10^{-4} of their peak values at $y \sim 15.0$. Hence it is sufficient to carry out the integration in a large enough finite interval. For the numbers used for the plot in Fig. 5.3 the interval used is (0, 50.0). The peaks become sharper away from the band edge, and shift gradually to 1.0 as the mobility edge is approached.

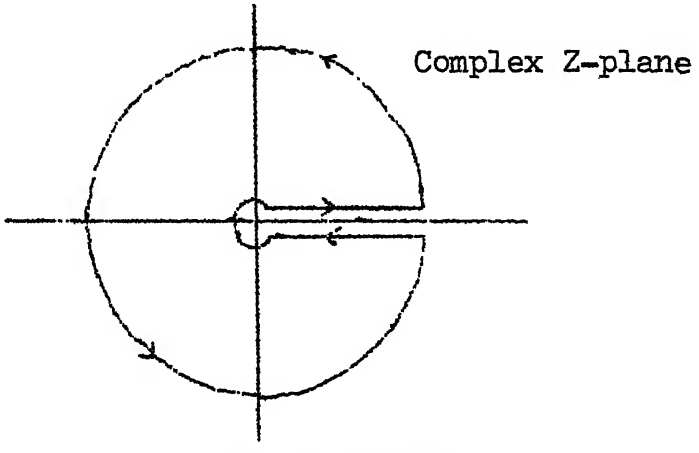

Fig. B.1: Contour of integration.

one régime the energy eigenvalues differ slightly from the harmonic oscillator levels (the near harmonic régime); in the other they differ slightly from the pure quartic oscillator eigenvalues (the near quartic régime). By using Bargmann representation they developed fast converging algorithms from which the energy eigenvalues in the small n régime may be computed. They also constructed several simple formulae with the use of best adjusted coefficients which when combined give good approximations (8 significant figures) to the energy eigenvalues except in a régime of values of (n, λ) called 'boundary layer' in which the energy eigenvalues are not 'near harmonic' or 'near quartic'. In contrast we present a method which applies with uniform and arbitrarily high accuracy for all values of n and λ. The method also yields eigenfunctions of accuracy comparable with that of the eigenvalues which are used for the computation of high accuracy matrix elements.

In a recent brief communication, Banerjee (1976) presented a method for eigenvalue problems. The essential feature of this work is the use of an appropriately scaled basis for the expansion of each eigenfunction:

$$\psi_n(\lambda) = e^{-\alpha x^2} \sum_{m=0}^{\infty} a_m x^m, \tag{1}$$

where the scaling is introduced through the parameter α. For an effective expansion the scale of coordinates is chosen so that sufficient lower members of the basis functions $\{x^m e^{-\alpha x^2}\}$ in the expansion (1) have appreciable values in the region of oscillation of the actual eigenfunction and decay outside the region of oscillation. Since the region of oscillation of an eigenfunction is determined by the values of n and λ, the appropriate scaling must also depend on n and λ. A simple criterion may be postulated: the region of oscillation of the nth eigenfunction (*ca.* $\lambda^{-\frac{1}{4}} n^{\frac{1}{2}}$ in the W.K.B. estimate) is set equal to the width of the nth basis function (*ca.* $\alpha^{-\frac{1}{2}} n^{\frac{1}{2}}$) which yields

$$\alpha(n, \lambda) \sim n^{\frac{1}{2}} \lambda^{\frac{1}{2}}.$$

This puts the span of the first n (or a number proportional to n) basis functions in the region of oscillation of the nth eigenfunction *for all* n, just as required for an effective expansion. In view of the W.K.B. estimate and large λ assumption implicit in the above scaling formula it is not expected to be good when n or λ is small. However, for $\lambda \to 0$ or for small n, the scaling must approach the value $\frac{1}{2}$ appropriate for the harmonic oscillator. Hence the scaling formula for all régimes of n and λ is

$$\alpha(n, \lambda) = \tfrac{1}{2} + B n^{\frac{1}{2}} \lambda^{\frac{1}{2}}, \tag{2}$$

where the constant B is to be adjusted empirically. The effect of using an appropriately scaled basis is remarkable. It is now possible to compute eigenvalues in any régime of n and λ with arbitrarily high accuracy.

2. Method

The expansion (1) on substitution into the Schrödinger equation, $H\psi = E\psi$, yields a four-term recursion formula connecting the alternate expansion coefficients:

$$a_{m+2} + d_{m,m}a_m + d_{m,m-2}a_{m-2} + d_{m,m-4}a_{m-4} = 0, \tag{3}$$

where $$d_{m,m} = -\frac{(4\alpha m + 2\alpha - E)}{(m+1)(m+2)}, \quad d_{m,m-2} = \frac{4\alpha^2 - 1}{(m+1)(m+2)},$$

and $$d_{m,m-4} = -\frac{\lambda}{(m+1)(m+2)}.$$

The even and odd parity solutions are obtained respectively by assigning the initial conditions (i) $a_0 = 1$, $a_1 = 0$; (ii) $a_0 = 0$, $a_1 = 1$. The recursion (3) may be viewed as an infinite set of linear homogeneous equations in unknowns $\{a_m\}$. For self-consistency the determinant

$$\Delta(E) = \begin{vmatrix} d_{00} & 1 & 0 & \dots & & & \\ d_{20} & d_{22} & 1 & 0 & \dots & & \\ d_{40} & d_{42} & d_{44} & 1 & 0 & \dots & \\ 0 & d_{62} & d_{64} & d_{66} & 1 & 0 & \dots \\ \dots & 0 & d_{m,m-4} & d_{m,m-2} & d_{mm} & 1 & 0 \\ \dots & \dots & \dots & \dots & \dots & \dots & \dots \end{vmatrix} = 0. \tag{4}$$

The roots of this trancandental equation are the eigenvalues. This mode of writing the characteristic equation in the form of an infinite determinant is known from the eigenvalue problem associated with Hill's equation (Whittaker & Watson 1927). Its applications in physical problems, however, had a limited success (Kerner 1951). In the typical case of the anharmonic oscillator (Biswas *et al.* 1973) the lowest eight eigenvalues were thus obtainable until the numerical errors became too severe. The reason for this is the use of a fixed scale expansion (like (1) with α = constant) in these works. A fixed scale expansion is suitable in a small régime of values of (n, λ) where the scale *happens* to be close to the appropriate value given by (2). Outside this régime the basis becomes unfavourable for expansion. To find the zeros of $\Delta(E)$ it may be noted that the determinant Δ_{m+2}, obtained by omitting all rows and columns beyond the element, d_{mm}, may be expanded into a four-term recursion between alternate determinants of lower orders:

$$\Delta_{m+2}(E) - d_{m,m}(E)\Delta_m(E) + d_{m,m-2}\Delta_{m-2}(E) - d_{m,m-4}\Delta_{m-4}(E) = 0. \tag{5}$$

With $\Delta_0 = 1$ normalization, the determinants up to any even order (for odd orders, $\Delta_0 = 0$, $\Delta_1 = 1$) may be computed successively from the recursion (5). The determinant $\Delta_{2m}(E)$ is a polynomial in E of degree m. In the limit of $m \to \infty$ this defines $\Delta(E)$. The zeros of $\Delta_m(E)$ are stable for large m (shown in the next section) and may

be obtained numerically by Newton's method which requires both $\Delta_m(E)$ and $\Delta'_m(E)$. The latter are obtained by differentiating (5) with respect to E,

$$\Delta'_{m+2}(E) - d'_{m,m}\Delta_m(E) - d_{m,m}(E)\Delta'_m(E) + d_{m,m-2}\Delta'_{m-2}(E) - d_{m,m-4}\Delta'_{m-4}(E) = 0, \quad (6)$$

and computing recursively therefrom. The recursions (5) and (6) used for computing the eigenvalues are numerically stable for large m. The accuracy of the computations is therefore limited only by the precision of the arithmetic used (16 significant figures here). Owing to the quadratic convergence of Newton's method it is possible to refine a rather crude initial estimate for an eigenvalue (say, within a small percentage) to a 15 figure accuracy in a very short time on the computer. The time on IBM 7044 for the first 100 eigenvalues is a total of two minutes. For the 10 000th eigenvalue the time required is about three minutes. The initial estimates used for higher eigenvalues are the W.K.B. values. For lower eigenvalues a sufficiently large order determinant Δ_M is computed recursively from (5) at various E points. Opposite signs of Δ_M for two neighbouring E values indicates that an eigenvalue is crossed which provides a sufficiently accurate estimate for Newton's method. The

TABLE 1. EIGENVALUES OF THE QUARTIC OSCILLATOR ($H = p^2 + x^4$) AND THE ANHARMONIC OSCILLATOR ($H = p^2 + x^2 + \lambda x^4$) FOR $\lambda = 1$

quantum number, n	quartic oscillator eigenvalues	anharmonic oscillator eigenvalues
0	1.060 362 090 484 18	1.392 351 641 530 29
1	3.799 673 029 801 40	4.648 812 704 212 08
2	7.455 697 937 986 74	8.655 049 957 759 31
3	11.644 745 511 378 2	13.156 803 898 049 9
4	16.261 826 018 850 2	18.057 557 436 303 3
5	21.238 372 918 236 0	23.297 441 451 223 2
6	26.528 471 183 682 5	28.835 338 459 504 2
7	32.098 597 710 968 3	34.640 848 321 111 3
8	37.923 001 027 034 0	40.690 386 082 106 4
9	43.961 158 097 289 7	46.965 009 505 675 5
10	50.256 254 516 682 9	53.449 102 139 665 3
11	56.734 214 055 173 0	60.129 522 959 157 8
12	63.403 046 986 718 9	66.995 030 001 247 2
13	70.252 394 628 616 6	74.035 874 359 102 5
14	77.273 200 481 984 0	81.243 505 050 767 2
15	84.457 466 274 942 0	88.610 348 800 799 2
16	91.798 066 808 991 2	96.129 642 045 234 1
17	99.288 606 660 493 3	103.795 300 322 273
18	106.923 307 381 733	111.601 815 045 173
19	114.696 917 384 985	119.544 170 733 050
20	122.604 639 000 999	127.617 777 795 355
21	130.642 068 748 630	135.818 417 325 610
22	138.805 147 911 395	144.142 195 296 398
23	147.090 121 257 604	152.585 504 205 574
24	155.493 502 268 682	161.144 990 694 513

TABLE 1 (*cont.*)

quantum number, n	quartic oscillator eigenvalues	anharmonic oscillator eigenvalues
25	164.012 043 622 865	169.817 528 001 595
26	172.642 711 962 845	178.600 192 366 876
27	181.382 666 185 768	187.490 242 692 950
28	190.229 236 652 463	196.485 102 910 221
29	199.179 918 823 747	205.582 346 604 423
30	208.232 339 005 166	214.779 683 549 177
31	217.384 261 674 103	224.074 947 352 600
32	226.633 563 481 138	233.466 087 479 375
33	235.978 250 361 696	242.951 154 951 147
34	245.416 393 791 936	252.528 299 061 493
35	254.946 197 970 798	262.195 757 468 520
36	264.565 917 814 499	271.951 850 050 007
37	274.273 307 658 941	281.794 972 923 820
38	284.068 590 581 401	291.723 593 051 018
39	293.948 458 266 006	301.736 243 351 187
40	303.912 066 348 384	311.831 518 269 701
41	313.958 030 183 978	322.008 069 744 845
42	324.085 020 992 133	332.264 603 530 091
43	334.291 762 334 482	342.599 875 332 547
44	344.577 026 891 585	353.012 690 233 780
45	354.939 633 506 395	363.501 894 863 479
46	365.378 444 467 063	374.066 379 600 092
47	375.892 363 004 933	384.705 074 675 721
48	386.480 330 986 517	395.416 946 465 263
49	397.141 326 780 674	406.200 997 442 128
50	407.874 363 284 438	417.056 263 284 848
100	1020.989 992 105 37	1035.544 183 138 91
1000	21865.262 118 137 7	21932.783 710 666 9
10000	470790.294 427 028	471103.777 790 809

sign change of a sufficiently large order determinant between two neighbouring E values may be used successively to yield increasingly accurate upper and lower bounds for the eigenvalues. As a method for the computation of eigenvalues this is much slower than Newton's method. However, an eigenvalue computed by Newton's method may be checked and in the process be upper and lower bounded by the sign check described above. The eigenvalues computed in this work were evaluated to 16 significant figures, upper and lower bounded in the 16th figure, and then rounded off to 15 figures for the tables 1 and 2. Table 1 lists some of our results for the anharmonic oscillator ($H = p^2 + x^2 + \lambda x^4$) and the quartic oscillator

$$(H = p^2 + x^4).$$

Each eigenvalue in the tables has been rechecked by using several values of α in the range

$$\alpha = \tfrac{1}{2} + (1.2 \quad \text{to} \quad 1.4)\, n^{\frac{1}{2}} \lambda^{\frac{1}{3}}, \tag{7}$$

in which the constant within brackets (1.2 to 1.4) is set empirically. The effect of using different αs from (7) in the computation of eigenvalues is that the stabilization of the initial estimate for an eigenvalue to 16 figures occurs at a slightly different point in the recursion. It emphasizes the point that though the scaling must be in the correct range for an effective expansion there is no exact scaling necessary. Table 2 demonstrates the uniform applicability of this method for all values of n and λ. We focus on the régimes of extreme values of (n, λ). Hioe *et al.* (1975, 1976) give different formulations of the eigenvalue problem in each of these régimes, which cannot be extended into the other régimes because of the 'boundary layer' in between. The eigenvalue corresponding to $n = 1000, \lambda = 10^{-4}$ is in the 'boundary layer' and also in the awkward high n, low λ régime (Hioe *et al.* 1976). In the present approach this eigenvalue is obtained by the same technique and with the same accuracy as any other, highlighting the scope of computation with an appropriately scaled basis.

TABLE 2. EIGENVALUES OF THE ANHARMONIC OSCILLATOR ($H = p^2 + x^2 + \lambda x^4$) IN RÉGIMES OF EXTREME VALUES OF (n, λ).

λ / n	0.0001	40000
0	1.000 074 986 880 20 (near harmonic régime)	36.274 458 133 736 8 (near quartic régime)
1000	2134.242 545 232 21 (boundary layer)	747 783.421 502 834 (near quartic/W.K.B. régime)

3. STABILITY OF ZEROS OF $\Delta_m(E)$

The recursive evaluation of the determinants $\Delta_m(E)$ and the stability of their zeros for large m will now be considered in some detail. It may be noted that the recursion (5) is obtained from the recursion (3) by replacing a_m with Δ_m and changing the sign of every alternate term. This prescription is valid when the coefficient of the highest order term in the $\{a_m\}$ recursion is set unity (by properly dividing if necessary). Then

$$\left.\begin{aligned} \Delta_m &= (-1)^{\frac{1}{2}m} a_m, \quad m = 0, 2, 4, \ldots, \\ \Delta_m &= (-1)^{\frac{1}{2}(m-1)} a_m, \quad m = 1, 3, 5, \ldots. \end{aligned}\right\} \tag{8}$$

The asymptotic behaviour of the solution of Schrödinger equation for the anharmonic oscillator approaches $\exp(\pm\frac{1}{3}|x|^3)$, which gives

$$a_{m+2}/a_{m-4} \sim \lambda/m^2, \quad m \to \infty, \tag{9}$$

for the coefficients in the series solution (1). It follows immediately from the relations (8) that

$$\Delta_{m+2}/\Delta_{m-4} \sim -\lambda/m^2, \quad m \to \infty. \tag{10}$$

The asymptotic relation (10) implies a sequence of decreasing determinants beyond a sufficiently large m. This zeroing for large m must be isolated from the deter-

mination of the eigenvalues which are the zeros of $\Delta(E)$ for values of E. It is possible to achieve this quite simply by multiplying the recursion (5) by a large number whenever, while applying Newton's method, the recursively computed determinants become too small in magnitude. This renormalization amounts to starting the recursion with a higher value of the arbitrary constant Δ_0. More generally, other recursively connected sequences of determinants $\{\bar{\Delta}_m\}$ may be defined such that the zeros of $\bar{\Delta}_m(E)$ and $\Delta_m(E)$ are common but $\bar{\Delta}_m(E)$ may be given any desired asymptotic behaviour for large m. This is done by multiplying the recursion (3) by a function of m, say $f(m)$. The corresponding infinite determinant $\bar{\Delta}(E)$ and its various order truncations are related to the respective quantities for $\Delta(E)$ by the relation

$$\bar{\Delta}_m(E) = f(m-2)f(m-4)\ldots f(0 \quad \text{or} \quad 1)\Delta_m(E), \tag{11}$$

where the right hand side contains $f(0)$ (or $f(1)$) for the even (or odd) eigenvalues. Clearly, $\bar{\Delta}_m(E)$ can be given any asymptotic behaviour for large m by properly choosing the function $f(m)$. Since $f(m)$ is independent of E by definition, the zeros of $\bar{\Delta}_m(E)$ and $\Delta_m(E)$ are common and they are equally suited for the computation of the eigenvalues. The 'renormalization suggested above is a special case of this multiplication' in which all rows of $\Delta(E)$ are left intact except one which is multiplied by a large number.

To see the stability of the zeros of $\Delta_m(E)$ as $m \to \infty$ we first consider the same problem for the harmonic oscillator which is exactly soluble. In the case of the harmonic oscillator the zeros of the characteristic polynomial $\Delta_m(E)$ are real and the ratio of successive polynomials is

$$\frac{\Delta_{m+2}(E)}{\Delta_m(E)} = -\frac{(2m+1-E)}{(m+1)(m+2)}.$$

The zeros of $\Delta_{m+2}(E)$ consist of all the zeros of $\Delta_m(E)$ plus a zero at $E = 2m+1$. Thus the eigenvalues resulting from the solution of $\Delta_m(E) = 0$ are reproduced *exactly* by the solutions of $\Delta_{m+2}(E) = 0$ for all m. This is characteristic of an exactly soluble problem. For anharmonic oscillator the zeros of successive order polynomials are different. For a given E and sufficiently large m however,

$$\Delta_{m+2}(E)/\Delta_{m-2}(E) \sim -\lambda/m^2, \quad m \to \infty.$$

This implies that the largest order term in the ratio $\Delta_{m+2}(E)/\Delta_m(E)$ is independent of E for $m \to \infty$. The successive polynomials as functions of E therefore differ by a multiplicative constant (depending on m) for large m. Hence, the zeros of $\Delta_m(E)$ stabilize for large m.

4. Eigenfunctions and moments

The recursion (3) falls off for large m according as $a_{m+2}/a_{m-4} \sim \lambda/m^2$, $m \to \infty$. This ensures a rapidly decreasing (in magnitude) set of coefficients $\{a_m\}$ after a sufficiently large value of m. When E is set equal to a computed eigenvalue in recursion (3) the resulting coefficients $\{a_m(E)\}$ provide a very convenient representation for the corresponding eigenfunction through the expansion (1). To test how well the computed eigenfunctions satisfy the Schrödinger equation we compare the two sides of the test equality, $H\psi(x)/\psi(x) = E$, at various points x. For the first ten eigenfunctions which we have computed the test equality is satisfied to 13–14 significant figures from $x = 0$ to points well outside the classical region. For $|x| \to \infty$ the right hand side of (1) must go to $+\infty$ or $-\infty$ unless the value of E used in the computation of the solution is an exact eigenvalue (Titchmarsh 1961). The blow-up occurs in the non-classical region and shifts to large x as E approaches an eigenvalue. However, this large x behaviour does not affect the computation of accurate eigenfunctions significantly since well before the blow-up the computed eigenfunction reaches extremely small values in the non-classical region. The part of the computed eigenfunction where the blow-up occurs may therefore be replaced by zero without losing much information. In the typical case of the 10th eigenfunction of the pure quartic oscillator the test equality $H\psi_{10}/\psi_{10} = E_{10}$ is satisfied to at least 13 significant figures in the entire classical region ($x \approx \pm E_{10}^{\frac{1}{4}}$). At a point $x \approx 1.5E_{10}^{\frac{1}{4}}$ the test equality is still satisfied to 10 significant figures, where the value of the computed eigenfunction $\psi_{10}(x \approx 1.5E_{10}^{\frac{1}{4}})$ is $O(10^{-16})$ relative to $\psi_{10}(x = 0) = 1$. The transition moments between the anharmonic oscillator energy eigenstates, given by the matrix elements $\langle i|x^k|j\rangle$, may now be obtained from the computed eigenfunctions. It is shown in a recent brief report (Banerjee 1977) that these matrix elements satisfy an exact linear recurrence relation with respect to the index k:

$$\begin{aligned} 4k(k-1)\langle i|x^{k-2}V|j\rangle + 2k\langle i|x^{k-1}V'|j\rangle \\ = (E_i - E_j)^2\langle i|x^k|j\rangle + 2k(k-1)(E_i + E_j)\langle i|x^{k-2}|j\rangle \\ + k(k-1)(k-2)(k-3)\langle i|x^{k-4}|j\rangle, \qquad (12) \\ H|i\rangle = E_i|i\rangle, \end{aligned}$$

where the potential $V(x)$ could in general be any polynomial function. For the anharmonic oscillator therefore the lowest moment of any particular transition is sufficient for the computation of all higher moments (of that transition) recursively, using the eigenvalues obtained above. The computation of the matrix elements $\langle i|x|j\rangle$ and $\langle i|x^2|j\rangle$ is done as follows (i) each eigenstate is defined by including as many terms in the expansion (1) as are needed to obtain the corresponding eigenvalue to 16 significant figures; (ii) as described earlier, the computed eigenfunction falls off to very small magnitudes in the non-classical region before finally increasing for $x \to \pm\infty$. The range of integration for the evaluation of the matrix elements is therefore truncated at a point at which the computed

TABLE 3. THE NON-ZERO MATRIX ELEMENTS $\langle i|x|j\rangle$ AND $\langle i|x^2|j\rangle$ BETWEEN THE LOWEST TEN EIGENSTATES OF THE QUARTIC OSCILLATOR

$\langle i|x|j\rangle$

i \ j	0	2	4	6	8
1	0.600 804 942 334	−0.734 340 766 283	0.037 148 375 006	−0.001 717 039 807	0.000 077 833 558
3	−0.032 461 289 392	0.838 903 284 915	−0.922 557 714 350	0.044 496 328 098	−0.002 017 187 983
5	0.001 526 391 867	−0.041 176 337 805	0.993 412 432 308	−1.055 437 316 854	0.049 916 105 158
7	−0.000 069 750 597	0.001 881 766 737	−0.047 366 390 038	1.110 946 812 523	−1.161 417 539 380
9	0.000 003 142 839	−0.000 084 789 094	0.002 134 420 223	−0.052 223 616 778	1.207 855 178 442

$\langle i|x^2|j\rangle$

i \ j	0	2	4	6	8
0	0.362 022 648 789				
2	−0.468 490 426 792	1.244 714 121 511			
4	0.053 785 987 462	−0.842 210 662 995	1.841 609 138 522		
6	−0.004 164 678 784	0.084 143 031 237	−1.142 331 998 243	2.352 866 384 212	
8	0.000 273 248 428	−0.006 092 887 947	0.109 046 749 878	−1.406 256 536 322	2.813 476 631 178

$\langle i|x^3|j\rangle$

i \ j	1	3	5	7	9
1	0.901 605 895 819				
3	−0.669 891 863 409	1.557 909 193 537			
5	0.069 874 305 670	−0.998 136 794 911	2.105 010 651 065		
7	−0.005 181 476 173	0.097 059 890 197	−1.277 762 011 524	2.588 299 362 716	
9	0.000 331 500 121	−0.006 913 995 758	0.120 340 586 778	−1.529 062 457 270	3.029 980 037 256

Bender, C. M. & Wu, T. T. 1976 *Phys. Rev. Lett.* **37**, 117.
Biswas, S., Datta, K., Saxena, R., Srivastava, P. & Varma, V. 1973 *J. Math. Phys.* **14**, 1190.
Chan, S. I. & Stelman, D. 1963 *J. Molec. Spectrosc.* **10**, 278.
Hioe, F. T. & Montroll, E. W. 1975 *J. Math. Phys.* **16**, 1945.
Hioe, F. T., MacMillen, D. & Montroll, E. W. 1976 *J. Math. Phys.* **17**, 1320.
Kerner, E. H. 1951 *Phys. Rev.* **83**, 71.
Reid, C. E. 1970 *J. Molec. Spectrosc.* **36**, 183.
Simon, B. 1970 *Ann. Phys.* **58**, 76.
Titchmarsh, E. C. 1961 *Eigenfunction expansions*, part I. Oxford: Oxford University Press.
Whittaker, E. T. & Watson, G. N. 1927 *Modern analysis*, § 19.42. Cambridge University Press.

Reprint from proceedings of the
Nuclear Physics and Solid State Physics Symposium
Pune, December 26-30, 1977
Vol. 20C : Solid State Physics

LOCALISATION - ELECTRONS IN DISORDERED SYSTEMS

A. Mookerjee and V. Choudhury
Department of Physics
Indian Institute of Technology, Kanpur 208016

I. INTRODUCTION

Various localisation criterion that have been proposed in the past have successfully shown the existence of localised electron states in disordered systems, but fail to show the important feature, viz. the transition to Bloch type non-normalisable states across the mobility edge. In the treatment of Abou Chacra et.al[1] the mobility edge E_c does not approach the band edge E_b, as the disorder $\delta \to 0$. The criteria suggested by Anderson[2] and Ishii[3], although rigorous in principle are mathematically intractable keeping the rigour. Drastic simplifying assumptions are therefore made. We have tried to look at the radius of localisation in the localised energy regions. We take as the delocalisation criterion itself, the probabilistic divergence of the localisation domain. For the weak disorder limit, the mobility edge E_c is thus located within the band (this has been reported by Kumar et.al.[4]) and is obtained as a function of the disorder parameter. The analysis in the case when disorder is larger leading to Anderson transition is possible. Further, the behaviour of the averaged size of the localisation domain and the way it diverges as $E \to E_c$ is looked at. The localisation length is a parameter that enters the expressions for various physical properties eg. phonon assisted hopping conduction[5] and hence the motivation for the calculation for the same.

II. FORMULATION

Consider the Anderson Hamiltonian

$$H = \sum_i \epsilon_i P_i + \sum_{i,j} V_{ij} T_{ij} \qquad \ldots (1)$$

and $G_{00}(z)$, a representation of the resolvent $(zI-H)^{-1}$. If an electron is placed at site r_0 at time $t = 0$, the probability that it is there at $t \to \infty$ [2] is

$$P_0 = \int_{-\infty}^{\infty} dE \lim_{\eta \to 0^+} \frac{\eta}{\pi} \left| G_{00}(E+i\eta) \right|^2 \qquad \ldots (2)$$

Now, if $G_{00}(z) = [z - \epsilon_0 - S_0(z)]^{-1}$ in the Cayley Tree Approximation (CTA), $S_0(z)$ being the self energy function, then

$$P_0 = \int_{-\infty}^{\infty} dE \; n_0(E) \left(1 - \frac{dS_0}{dE}\right)^{-1} \qquad \ldots (3)$$

In a band (i.e $n_0(E) \neq 0$), for extended states, dS_0/dE diverges and $P_0 = 0$, while for localised states dS_0/dE and P_0 are finite. For disorder $\delta \to \infty$, dS_0/dE is 0 and $P_0 = 1$. We thus identify $L_0(E)$, the localisation length with $(1-dS_0/dE)$. Further support of this is from the fact that residue of G_{00} at its poles is $(1-dS_0/dE)^{-1}$ which must

also be $\sim 1/L$ for a state localised over L sites.

Let $P(E_j, l_j)$ be the probability distribution over E_j, l_j, where $l_j = d\delta_0 / dN$. Then $\hat{P}(k, s)$, its Fourier-Laplace transform is found to satisfy the following non-linear integral equation.

$$\hat{P}(k,s) = \left\{ \frac{1}{\pi\delta} \int_{-\infty}^{\infty} dx \int_{-\infty}^{\infty} dk' \hat{p}(k') \hat{P}\left(k', \frac{sv^2}{x^2}\right) \exp\left[-ik'(E-x) - s\frac{kv^2}{x^2} - \frac{sv^2}{x^2}\right] \right\}^k \quad \ldots (4)$$

We first attempt a solution of the type

$$\hat{P}(k,s) = \hat{f}\left(k, \{x_\lambda\}\right) \hat{P}\left(s, \{x_\lambda\}\right) \quad \ldots (5)$$

where $\{x_\lambda\}$ denotes a set of parameters describing the probability density of E_j which is independent of the probability density of l_j and not vice versa. The variables l_j and E_j are, however, dependent. The above form thus does not imply stastical independence of E_j and l_j, but is an approximation none-the-less. In particular,

$$\hat{P}(k,s) = \hat{f}(k)\, \hat{P}(s) \quad \ldots (6)$$

Taking $p(\epsilon)$ to be a Cauchy distribution, we have

$$\hat{f}(k) = e^{i z_\lambda k - z_i \mathrm{sgn}(k) k} \quad \ldots (7)$$

and $\hat{P}(s)$ satisfying the following equation

$$\hat{P}(s) = \left\{ \int_{-\infty}^{\infty} \frac{(r+z_i)/\pi}{(E-z_\lambda - x)^2 + (r+z_i)^2} \hat{P}\left(\frac{sv^2}{x^2}\right) \exp\left(-\frac{sv^2}{x^2}\right) \right\}^k \quad \ldots (8)$$

z_i and z_r being given by

$$z_\lambda + i z_i = \frac{kv^2}{(E - z_\lambda) - i(r + z_i)} \quad \ldots (9)$$

$\hat{P}(s)$ cannot be solved for analytically from (8) because of the $\exp(-sv^2/x^2)$ factor. But in the weak disorder limit ie $(r+z_i) \ll 1$ it admits the following solution

$$\hat{P}(s) = e^{-as} \exp\left(-s^\alpha \sec\frac{\pi\alpha}{2}\right) \quad \ldots (10)$$

where

$$a = \frac{kv^2}{(E-z_\lambda)^2 - kv^2}, \qquad \alpha = \frac{1}{2} \frac{\ln(k)}{\ln\left(\frac{E-z_\lambda}{v}\right)} \quad \ldots (11)$$

and $$\hat{P}_0(s) = \left[\hat{P}(s)\right]^{\frac{k+1}{k}} \quad \ldots (12)$$

$P_0(y)$, the probability distribution of the localisation length is then obtained as the Laplace inverse of $\hat{P}_0(s)$. These are curves of the type shown in Fig. 1. Since this has a long tail, $\langle L_0 \rangle$ is found to diverge. We thus define the average localisation length as

... (13)

For $E \to E_c$, $\kappa \to 1$, and $P(\delta)$ approaches a δ-function and

$$\langle L_0^{-1} \rangle^{-1} \longrightarrow \left\{ \left(\frac{\kappa+1}{\kappa} \sec \frac{\pi\kappa}{2} \right)^{1/\kappa} + a \cdot \frac{\kappa+1}{\kappa} + 1 \right\} \qquad \ldots (14)$$

The divergence of $\bar{L}_0$ near E_c may be seen to be linear as would be expected from a mean field theory. The CPA is akin to such an approximation. The numerical results are shown in Fig. 2.

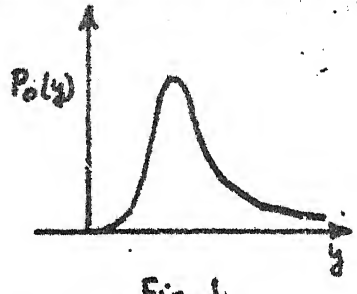

Fig. 1.

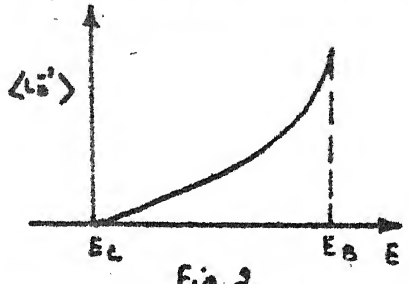

Fig. 2.

For somewhat larger disorder, an iterative calculation is made taking the small disorder limit solution given by (10) as the zeroth iterant. $P(y)$ is qualitatively unchanged and becomes only more peaked as expected. Also the linear divergence of $\langle L_0^{-1} \rangle$ near E_c is retained.

REFERENCES

1. R. Abou Chacra, P.W. Anderson and D.J. Thouless, J.Phys.C: Solid St. Phys. 6, 1734-52 (1973).

2. P.W. Anderson, Phys. Rev. 109, 1492-1505 (1958).

3. K. Ishii, Prog. Theor. Phys. Suppl. 53, 77 (1973).

4. N. Kumar, J. Heinrichs and A.A. Kumar, Solid State Commun. 17, 541-44 (1975).

5. I.G. Austin and N.F. Mott, Advan. in Phys. 18, 14-102 (1969).

But as n increases this compromise scaling becomes unfavourable for more and more eigenvalues. The way out is to compute each eigenvalue separately by using an appropriately scaled set of basis functions. This is intractably laborious in a variational scheme. In our method the use of an appropriately scaled basis merely requires that a proper value of α obtained from the formula (7) be used in the recursions (3), (5) and (6). Since each eigenvalue is computed individually there are no carryover errors.

(v) Computation with a larger basis is very simply done in this method by continuing the recursions (3), (5) and (6) for increasing m. In contrast, a variational calculation with a larger basis requires integration and the subsequent diagonalization of a large matrix which beyond a certain size is intractable. For instance, the 10000th eigenvalue of the anharmonic oscillator stabilizes to a 15 figure accuracy (in three minutes on IBM 7044) at a point in the recursions which corresponds to the use of nearly 17500 terms in the expansion (1). A variational calculation of this size is inconceivable.

(vi) The eigenvalue problem of the general anharmonic oscillator

$$H = p^2 + x^2 + \lambda x^{2\mu},$$

$\mu = 2, 3, 4, \ldots$ is solvable precisely along the same lines. The generalized scaling formula is

$$\alpha(n, \lambda) = \tfrac{1}{2} + n^{(\mu-1)/(\mu+1)}\lambda^{1/(\mu+1)}. \tag{2'}$$

Thus the following régimes may be distinguished:

$n^{(\mu-1)/(\mu+1)}\lambda^{1/(\mu+1)} \ll \frac{1}{2}$ is the near harmonic régime,

$n^{(\mu-1)/(\mu+1)}\lambda^{1/(\mu+1)} \gg \frac{1}{2}$ is the near pure anharmonic régime,

$n^{(\mu-1)/(\mu+1)}\lambda^{1/(\mu+1)} \approx \frac{1}{2}$ is the boundary layer between the above two régimes.

The importance of the combination $n^{\mu-1}\lambda$ in determining the above régimes was recognized by Hioe *et al.* (1976) on essentially empirical grounds. It is in the present work that the combination $n^{\mu-1}\lambda$ is shown to determine the characteristic scaling in a given régime of (n, λ) through the relation (2'). This observation leads to the construction of a scale adapted basis and to a uniform treatment of the problem in all régimes of (n, λ). The detailed results on the general anharmonic oscillator problem will be reported later.

Computational assistance from Mr M. Ramesh is gratefully acknowledged.

References

Banerjee, K. 1976 *Lett. Math. Phys.* **1**, 323.
Banerjee, K. 1977 *Phys. Lett.* A **63**, 223.
Bender, C. M. & Wu, T. T. 1969 *Phys. Rev.* **184**, 1231.

occur in the 7 x 7 matrix $\underline{G}^{(7)}$. Interactions between these bonds specific to each of the constituents (GaAs and InAs in case of $Ga_xIn_{1-x}As$ alloys) are used to determine the elements of the 7 x 7 matrix $\underline{H}^{exact}$ for each configuration and then the 7 x 7 matrix $\underline{G}^{M}$ is determined from Eq. (3.28). Finally, a weighted average of the (1,1) element of these $\underline{G}^{(M)}$ (since the central bond is numbered 1) yields the configurationally averaged diagonal Green's function sought.

(e) Finally, a cluster of six bonds, forming the characteristic ring in diamond structures, is considered. The configurations and their respective statistical probabilities of occurrence are shown in Fig. 3.7(e). Again, the 6 x 6 matrices for $\underline{H}^{exact}$, $\underline{H}^{(6)}$ and $\underline{G}^{(6)}$ are written down and $\underline{G}^{M}$ determined from Eq.(3.28). An average over the trace of the weighted averaged of the $\underline{G}^{M}$ corresponding to each configuration of the cluster is taken. This is the diagonal Green's function sought, averaged over configurations of the ring.

The effect of such ring clusters is important. In amorphous alloys, when the orbitals are distorted, we often get five and other odd membered rings. The effect of such rings on the density of states is a matter of much interest. It is important, therefore, to first study the effect of rings in the crystalline materials and alloys.

$Ga_{0.5}\ In_{0.5}\ As$

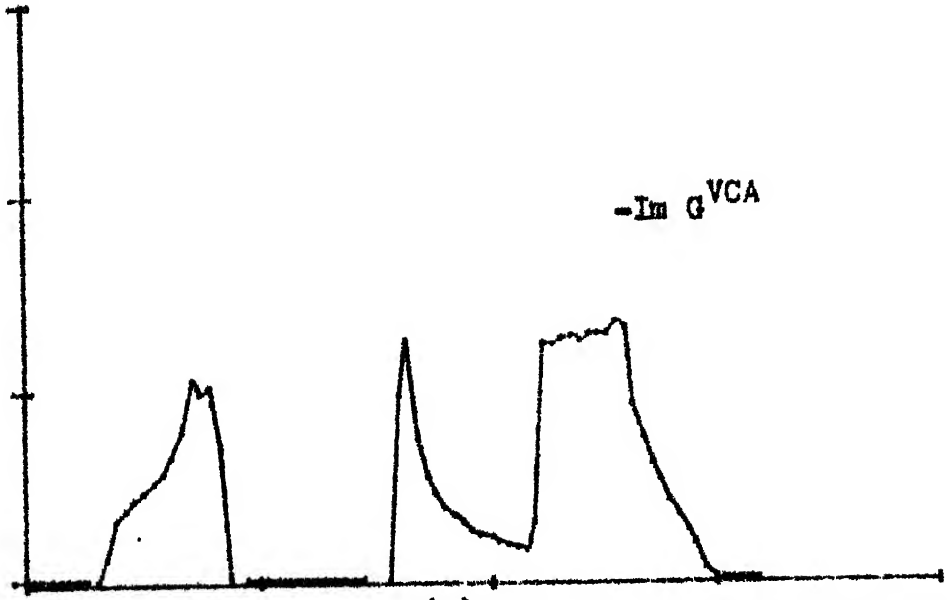

(i)

Range

abscissa: -20 eV to 0 eV
ordinate: 0 to 3

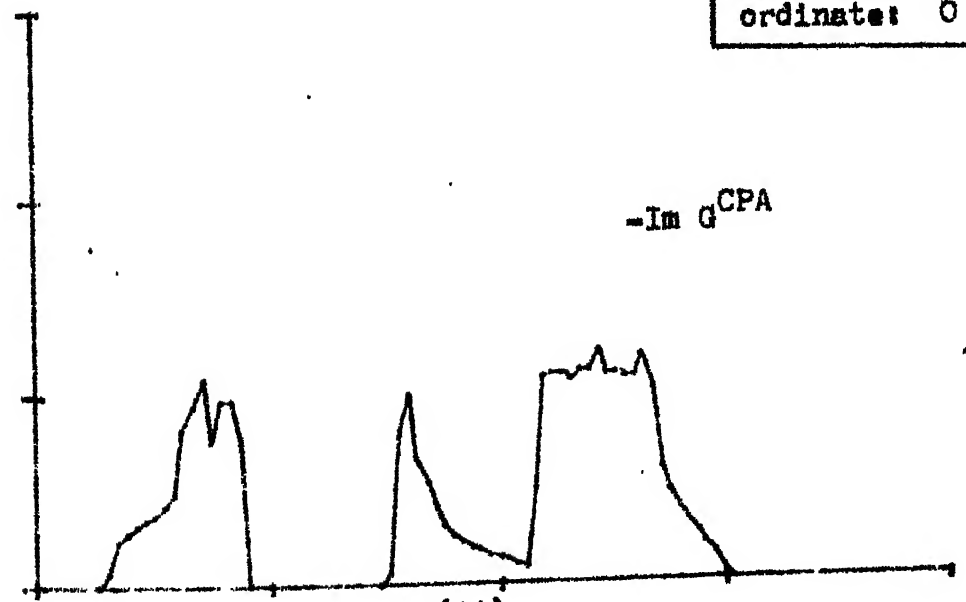

(ii)

Fig. 3.12: (i) $-\mathrm{Im}\ G^{VCA}$ and (ii) $-\mathrm{Im}\ G^{CPA}$ for $Ga_{0.5}\ In_{0.5}\ As$ using the fitted parameters.

This effect of non-orthogonality has been argued away by Chen and Sher but their arguments are weak and difficult to justify.

In this chapter, an ab initio chemical pseudopotential scheme originally introduced by Anderson (1969) and later developed by Bullett (1975) is used with the aim of overcoming the above shortcomings. Herman-Skillman tables of self consistent Hartree-Fock atomic orbitals and potentials are employed as the starting point to determine the pseudo-Hamiltonian matrix elements characterising the III-V semiconductors under consideration. While no claim of extra-ordinary accuracy of the parameters so obtained is made, the procedure is superior to parametric fitting since it does not depend on experimental results. Further, non-orthogonality of the basis set is present naturally in the scheme and no approximation is made on its account. This is where the main thrust of the scheme lies.

The procedure is described in the following (Sec.4.2). It was pioneered by Austin (1962) and Anderson (1969) and extended for application to the cases of homopolar carbon and silicon in the bond basis by Bullett (1975), The chemical pseudopotential scheme has been further generalised in this work for application to heteropolar covalently bonded zinc-blende alloys. In Sec. 4.3 this is applied to the cases of

calculation on benzene in the site orbital basis. This consists of defining the Wigner-Seitz cells corresponding to each bond, considering these to be situated at the centres of the lines connecting the neighbouring bonding sites. Operationally, this is done by checking that each point in the Wigner-Seitz cell corresponding to a bond is not closer to any other bond centre than its own. The 'Wigner trick' involves assuming that an electron at any point sees the potential due to the cell in which the point is situated only, while the potentials due to all others is screened by the Fermi sea. This is equivalent to dividing the crystal into Wigner-Seitz cells, and the potential in each of these is only its own bond potential. Under this approximation, the pseudo-Hamiltonian matrix elements are like

$$\langle a'c'|V_{a\,c}^{(ac)}|ac\rangle = \int_{W_{a'c'}} \phi_{a\,c}\,(V_{a'c'} - V_{ac})\,\phi_{ab}\,d^3\vec{r}$$

$$= \frac{1}{2(1+S)} \int_{W_{a'c'}} [-\{V_a-\varepsilon_a)\,\phi_a$$

$$+ (V_c-\varepsilon_c)\phi_c\}\phi_{a'c'} + \{(V_{a'}-\varepsilon_{a'})\phi_{a'}$$

$$+ (V_{c'}-\varepsilon_{c'})\,\phi_{c'}\}\,\phi_{ab}]\,d^3\vec{r}$$

the integration being over the Wigner-Seitz cell $W_{a'c'}$ corresponding to the bond orbital $|a'c'\rangle$ only.

four alloyed cation sites respectively, the seven bond clusters C_7 and the six bond ring clusters C_6 are embedded in the 1-CPA medium as an approximation to the corresponding n-CPA self-consistent medium as before. Density of states per bond (in units of π^{-1}) corresponding to each configuration of each cluster and the configurationally averaged ones are calculated and graphical results for $Ga_{0.1}$ $In_{0.9}$ As are presented in Fig. 4.5 and in Fig. 4.8 to $Ga_{0.5}$ $In_{0.5}$ As π times the density of states per bond corresponding to the VCA and the 1-CPA are shown on a larger scale in Figs.4.6 and 4.9 for the same alloys. In Figs. 4.7 and 4.10 again, (a) $-\mathrm{Im} \langle\langle G \rangle\rangle_{C_1}$, (b) $-\mathrm{Im}\langle\langle G \rangle\rangle_{C_4}$, (c) $-\mathrm{Im}\langle\langle G \rangle\rangle_{C_4}$, (d) $-\mathrm{In}\langle\langle G \rangle\rangle_{C_7}$ and (e) $\langle\langle G \rangle\rangle_{C_6}$, averaged over configurations of clusters C_1, C_4, $C_{4'}$, C_7, C_6 (See Fig. 3.7(a) to (e)) respectively are shown in a larger scale for clarity.

The comments regarding these results are exactly analogous as those for the fitted parameters. The effect of clusters is the same as before. In the x = 0.1 case there is an enhancement of the upper lying states, arising mainly out of isolated clusters immersed in the medium. There is now also some effect in the s-like part - again an enhancement of the upper like peak. The 50 - 50 case shows less effect, but with perceptible filling in of the upper lying states near the upper band edge.

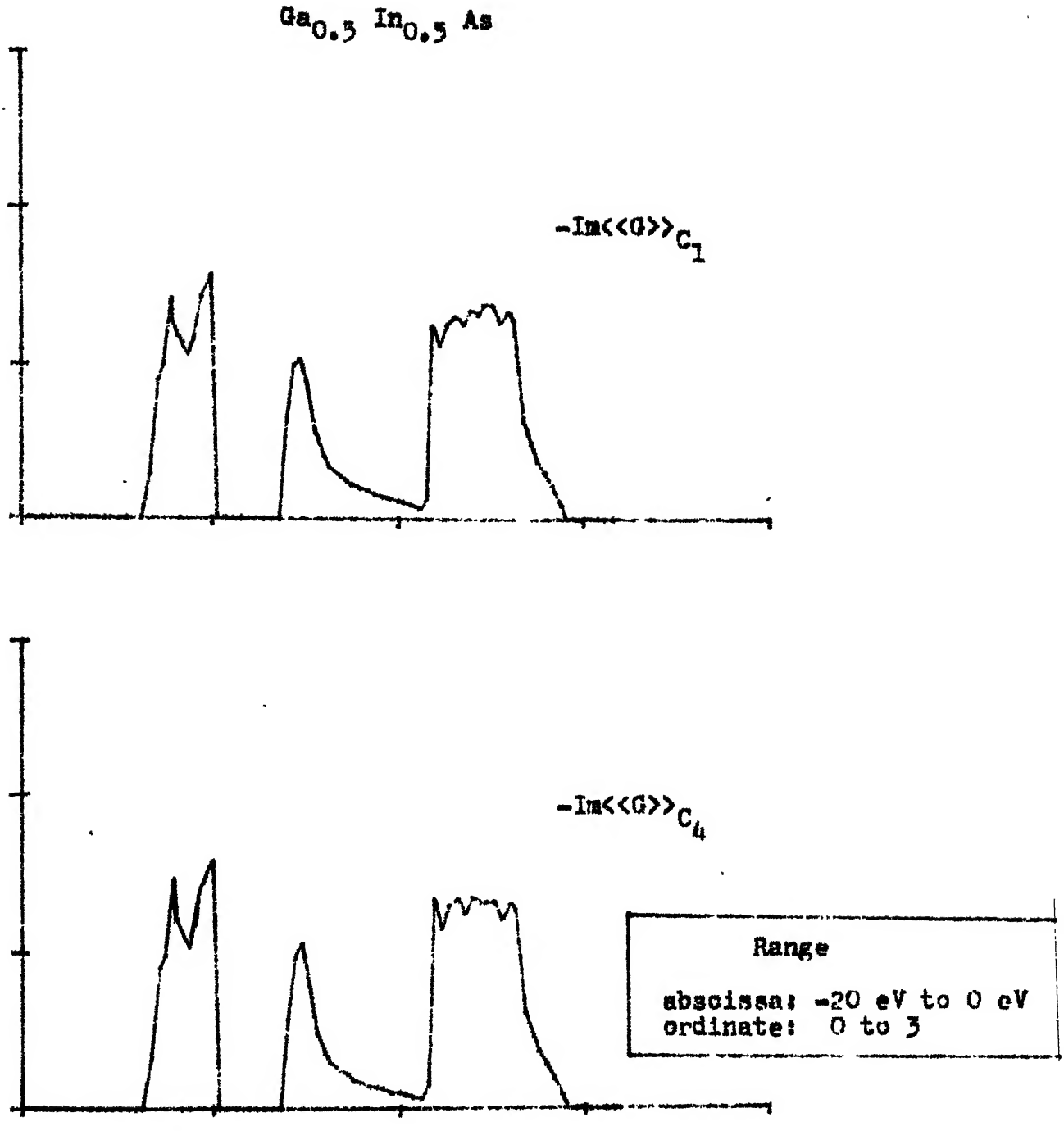

Fig. 4.10 (a) and (b) continued.

of disorder → ∞. This immediately suggests the following identification of the size of the localised state,

$$L_0(E) = \left(1 - \frac{d\sigma_0}{dE}\right) \tag{5.3}$$

The identification is justified if we also note that the residue of G_{00} at its pole is $\left(1 - \frac{d\sigma_0}{dE}\right)^{-1}$.

For states localised over L sites, using the probability interpretation, this is also ~ 1/L. Hence a justification of (5.3). Unfortunately, as we shall see, the probability density of $L_0(E)$ has a long tail leading to divergence of $\langle L_0(E)\rangle$. However, $\langle L_0^{-1}(E)\rangle$ exists and it is more profitable to directly look at this quantity and define the averaged size of the localised state as $\bar{L}_0(E) = \langle L_0^{-1}(E)\rangle^{-1}$.

5.3 The Probability Density:

We shall study the simple model of diagonal disorder with non-random, nearest-neighbour overlap. Within the Anderson tight-binding Hamiltonian,

$$H = \sum_i \varepsilon_i \underline{P}_i + \sum_{i,j} V_{ij} \underline{T}_{ij}$$

$$V_{ij} = V \, \delta(\vec{r}_j - \vec{r}_i - \vec{x})$$

where $\vec{x}$ is a lattice vector, and $\{\varepsilon_i\}$ form a set of statistically independent, identically distributed variables with probability density $p(\varepsilon)$.

$$Q_0(y) \cong \delta\left[y - \left(\frac{K+1}{K} \operatorname{Sec} \frac{\pi\alpha}{2}\right)^{1/\alpha}\right]$$

when,

$$\langle L^{-1}\rangle^{-1} = \left\{\left(\frac{K+1}{K} \operatorname{Sec} \frac{\pi\alpha}{2}\right)^{1/\alpha} + a_0 + 1\right\} \qquad (5.20)$$

We note that near $E = E_c$, $\langle L_0^{-1}\rangle^{-1}$ diverges linearly. This is the familiar result we would expect from a mean field theory . The CTA is akin to such an approximate theory. We cannot compere this with Anderson's prediction of a 3/5 power-law divergence. His argument was based on the study of G_{on} on a real lattice, and the 3/5 power law near E_c depended on the statistics of closed, non-repeating paths in the lattice. Such a result cannot be expected within our CTA. Departure from the linear law is evident away from E_c.

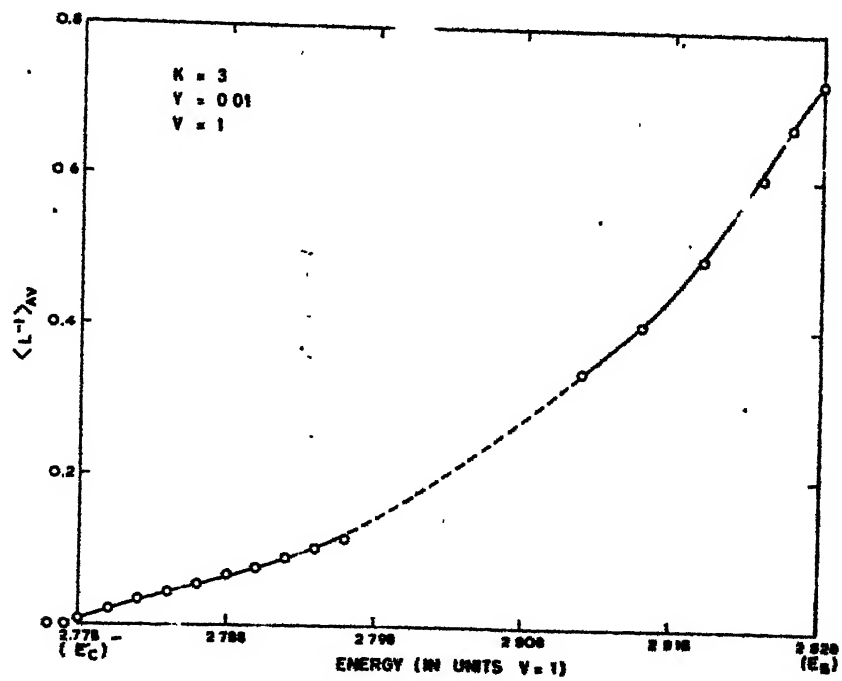

Fig. 1. Averaged value of the inverse size of localisation domain in the localised regime for a very weakly disordered system. Site energies are Lorenzians with very narrow width $\gamma/v = 0.01$.

REFERENCES

Abou-Chacra, Anderson, P.W., Thouless, D.J. (1973), J. Phys. C6 1734.

Adams, W.H. (1961) J. Chem. Phys. 34 89.
(1962) J. Chem. Phys. 37 2009.
(1971a) Chem. Phys. Lett. 11 71.
(1971b) Chem. Phys. Lett. 11 441.
(1971c) Chem. Phys. Lett. 12 295.

Alben, R., Blume, M., Krakauer, M. and Schwartz, L.(1975) Phys. Rev. B12 4090.

Anderson, P.W. (1958) Phys. Rev. 109 1492.
(1968) Phys. Rev. Lett. 21 13.
(1969) Phys. Rev. 181 25.
(1970) Comm. on Solid State Phys. 2 193.
(1972) Proc. Nat. Acad. Sci. USA 69 1097.

Austin, B.J., Heine, V., Sham, L.J. (1962) Phys. Rev. 127 276.

Austin, I.G., Mott, N.F. (1969) Adv. in Phys. 18 14.

Banerjee, K. (1976) Lett. Math. Phys. 1 323.
(1977) Phys. Lett. A 63 223.
(1978a) Proc. Roy. Soc. (Lond) A 363 147.
(1978b) Proc. Roy. Soc. (Lond) A 364 265.
(1979) Proc. Roy. Soc. (Lond) A 368 155

Banerjee, K., Bhatnagar, S.P., Choudhry, V. and Kanwal, S.S., Proc. Roy. Soc. (Lond) A 365 575 (reprinted in Appendix C).

Bansil, A., Schwartz, L. and Ehrenreich, H. (1975) Phys. Rev. B12 2893.

Bellman, R. (1960) Introduction to Matrix Algebra, McGraw Hill Books Ltd., pp. 61.

Bennett, L.H., Swartzendruber, L.J. and McNeil,M.B. (1974).

Proc. of the 3rd Int. Cong. on Marine Corrosion and Fouling.

National Bureau of Standards Publications.

of the square face. The IBZ is then 1/48th of the BZ since there are eight hexagonal faces and six square faces. The tetrahedrons ΓLAK, ΓLUA, ΓUXA into which the IBZ is divided are of volumes 32, 32, 32 2/3 respectively in units of $(\pi/16a)^3$. For the calculation, each tetrahedron is subdivided into 64 TT's since finer division does not reveal any additional features in the Green's functions evaluated. Energy eigenvalues have been determined at five points besides Γ, the tip of each TT, spaced evenly along axes of each TT and 6-point Lagrange's interpolation formula

$$f(x + ph) = -\frac{p(p^2-1)(p-2)(p-3)}{120} f_{-2} + \frac{p(p-1)(p^2-4)(p-3)}{24}$$

$$- \frac{(p^2-1)(p^2-4)(p-3)}{12} f_o + \frac{p(p+1)(p^2-4)(p-3)}{12}$$

$$- \frac{p(p^2-1)(p+2)(p-3)}{24} f_2 + \frac{p(p^2-1)(p^2-4)}{120} f_3$$

is used where f_i, i = -2 to 3 are the known values of the function f(x + ih) for i = -2 to 3, i.e. at intervals of h around x. The values of α_r such that $E = E_r$ have been obtained by Newton Raphson's method.

For the imaginary part of the diagonal element of the Green's function in the coordinate space bond bases set $|\vec{r}\ \alpha\rangle$, $f(\vec{k}) = 1$ and the above procedure is complete. In general,

$$\langle \vec{r}\alpha | G | \vec{r}'\alpha' \rangle = \frac{1}{N} \sum_{\substack{k,n \\ (BZ)}} e^{i\vec{k}\cdot\vec{\tau}_{\alpha\alpha'}} \frac{\phi(kn\alpha)\ \phi(kn\alpha')}{E - \varepsilon_n(\vec{k})} \qquad (A.2)$$

Proc. R. Soc. Lond. A. 360, 575–586 (1978)
Printed in Great Britain

The anharmonic oscillator

By K. Banerjee, S. P. Bhatnagar,
V. Choudhry and S. S. Kanwal

Physics Department, Indian Institute of Technology, Kanpur 208016, *India*

(*Communicated by D. R. Bates, F.R.S. – Received 7 September* 1977)

Accurate eigenvalues and eigenfunctions of the anharmonic oscillator ($H = p^2 + x^2 + \lambda x^4$, $\lambda > 0$) and the quartic oscillator ($H = p^2 + x^4$) are obtained in all régimes of the quantum number n and the anharmonicity constant λ. Transition moments of comparable accuracy are obtained for the quartic oscillator.

The method, applicable quite generally for eigenvalue problems, is non-perturbative and involves the use of an appropriately scaled basis for the determination of each eigenvalue. The appropriate scaling formula for a given régime of (n, λ) is constructed from the oscillation properties of the eigenfunctions. More general anharmonic oscillators are also discussed.

1. Introduction

The quantum mechanical anharmonic oscillator described by the Hamiltonian $H = p^2 + x^2 + \lambda x^4$, where $p = -\mathrm{i}\,\mathrm{d}/\mathrm{d}x$ and $\lambda > 0$ is the anharmonicity constant, has been the subject of very general interest. The investigations from the points of view of molecular physics and field theory are referred to in the works of Reid (1970) and Bender & Wu (1976) respectively. A general account may be found in Hioe & Montroll (1975) and Hioe, MacMillen & Montroll (1976).

The perturbation expansion for the eigenvalues $E_n(\lambda)$ in powers of the anharmonicity constant λ is not convergent but asymptotic (Bender & Wu 1969; Simon 1970). Such investigations have been confined to the computation of the lowest few eigenvalues for various λ. Variational calculations using a harmonic oscillator basis have been more successful. Reid (1970) thus obtained the first 25 eigenvalues of the quartic oscillator ($H = p^2 + x^4$) to 12 significant figures. For higher eigenvalues the variational calculations become forbiddingly laborious. Moreover, the variationally obtained eigenfunctions are far less accurate than the corresponding eigenvalues and are therefore unsuitable for the computation of matrix elements of operators. Biswas *et al.* (1973) used the Hill determinant method to obtain eight eigenvalues of the anharmonic oscillator for various λ in the range $0 < \lambda \leqslant 100$. For higher eigenvalues or for higher λ the numerical errors in their work become too severe. The most comprehensive work on this problem is due to Hioe & Montroll (1975) and Hioe *et al.* (1976); they distinguished two limiting régimes of values of the quantum number n and the anharmonicity constant λ. In